# SUPERHYDROPHILIC AND SUPERHYDROPHOBIC TEXTILES FOR RAPID CONTACT-KILLING OF AIRBORNE BACTERIA

**ZHAO YUANYUAN**

**PhD**

**The Hong Kong Polytechnic University**

**2025**

**The Hong Kong Polytechnic University**

**School of Fashion and Textiles**

# Superhydrophilic and Superhydrophobic Textiles for Rapid Contact-Killing of Airborne Bacteria

**Zhao Yuanyuan**

**A thesis submitted in partial fulfilment of the**

**requirements for the degree of Doctor of Philosophy**

**December 2024**

CERTIFICATE OF ORIGINALITY

I hereby declare that this thesis is my own work and that, to the best of my knowledge and belief, it reproduces no material previously published or written, nor material that has been accepted for the award of any other degree or diploma, except where due acknowledgement has been made in the text.

_____ (Signed)

ZHAO YUANYUAN (Name of student)

# Abstract

In this study, three kinds of new antibacterial materials with different functions were developed to solve the problem of contact killing of bacteria in air aerosols, and their properties and application potential were systematically studied. Firstly, the superhydrophilic nanofiber layer modified with silver nanoparticles enables the rapid capture and effective killing of bacteria in bioaerosols by efficiently capturing airborne bacteria and releasing silver ions. This kind of superhydrophilic fiber material combines breathability and antibacterial properties, capable of significantly reducing the survival rate of the bacteria in a short time. Secondly, polyvinylpyrrolidone (PVP) was modified on the surface of zinc oxide nanorods (ZnO NRs) to construct superhydrophilic nanostructures. This strategy utilizes capillary condensation and liquid bridge stretching effect to produce strong and controllable mechanical stress under moderate humidity conditions, directly destroying bacterial cell membranes, and achieving the purpose of efficient contact killing. Thirdly, by introducing polycation (PCa), the nanorod surface transforms from hydrophilic to superhydrophobic, and produces extremely high charge density in the microregion. This local charge enrichment can not only strengthen the binding of bacteria to the surface, but also use hydrophobic chain segments to disturb the cell membrane structure, and finally achieve rapid and complete bacterial killing in 3 minutes.

This study applied antibacterial materials to polypropylene (PP), polyethylene terephthalate (PET) and nylon textiles, which greatly improved their antibacterial property. After long-term testing, the modified textile has continued to achieve zero bacterial survival in several weeks, providing strong support for practical applications such as medical protective clothing, masks, and air filters. The above results reflect the organic integration of air aerosols, antibacterial materials, textiles and contact sterilization technology, opening a new path for the development

of efficient, green and sustainable antibacterial protection products, and provide an important reference for addressing public health challenges and improving biosecurity.

# List of Publications

Related journal publications

1. **Y. Zhao**[#], H. A[#], Y. H. Cheung, Y. Lam, J. Tang, H. Li, Z. Yang[*], J. H. Xin[*], Capillary Condensation Mediated Fluidic Straining for Enhanced Bacterial Inactivation. *Adv. Funct. Mater.* 2024, 34:2314581.
2. **Y. Zhao**[#], Y. Luo[#], Y. Chai[#], Y. Lam, Y. Gong, K. Chen, G. Lu, G. Xia, Y. Chang, M, Yang, Y. Xu[*], J. H. Xin[*], Precise Oligomer Organization Enhanced Electrostatic Interactions for Efficient Cell Membrane Binding. *Nano Lett.* 2025, 25:8488–8494.

Other journal publications

1. **Y. Zhao**[#], J. Liu[#], G. Lu[#], J. Zhang, L. Wan, S. Peng, C. Li[*], Y. Wang[*], M. Wang, H. He, John H. Xin[*], Y. Ding, S. Zheng[*], Diurnal Humidity Cycle Driven Selective Ion Transport Across Clustered Polycation Membrane. *Nat. Commun.* 2024, 15:7161.
2. **Y. Zhao**, S. Shi, J. H. Xin[*], and S. Zheng[*], Phase Separation Regulated Microfiber Networking for Strain-Insensitive Electronics, *Matter* 2024, 7(8): 2626-2788.
3. **Y. Zhao**, G. Xia, Y. Lam, J. H. Xin[*], Interfacial Friction Induced Capillary Flow within Nanofiber-supported Ionic Liquid Droplets. *Green Energy Environ.* 2024, 9(5):789-791.
4. J. Tang[#], **Y. Zhao**[#], M. Wang, D. Wang, X. Yang, R. Hao, M. Wang, Y. Wang, H. He[*], J. H. Xin, S. Zheng[*] Circadian Humidity Fluctuation Induced Capillary Flow for Sustainable Mobile Energy. *Nat. Commun.* 2022, 13:1291.

5. G. Xia, X. Bian, Y. Wang, Y. Lam, **Y. Zhao**, S. Fan, P. Qi, Z. Qu, J. H. Xin*, Janus Outdoor Protective Clothing with Unidirectional Moisture Transfer, Antibacterial, and Mosquito Repellent Properties, *Chem. Eng. J.*, 2024, 490:151826.

Conferences

1. **Y. Zhao**, J. H. Xin, "Improved Bacterial Elimination Using Fluid Straining via Capillary Condensation" During the session "E02_E-textiles and Functionalisation 1" of Symposium E, European Materials Research Society (E-MRS) Spring Meeting, Strasbourg, France, 2024

Patent

1. H. Xin, **Y. Zhao**, Nanocomposite Materials, Their Preparation Methods, and Applications. 2024, Chinese Patent Application No. CN202410353976.0.

# Acknowledgements

First of all, I would like to express my heartfelt thanks to my supervisor, Professor John Xin. He not only gave me this valuable academic opportunity, but also provided me with a flexible working environment that gave me the freedom to explore different areas of research. Professor Xin has always given me meticulous guidance and support during my research and learning process. In the past three years of study, his insightful and patient guidance has helped me to develop a deeper understanding and richer research experience in this field from my initial attempt in the field of antibacterial textiles to today, which is a lifelong wealth for me.

In addition, I would like to thank the Hong Kong Polytechnic University and the School of Fashion and Textiles for providing an ideal platform for my research. In this supportive environment, I was able to keep improving. Meanwhile, I would like to take this opportunity to express my heartfelt thanks to all the colleagues in Professor Xin's group for their collaboration and support in making this scientific research journey more fulfilling and meaningful.

Lastly, I would like to extend my special thanks to my family. They have stood beside me at all moments and made this hard path of scientific research warm and hopeful. Their encouragement is my power that overcame every hard situation and made it easy for me to progress. Thanks again to everybody who helped me and stood by me during this journey!

# Table of Contents

# List of Figures, Tables and Abbreviations

List of Figures

List of Tables

List of Abbreviations

| | |
|---|---|
| Ag NPs | Silver nanoparticles |
| $Ag^+$ | Silver ions |
| $AgNO_3$ | Silver nitrate |
| BE | Binding energy |
| CA | Contact angle |
| CFU | Colony forming unit |
| CTA | Chain transfer agent |
| DI water | Deionized water |
| DMAc | N,N-Dimethylacetamide |
| *E. coli* | *Escherichia coli* |
| EDS | Energy dispersive X-ray spectroscopy |
| FESEM | Field emission scanning electron microscope |
| FTIR | Fourier-transform infrared spectroscopy |
| $\gamma$ | The surface tension |
| HRTEM | High-resolution transmission electron microscopy |
| ICP | Inductively coupled plasma |
| LB | Luria-Bertani |

| | |
|---|---|
| ILs | Ionic liquids |
| MD | Molecular dynamics |
| MOFs | Metal-organic frameworks |
| NMR | Nuclear magnetic resonance |
| NVP | N-Vinylpyrrolidone |
| NR | Nanorods |
| $P$ | Partial pressure |
| $P_0$ | Below the saturation vapor pressure |
| PBS | Phosphate-Buffered Saline |
| PCa | Polycation |
| PCaNR | Polycationic zinc oxide nanorods |
| PET | Polyethylene terephthalate |
| PI | Prodium iodide |
| PP | Polypropylene |
| PVP | Polyvinylpyrrolidone |
| QAC | Quaternary ammonium compounds |
| $r_1$ | The meniscus curvature radius of the condensed water |
| RAFT | Reversible Addition–Fragmentation chain-Transfer |

| | |
|---|---|
| RH | Relative humidity |
| ROS | Reactive oxygen species |
| RSV | Respiratory syncytial virus |
| *S. aureus* | *Staphylococcus aureus* |
| S-NRs | Superhydrophilic nanorods |
| SARS | Severe acute respiratory syndrome |
| SAXS | Small-angle X-ray scattering |
| SEM | Scanning electron microscopy |
| TEM | Transmission electron microscopy |
| $\theta$ | Contact angle of the water against the solid wall |
| UV | Ultraviolet |
| $V_m$ | Molar volume of the condensate |
| XPS | X-ray photoelectron spectroscopy |

# 1 Introduction

## 1.1 Research Background

Bioaerosols can be defined as aggregated solid or liquid particles that contain bacteria, viruses, pollen, and fungi, which, due to being dispersed in gaseous environments, are produced from numerous natural and anthropogenic processes [1]. Such particles, though their conveyance takes place through the air, are known to be capable of grave health consequences with potential influencing factors on medical and industrial environments. The airborne pathogens usually come from soil, water, and human activities. A typical example, especially the airborne bacteria infected in the respiratory system via inhalation and extended to further organs [1, 2]. Besides, several serious pandemic viruses that have occurred in the history of humans are a result of airborne viruses. Many include the Spanish flu, severe acute respiratory syndrome (SARS) virus, and influenza A viruses, including the recent coronavirus disease 2019 (COVID-19) virus pandemic [3].

Surfaces such as medical devices and air filtration devices are vulnerable to bioaerosol contamination, leading to bacterial colonization, infection, increasing the difficulty and cost of treatment [4, 5]. Although antibiotic drug treatment is effective, this method currently faces challenges such as increasing bacterial resistance. Antibiotic resistance is increasing in common pathogens. At the same time, traditional filters and textiles cannot effectively kill attached bacteria. Therefore, the development of efficient and sustainable antibacterial materials has become a research focus.

The existing antibacterial technologies mainly include ultraviolet (UV) antibacterial, microwave antibacterial, high-temperature antibacterial and other physical ways to kill bacteria or inhibit their growth, usually used in non-contact or indirect antibacterial scenarios; Chemical disinfectants (such as alcohol, sodium hypochlorite), gases (such as ozone, ethylene oxide) kill microorganisms through chemical oxidation; And contact antibacterial through the special structure of the surface or the antibacterial component in the coating and the bacteria in direct contact to achieve the bactericidal effect.

Surface contact antibacterial mainly includes chemical antibacterial (such as silver nanoparticles) and physical antibacterial (such as mechanical sterilization nanostructure surfaces) [6, 7]. For example, the chemical antimicrobial mechanism of silver nanoparticles is that silver nanoparticles destroy the structure of bacterial cell membranes by releasing silver ions ($Ag^+$), inhibit protein synthesis, and interfere with DNA replication, thereby inhibiting bacterial growth and reproduction [8-10]. Silver ions can also further disrupt cell metabolism through the generation of reactive oxygen species (ROS) to achieve broad-spectrum antibacterial effects [11-14]. Silver nanoparticles antibacterial does not rely on chemical disinfectants, silver nanoparticles combined with electrospinning technology of superhydrophilic fiber membrane can be used for bioaerosol capture and inactivation. On the other hand, as an advanced physical antibacterial method, the mechano-bactericidal surface uses nanostructures to exert mechanical stress on the bacterial cell wall, resulting in cell rupture and death [15-17]. Notably, liquid behavior (such as capillary condensation) plays a key role in enhancing mechanical sterilization in bioaerosol applications: superhydrophilic surfaces are enhanced by capillary strain. The chemical antibacterial properties are combined with the functional surface of mechanical sterilization, the antibacterial properties can be further enhanced, especially for the sterilization of bioaerosols in complex environments.

Functional textiles have strong antibacterial potential and are becoming the focus of research on the next generation of antibacterial materials. First, textiles have the characteristics of flexibility, good air permeability, large specific surface area, lightweight nature makes them in terms of portability and wearability has a significant advantage, is an ideal substrate for antibacterial materials. In addition, textiles are easy to be modified by nanoparticles or nanostructures to give specific functions (such as superhydrophilic or superhydrophobic), thus realizing the antibacterial needs of multiple scenarios. From the perspective of industrialization and application, textiles are easier to achieve large-scale production than other materials, and the manufacturing cost is low, especially in the fields of medical protective clothing, masks, filtration materials and other important application potential.

Currently, antibacterial textiles are important in hospitals, the environment, and in places of high microbial risk. In these settings, the clothing worn by patients, health care workers and doctors can carry many microorganisms and can be transmitted between different populations through clothing. Antibacterial textiles have great commercial potential in controlling the spread of infectious microorganisms. Antibacterial textiles can be divided into coating antibacterial textiles, composite antibacterial textiles, nano-modified antibacterial textiles, fiber functional antibacterial textiles according to the functional classification. Coating type antibacterial textiles refers to the coating of antibacterial agents on the surface of textiles, such as silver nanoparticle coating and photocatalytic coating. This kind of textile has strong antibacterial properties, suitable for a variety of substrates, and is generally used in protective clothing and filtration materials. Composite antibacterial textiles refer to the direct incorporation of antibacterial materials into the substrate (such as polyester, nylon) in the fiber manufacturing stage. It is characterized by the uniform distribution of antibacterial agents, long service life, and is generally used in sports clothing and medical sheets. Nano-modified

antibacterial textiles generally modify the textile surface through nano-structures to achieve super hydrophilic or super hydrophobic properties and enhance the antibacterial effect. This kind of textile is characterized by both physical anti-adhesion and chemical antibacterial functions, and is generally used in outdoor clothing, high-end protective equipment, and other fields. Finally, fiber functionalized antibacterial textiles are textiles that introduce antibacterial functional groups on the fiber surface through chemical grafting or modification technology. Its most notable feature is that its antibacterial properties can be adjusted to meet different needs, and it is generally used in medical dressings and special purpose textiles.

In this thesis, the design and application of antibacterial textiles were carried out as follows. First, the superhydrophilic electrospun nanofiber layer doped with silver nanoparticles was prepared for antibacterial purposes. In the second work, textiles with polyvinylpyrrolidone-modified zinc oxide nanorods were fabricated, using capillary condensation effect to enhance bacterial capture and mechanical sterilization. In the third work, textiles were further modified by polycationic zinc oxide nanorods, combined with chemical action and mechanical sterilization behavior, to improve the antibacterial ability. In conclusion, these three works integrated the chemical and mechanical bactericidal properties of nanomaterials to functionalize textiles with silver nanoparticles, PVP modified zinc oxide nanorods and polycationic modified zinc oxide nanorods, respectively, providing diversified design strategies for the development of efficient, broad-spectrum, and environmentally friendly antibacterial textiles.

Functional textiles combine chemical and mechanical antibacterial strategies to provide green solutions and show great potential in the field of medical protection. Its antibacterial properties are significant, while reducing environmental impact and meeting the needs of sustainable development. In the field of public health, antibacterial textiles can be used in high-contact

items such as towels, curtains, and vehicle seat cover to effectively reduce pathogen transmission and reduce the risk of cross-infection. In terms of medical protection, antibacterial protective clothing, surgical gowns, and masks provide important barriers for medical workers, significantly reduce hospital infections, and can achieve comprehensive properties such as antibacterial, waterproof, and protective through multi-functional design. In the field of air purification, antibacterial textiles act as efficient filtration materials to capture pathogens in the air, improve air quality and reduce disease transmission. With the development of nanotechnology and electrospinning processes, functional textiles will play a greater role in extreme environmental protection, personal care, making important contributions to human health and sustainable development.

## 1.2 Research Gaps and Objectives

Although there has been a lot of research in the field of antibacterial materials, there are still several key deficiencies. First, the lack of strategies that can achieve rapid and effective contact sterilization limits the actual antibacterial efficiency of the materials. In response to this, this study designed three rapid contact sterilization strategies to achieve efficient inactivation of bacteria upon contact. Secondly, the physical and chemical mechanisms of the nano-bio-interface during contact sterilization were not fully understood. This work integrated multi-scale experimental and theoretical evidence to deeply reveal the mechanism of interfacial bacterial inactivation. Third, the high-performance mechanical sterilization materials commonly used in the laboratory were mostly based on rigid substrates, which were difficult to directly apply to real textile materials and wearable products. To solve this problem, this study successfully transformed the laboratory strategy into functional textiles to promote its practical application in mask filters and protective clothing. From mechanism analysis to

practical application, this study systematically promoted the design and development of antibacterial textiles.

This research focuses on the contact antibacterial challenge of bacteria in bioaerosols, combines the advantages of chemical antibacterial and physical mechanical antibacterial, and develops functional textile materials, aiming to provide efficient, green and sustainable antibacterial solutions. The specific objectives are as follows:

1. Develop efficient antibacterial materials. The superhydrophilic fiber layer containing silver nanoparticles was prepared by electrospinning technology, and the bacteria in bioaerosol were captured and quickly killed by its chemical antibacterial properties and superhydrophilic property. Superhydrophilic (PVP modification) and superhydrophobic (polycationic modification) textile materials were designed using the surface modification technology of zinc oxide nanorods, and their bactericidal ability was explored.

2. Optimize contact sterilization technology. The function of chemical antibacterial (such as silver nanoparticles, polycations) and mechanical antibacterial (nanostructured surface) was discussed, and multi-functional antibacterial textiles were designed to realize the comprehensive performance of efficient sterilization and superhydrophilic and superhydrophobic surface. This study also integrated multi-scale evidence to uncover the physical and chemical killing mechanisms at the nano-bio interface.

3. Promote the practical application of antibacterial textiles. To provide scientific basis for large-scale production and commercialization of antibacterial textiles, design specifications and optimization strategies based on bioaerosol treatment were proposed. Through

experimental verification, the application prospect of functional textiles in medical protection, public health and environmental governance was demonstrated.

## 1.3 Research Methodologies

In this study, a combination of experimental design, material preparation and characterization were adopted to conduct research on bacterial contact sterilization in bioaerosols. Specific research methods were as follows:

Material preparation. For the superhydrophilic silver nanoparticle electrospinning nanofiber film, cellulose acetate nanofiber film containing silver nitrate was firstly prepared by electrospinning technology, and then reduced to silver nanoparticles by ultraviolet light. In addition, the wettability of the surface of the alkali-treated fiber layer was adjusted to superhydrophilic property. For superhydrophilic PVP modified zinc oxide nanorods textile, zinc oxide nanorods were firstly modified on textile substrates, and then modified zinc oxide surface with PVP to give the textile super hydrophilic properties. For superhydrophobic polycationic modified zinc oxide nanorods, zinc oxide nanorods were firstly modified on textile substrates, and then introduce polycationic modification on the surface of zinc oxide nanorods to give super hydrophobic properties of the textile.

Material characterization. For morphology and structure characterization, this study used scanning electron microscopy (SEM) to observe the micro/nano structures of nanofibers, zinc oxide nanorods and textile surfaces to confirm the preparation and morphological characteristics of the materials. The dispersion and size distribution of silver nanoparticles were analysed by transmission electron microscopy (TEM). In this study, static water contact angles were measured to evaluate the wettability of superhydrophilic and superhydrophobic surfaces.

For chemical composition characterization, Fourier-transform infrared spectroscopy (FTIR), X-ray photoelectron spectroscopy (XPS), energy dispersive X-ray spectroscopy (EDS) were used to analyse the chemical composition and element distribution on the surface of the material.

Contact antibacterial performance test. Bioaerosol contact sterilization experiment, preparing aerosols containing bacteria, spraying them on the surface of functional textile materials, and evaluating the time required to kill bacteria on the surface of the material under different conditions. The survival rate of bacteria after contact sterilization was measured by standard plate counting method, and the antibacterial properties of different materials were compared. The bacteria on different antibacterial surfaces were fixed by glutaraldehyde after contact with bioaerosol for a period, and the death state of bacteria was observed by SEM. Cell fluorescence staining (such as live/dead staining) was used to observe the death state of bacteria and determine the survival rate of bacteria after contact sterilization.

Performance comparison and mechanism study. The antibacterial properties and application scenarios of silver nanoparticle fiber layer, superhydrophilic and superhydrophobic zinc oxide nanorods were compared. The antibacterial efficiency of the material under different humidity conditions was analysed, and the adaptability of the material function to the actual application environment was discussed. The bactericidal mechanism was studied by SEM and live/dead staining to analyse the damage morphology of bacteria and verify the synergistic effect of mechanical bactericidal and chemical bactericidal. The key mechanisms of capillary condensation, superhydrophilic and electrostatic action of polycations in the antibacterial process were discussed.

Practical application testing. Evaluation of functional textiles in a practical scenario, functional textile materials were applied to the middle layer of a mask to test its antibacterial ability and durability. Through the above research methods, this study systematically explored the preparation, performance and practical application potential of functional antibacterial textile materials and provide theoretical basis and technical support for bioaerosol sterilization.

## 1.4 Significance and Values

This study systematically has explored the preparation, properties and practical application potential of functional antibacterial textile materials and provided theoretical basis and technical support for bioaerosol sterilization.

This research has innovative basic scientific significance. This study has expanded the theoretical basis in the field of contact sterilization, combined the two strategies of chemical antibacterial and physical mechanical antibacterial, systematically studied the performance of chemical components (such as silver nanoparticles, polycations) and nanostructured physical mechanical antibacterial surfaces in bioaerosol contact sterilization, and provided a new idea for the design of antibacterial materials. In addition, this study also has explored the mechanism of the influence of liquid behaviour (such as capillary condensation and droplet rolling) on the mechanical sterilization performance, revealed the internal relationship between wettability and sterilization efficiency, and expanded the existing research. Second, this study has emphasized the design of innovative multi-functional antibacterial materials. The nanostructured surface was used to develop functional textiles with super-hydrophilic or super-hydrophobic properties, providing efficient, green solutions for multi-scenario applications. Third, at present, the problem of antibiotic resistance is becoming increasingly serious, and this study provides a new method of non-traditional sterilization, reducing the dependence on

traditional antibiotics, and providing a scientific foundation for addressing with the challenge of bacterial resistance.

This research has not only reflected the significance of scientific basis, but also had practical application value and social importance. First, bioaerosols were important vectors for the spread of bacteria in medical settings, public spaces and industrial environments, and the development of highly effective antibacterial materials can help control the risk of airborne diseases. The results of this research have potential application value in the fields of protective clothing, masks, air filters, etc., especially in high humidity or polluted environments to provide feasible solutions. In response to public health challenges, this study has provided technical reserves for improving public health protection systems. Second, functional textiles were an ideal carrier for the industrialization of antibacterial materials because of their lightness, flexibility and good processability. This study has provided technical support for the design, optimization and large-scale production of textile antibacterial function. The low cost and sustainability of the materials helped promote the application of antibacterial textiles in medical, daily life and industry, and improved the level of public health protection. Thirdly, this study has been expected to promote the popularization of green and sustainable antibacterial technology. The research of mechanical sterilization technology could reduce the use of traditional chemicals such as antibacterial coatings and disinfectants and reduce environmental pollution. The reusable and durable materials enhanced the ecological benefits of antibacterial products and contribute to sustainable development.

From the scientific, practical, and social levels, this study has designed efficient and multi-functional antibacterial materials for bacterial threats in bioaerosols, which not only promote the development of contact sterilization technology, but also bring far-reaching impact on public health safety, environmental protection and textile industry upgrading.

## 1.5 Outline of the Thesis

This thesis is organized as follows:

The first chapter briefly introduces the research background of this paper: the harm of bioaerosol and its role in the transmission of infectious diseases; The development and potential of contact antibacterial technology (chemical antibacterial and mechanical antibacterial); Application advantages and prospects of functional textiles in antibacterial field. Research objectives are then proposed, including the development of highly effective antibacterial materials, the optimization of contact sterilization techniques, and the promotion of practical applications of antibacterial textiles. Then the methods of preparation, characterization and testing of antibacterial properties of the materials used in this paper are described briefly, as well as the strategies of practical application testing. Finally, the scientific significance, practical significance and social importance of this study are expounded, and its promoting effect on coping with the threat of bioaerosol and the development of antibacterial materials is explained.

In Chapter 2, the definition, composition and mode of transmission of bioaerosol are reviewed, and the harm to public health and the limitations of existing antimicrobial techniques are analysed. The research progress of contact sterilization technology was further discussed, including the principle, application and shortcomings of mechanical sterilization surfaces and chemical antibacterial strategies. Then, the unique mechanism of superhydrophilic and superhydrophobic surfaces in enhancing mechanical sterilization and realizing self-cleaning antibacterial was introduced. Finally, the application potential of nanoparticles and nanostructures in functional textiles is analysed, and their antibacterial prospects in medical and industrial fields are forecasted.

In Chapter 3, the superhydrophilic electrospinning fiber membrane of silver nanoparticles was prepared and characterized. The morphology, chemical composition and wettability of the materials were analysed by SEM, XPS and contact angle test. Then, the antibacterial efficiency of silver nanoparticle superhydrophilic electrospinning nanofiber textile against bioaerosol was tested, and the aerosol trapping ability of fiber membrane and the chemical antibacterial ability of silver nanoparticle were analysed.

In chapter 4, the rapid sterilization of super hydrophilic PVP modified zinc oxide nanorods textile was introduced. Firstly, zinc oxide nanorods were prepared, superhydrophilic properties were conferred by PVP modification, and the modification method of textile surface nanorods was optimized. Then the microstructure, chemical composition, wettability, and other properties of the materials were tested and characterized. Finally, the antibacterial performance was tested. Under different humidity conditions, the capturing and bactericidal capacity of the super-hydrophilic textile was evaluated, and the effect of capillary condensation effect on the mechanical bactericidal efficiency was analysed.

In Chapter 5, super hydrophobic polycationic modified zinc oxide nanorods textile was proposed to quickly kill airborne bacteria. Firstly, the superhydrophobic fabric of polycationic modified zinc oxide nanorods was prepared. Then the microstructure, chemical composition, wettability and other properties of the materials were tested and characterized. Finally, the antibacterial properties and antibacterial efficiency of super hydrophobic polycationic modified zinc oxide nanorods were tested.

Chapter 6 provides an overall summary of the research and outlines future directions for enhancing antibacterial textiles in the fight against bioaerosols.

# 2 Literature Review

## 2.1 Bioaerosols and Their Hazards

The spread of respiratory infectious diseases is a serious public health problem, attracting a lot of attention and research in many disciplines [18, 19]. SARS, the A (H1N1) virus, MERS, and the global COVID-19 outbreak in 2020 are examples of how these airborne public health problems are becoming more serious internationally [2, 20-22]. Most of the infected people are infected by inhaling bioaerosol particles carrying pathogens [23]. Therefore, it is significant to study the control measures of bioaerosol carrying pathogens.

### 2.1.1 Definition and Composition of Bioaerosols

Bioaerosol refers to a colloidal system composed of microorganisms suspended in the air, which is defined by the American Government Industrial Hygiene Association (ACGIH) as an aerosol particle with a particle size range of 0.1 to 100 μm [1, 24, 25]. These particles include viruses, bacteria, fungi and other microorganisms. For example, the particle size of the tuberculosis bacterium is usually 1 to 4 μm, the particle size of the foot-and-mouth disease virus is generally 10 to 22 nm, and the particle size of the SARS virus is 60 to 200 nm [26, 27]. Bioaerosols are a diverse and complex class of organic aerosols derived from a variety of biological materials, including bacteria, fungi, viruses, detritus, and by-products of biological activity [28, 29]. These by-products may be metabolites, peptidoglycans, endotoxins, mycotoxins, biopolymers, or small molecule compounds.

2.1.2 Transmission Modes of Bioaerosols

The transmission modes of bioaerosol mainly include contact transmission, droplet transmission and air transmission, as shown in Figure 2.1 [29-31]. The World Health Organization divides droplet nuclear transmission (≤5 μm) and droplet transmission (>5 μm) according to the size of the aerosol particle size of 5 μm, and the same pathogen can be transmitted through different modes of transmission [32].

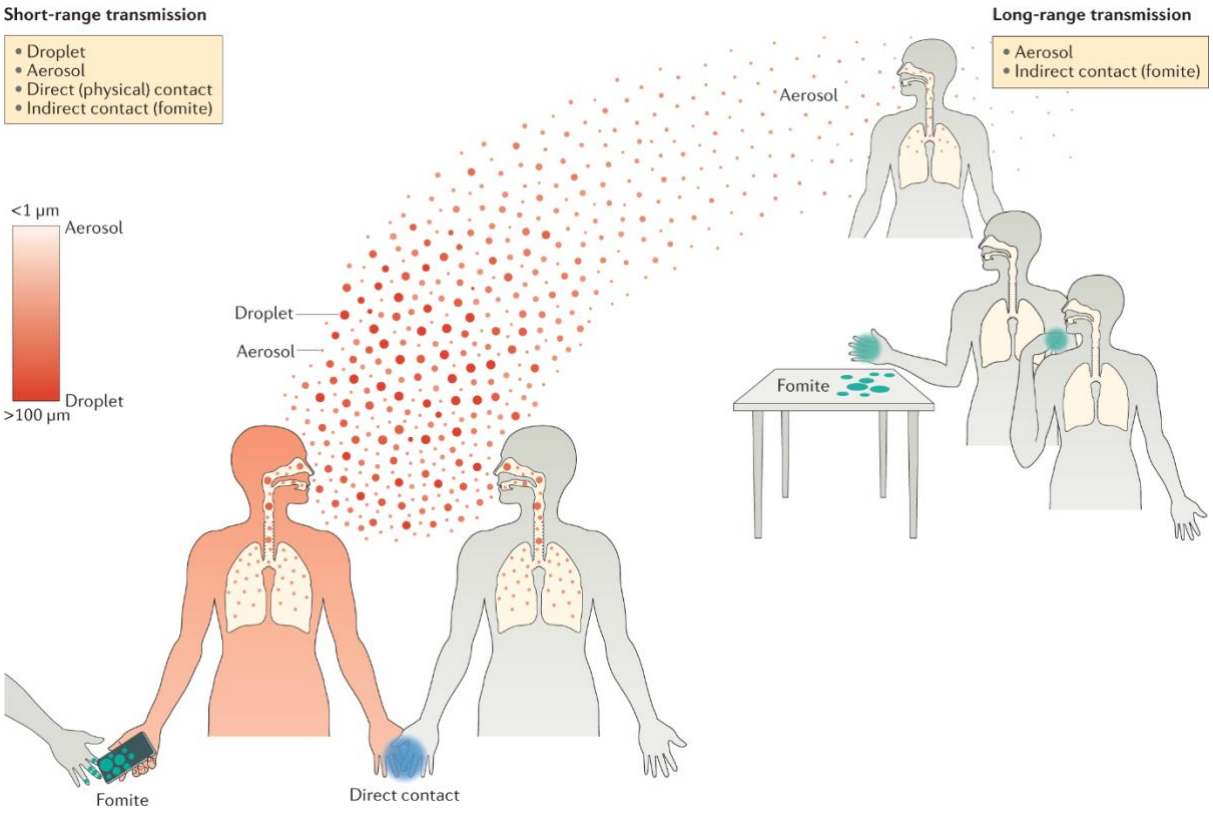


Figure 2.1 Primary mechanisms for the transmission of respiratory pathogens [30].

Contact transmission is mainly through direct human contact, which occurs more often between patients and health care workers, or indirect contact between an intermediate host carrying the pathogen and a susceptible person, such as when people come into contact with someone or

the environment that has been infected with the virus. Large droplet propagation is a form of contact propagation, with large droplet diameters generally >5 μm. Infected patients release many droplets, which deposit pathogens on the conjunctiva of susceptible hosts or on protective equipment such as masks. When the subsequent protective treatment is not appropriate, the pathogen will transfer to the skin of the body, and enter the human body through the mouth, nasal cavity, eye mucosa and other ways, and cause infection.

Droplet transmission is transmitted by droplets with a particle size of >5 μm containing pathogens. When the human body coughs or sneezes, droplets inside the respiratory tract, throat and nasal cavity will be released along with the air flow, and patients with pathogens, the released droplets will contain pathogens, and the droplets will settle on the surrounding objects or be inhaled by others [33, 34]. The particle size of these droplets is relatively large, and the sedimentation rate is fast, and the suspension time in the air is relatively short. Droplets containing pathogens may settle in other people's eyes, nasal passages, and oral mucosa after a period, resulting in susceptible people may be infected, especially for crowded enclosed Spaces, where droplet transmission of infection is higher.

Airborne transmission mainly refers to the transmission of pathogens by droplets with a particle size of <5 μm [35, 36]. Droplet nuclei are potentially infectious bioaerosols remaining in air, which are mainly formed by the evaporation of droplets released by human respiratory activities. The airborne mode has a higher risk than the indoor environmental mode of bioaerosol transmission. Indoor air conditioning and ventilation system determines the space air flow direction, and the air flow organization will strongly affect the propagation trajectory of bioaerosol. Bioaerosol droplets of different sizes are affected by other factors to different degrees during suspension. Large droplets have larger Stokes number (≥1) and are more affected by their own inertia. On the other hand, micrometer-sized droplets, micrometre-sized

droplets with very small Stokes numbers (much less than one) tend to follow the airflow, remain suspended for extended periods, and travel considerable distances, thereby increasing the risk of infecting susceptible individuals [37, 38].

### 2.1.3 Health Issues Associated with Bioaerosols

The health issues caused by bioaerosols depend on the pathogenicity or immunogenicity of the specific microbes and their associated compounds, as well as other factors—such as environmental conditions influencing microbial survival in the air and the dynamics of bioaerosol particles [20, 27, 39]. Diseases associated with bioaerosol exposure fall into two main categories: non-infectious diseases and infectious diseases.

Bioaerosols have been linked to a range of non-infectious diseases, such as hypersensitivity reactions, allergies and asthma [34, 40, 41]. Constant exposure to microorganisms in the air can lead to sensitization and occupational disease [42]. In a variety of occupational settings, workers continue to be diagnosed with hypersensitive pneumonia due to bioaerosol exposure [43, 44]. Microbial allergens and endotoxins (also known as lipopolysaccharides, LPS) produced by gram-negative bacteria are recognized significant health hazards. Research have shown that endotoxins may be a common cause of airway and intestinal inflammation, and can also cause symptoms like diarrhea, fatigue, and nasal irritation, which are prevalent in a variety of occupational settings [45].

Infectious diseases can result from bacteria, fungi, or viruses. When these microorganisms become airborne, they can spread to humans through inhalation. Among bacteria, Legionellosis, tuberculosis, and anthrax pose significant public health concerns due to their high infectivity at low doses. *Legionella pneumophila*, which causes legionellosis, can be spread by aerosol

from contaminated water [46]. Tuberculosis patients can spread droplets carrying *Mycobacterium tuberculosis* through coughing, sneezing and talking [47].

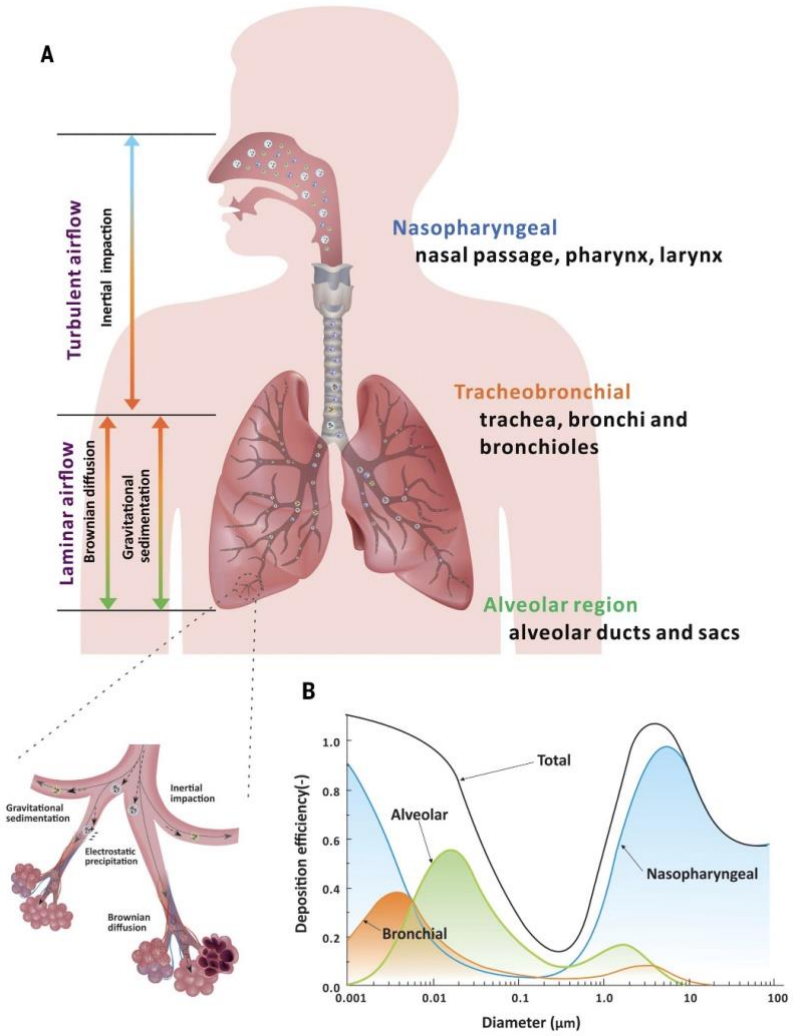


Figure 2.2 Mechanisms of aerosol deposition in the respiratory tract based on particle size [3].

The health effects of bioaerosol on human body include irritation of respiratory system and ocular mucosa, non-specific symptoms such as nausea and infectious diseases. The degree of harm caused by bioaerosols is controlled by several factors, including the way they are released from the body, aerosol concentration and particle size, and environmental physical properties.

After the bioaerosol is released by the human body, it will quickly spread around in the air, mainly through entering the human skin, respiratory tract and digestive tract mucosa and other ways to harm health. Different deposition locations will affect the pathogenesis, large droplets can splash into the eyes or mouth, and deposit in the upper respiratory tract; Small droplets can be inhaled into the lower respiratory tract, or even deeper into the lungs, with a relatively higher degree of harm. For example, respiratory viruses such as swine flu and Ebola virus are inhaled and spread by the human body in the form of droplets. The deposition locations corresponding to different particle sizes of aerosol particles are shown in Figure 2.2 [3].

### 2.1.4 Control Methods for Bioaerosol Transmission

The methods to control the concentration of indoor bioaerosol are divided into three types: control the release source, protect the susceptible population, and cut off the transmission route. One way to control release sources and protect vulnerable people in the public environment is to wear a mask. Some scholars have studied the protective effect of masks on bioaerosols and found that medical masks can reduce the risk of SARS infection to a certain extent, especially for bioaerosols that can be transmitted through air conditioning systems [48]. In addition, wearing masks can also help reduce individual cases of viral respiratory infections, but for infectious diseases such as tuberculosis and measles, surgical masks may not be enough to block bioaerosols, and filter masks are needed to play a role. A recent study showed that N95 masks are more effective than surgical masks in reducing the spread of coronavirus disease, preventing wearers from inhaling or releasing large particles of aerosol droplets to reduce the risk of infection [1, 49].

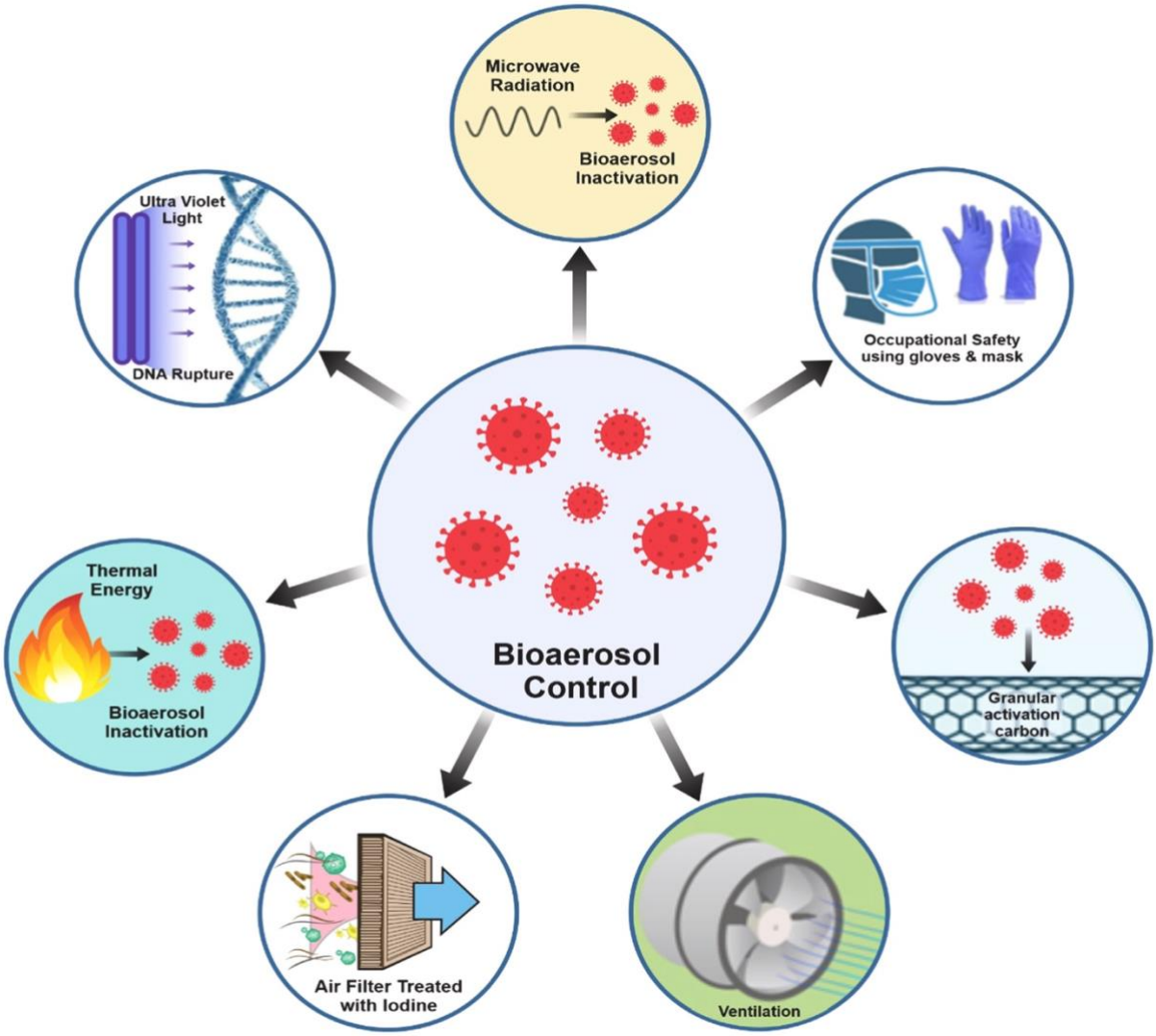


Figure 2.3 Widely used methods for controlling or inactivating bioaerosols [1].

The common methods to cut off transmission routes are ventilation dilution, filtration and dust removal, and disinfection and sterilization, as shown in Figure 2.3. First, ventilation can not only meet the comfort requirements of indoor personnel, but also reduce the concentration of bioaerosols in the air, reduce the spread of diseases and improve air quality. Increasing fresh air volume is the most used and effective method to control indoor bioaerosols. Second, filtration is currently the most conventional method of purifying air, and it is also the method used to control indoor microbial concentration in clean rooms and operating rooms in hospitals.

Finally, air disinfection not only effectively controls the source of contamination but also reduces the risk of cross-infection, making it an effective method for blocking transmission routes [50]. The principle and effect of different disinfection and sterilization methods are different, such as chemical disinfection, ultraviolet disinfection, photocatalytic disinfection, plasma disinfection, etc.

Although the existing bioaerosol transmission control methods are effective to a certain extent, there are still many shortcomings. First, in terms of source control, ordinary medical masks or surgical masks are difficult to completely block the spread of highly contagious diseases such as tuberculosis and measles, and although N95 masks have better protective performance, long-term wear will cause respiratory discomfort, and the filtration effect will decrease with the use of time. In terms of cutting off transmission routes, ventilation dilution, although a common method to reduce indoor bioaerosol concentrations, may not fully meet the needs in high-density human environments. Traditional air filtration technology has limited capture efficiency for small particle size aerosols (such as virus carrier particles), and efficient filtration equipment has high cost and high energy consumption, which is difficult to promote in a wide range of scenarios. Disinfection and sterilization technologies also have limitations, such as chemical disinfectants may cause secondary hazards to the environment and human health, and ultraviolet disinfection has limited effects on areas not covered by light, and photocatalysis and plasma technology may be difficult to maintain stability in practical applications.

In view of the above deficiencies, it is highly desirable to develop novel bactericidal materials. Novel bactericidal materials can exert efficient sterilization through multiple mechanisms: metal nanoparticles (such as silver, copper, zinc oxides) destroy cell membranes or generate reactive oxygen species, thus killing microorganisms; photocatalytic materials such as titanium dioxide produce bactericidal effects sustainably in ultraviolet or visible light. New materials

can provide broad protection with sustainable performance for a wide-spectrum, antimicrobial effect against bacteria, fungi, and viruses. This material also has the advantage of incorporation into current technologies that include high-efficiency filters, air purifiers, and masks by adding additional functionality to said devices, like antibacterial properties, waterproof, and dustproof, that further increase their utility.

## 2.2 Microorganisms and Current Antimicrobial Strategies

Microorganisms are widely distributed in nature and human life, including those that are highly beneficial to human health and the environment, as well as those that may cause diseases. Since the development and wide use of antibiotics and other chemical antimicrobials, antimicrobial strategies have been playing a very important role in medical treatments, food safety, and public health. However, with the improper use of antibiotics, resistance to drugs gradually appeared, and the drug-resistant bacterium has been a big challenge to traditional treatments [51]. To solve this problem, the current strategy against microbes does not restrict itself to antibiotic medicines but embraces all varieties of chemical anti-microbes and physical methods such as ultraviolet disinfection and high-temperature sterilization, to which the application of nanotechnology is also added. In addition, new nano-antibacterial materials and innovative technologies are developed to overcome these classic limitations. These strategies, taken together, have great importance not only in terms of controlling the spread of microbial infection-associated diseases and disorders but also for the safeguarding of future public health on sound scientific footing.

### 2.2.1 Microorganisms and Our Life

Microbes exist in every corner of nature, and human life is no exception. Microbes co-evolved with humans to live inside and outside the human body, forming host-related structures known as the "human microbiome." The number of microbes is so large, about ten times that of human cells, that they are considered symbiotic [52-54]. The human microbiome refers to the entire genome of microorganisms living in or on the human body. There are trillions of microorganisms in the human body, which are important in maintaining the normal function of the body's metabolism, physiology and immune system. The microorganisms that people come into contact with in daily life not only include beneficial microorganisms, but also include many harmful microorganisms, which may cause a variety of diseases. Animals are home to thousands of microbes, some of which are harmful and some of which are beneficial. Most bacteria are found in the gastrointestinal tract and account for about 70% of the body's microbial load (especially the large intestine), such as *Bacillus* and *Lactobacillus* [55, 56]. At the same time, many pathogens are present, such as *Mycobacterium tuberculosis, Corynebacterium, Streptococcus and Shigella*, which can become airborne agents of disease. So far, tuberculosis caused by *Mycobacterium tuberculosis* is still one of the most serious infectious diseases, and the incidence is still on the rise. Some common diseases caused by bacteria have been summarized, as shown in Table 2.1.

In addition to the large-scale infectious disease events in history, many common bacterial pathogens also appear in modern daily life, which affect people's normal life all the time. These pathogens that exist in every corner of the living environment threaten people's life, health, and safety, and have a huge impact on the environment, society and economy. Therefore, it is of great significance to raise people's awareness of safety prevention of infectious diseases and actively seek and develop new harmless pathogen inactivation methods and products.

Table 2.1 Common human pathogenic bacteria and related diseases.

| Pathogenic bacteria | Classification | Infectious diseases |
|---|---|---|
| *Mycobacterium tuberculosis* | Gram-positive bacteria | Tuberculosis |
| *Diphtheria* | Gram-positive bacteria | Diphtheria |
| *Staphylococcus aureus* | Gram-positive bacteria | Pneumonia |
| *Escherichia coli* | Gram-negative bacteria | Urethritis |
| *Shigella* | Gram-negative bacteria | Dysentery |
| *Pseudomonas aeruginosa* | Gram-negative bacteria | Uremia |
| *Proteus* | Gram-negative bacteria | Urinary tract infection |
| *Streptococcus* | Gram-positive bacteria | Erysipelas and acute cellulitis |

*E. coli* and *S. aureus* are both highly pathogenic to humans and other animals, and as representatives of Gram-negative and Gram-positive bacteria, both bacteria cause certain damage to human surface skin and internal organs. Therefore, the selection of these two bacteria as the target bacteria to study the antibacterial properties of the material has certain representative significance. (1) *E. coli*, a Gram-negative bacterium, was discovered in 1885. *E. coli* bacteria are covered with flagellates, can move, and usually reside in the intestines of humans and animals. *E. coli* O157:H7 can cause bloody diarrhea and can also cause severe uremic syndrome [57, 58]. If the immune system of the organism is weakened, *E. coli* can migrate to the urethra, gallbladder, and appendix, causing local or, in severe cases, systemic infection [59]. *E. coli* is mainly transmitted through contaminated food and water, so “fecal coliform” is usually monitored during food safety inspection and contaminated water treatment [60]. (2) *S. aureus*. Unlike *E. coli*, there is no flagella on the surface of the bacteria,

and the outer wall of the bacteria cells does not contain LPS [61]. *S. aureus*, a representative of Gram-positive bacteria, ranks second only to *E. coli* in causing foodborne diseases and is widely found in animal intestines, skin, air, water, and dust [62]. The infection of *S. aureus* has been reported to cause soft tissue and skin infections and even necrotic pneumonia [63].

### 2.2.2 Antibiotics and Antibacterial Resistance

Antimicrobial strategies can be divided into chemical and physical methods, each with its own unique means of inhibiting or destroying microorganisms. Chemical antimicrobials are substances or compounds that inhibit or kill microorganisms. These antimicrobials can be synthetic or naturally sourced and are widely used in areas such as healthcare, food preservation and water treatment. Antibiotics, once considered one of the greatest drugs of the 20th century, are the best solution to the problem of bacterial infections [64-66]. However, due to the misuse and overuse of antibiotics in the prevention and treatment of infections in humans, animals and plants, pathogenic microorganisms have gradually evolved protective mechanisms to circumvent the toxicity of antibiotics [67]. This phenomenon is called drug resistance.

Drug resistance is seen as a hidden global epidemic. The rapid spread of multidrug-resistant and pandrug-resistant bacteria (often referred to as “superbugs”) makes certain infectious diseases impossible to treat effectively with existing antibiotics [68-72]. According to statistics, about 700,000 people worldwide die every year from bacterial infections caused by antibiotic resistance, and this number is expected to increase to 10 million by 2050. More worryingly, because of biodiversity, different populations can act as “hosts” for resistant bacteria for long periods of time, co-existing with antibiotics, further exacerbating the problem.

The formation of resistance is mainly influenced by two factors: first, antibacterial agents or antibiotics, which destroy susceptible microorganisms at the same time, but also selectively promote the survival of resistant strains; The second is the resistance genes inside microorganisms, which are more easily retained and spread under the pressure of antimicrobials. When these two factors intersect in a particular environment or host, drug resistance can cause clinical problems. Under constant antimicrobial pressure, resistant genes and host bacteria proliferate and spread, not only exacerbating the problem of resistance, but also allowing it to spread to new hosts and regions.

Currently, antibiotics have been divided into more than 15 different classes, each targeting key physiological or metabolic processes in bacterial cells [73, 74]. However, no antibiotic can completely avoid the development of resistance mechanisms. Millions of kilograms of antimicrobial substances are utilized globally every year in humans, animals and agriculture, and this widespread use on the one hand eliminates susceptible strains, on the other hand promotes the survival of resistant strains, further exacerbating the resistance crisis.

Mechanism of resistance formation. The formation and spread of resistance genes are very dynamic. With mobile genetic elements, bacteria can exchange resistance genes in different taxonomic and ecological contexts (Figure 2.4) [73]. For example, some transposons contain integrons with complex structures that can integrate multiple antibiotic resistance genes and other gene boxes and achieve unified expression through a single promoter. Take the tetracycline resistance gene tet(M), which is usually located on transposon Tn*916* and has been found to be widely present in different bacteria and environments. In addition, resistance genes can also be spread through transformation. In this process, bacteria acquire chromosomal resistance genes by absorbing DNA released by other microorganisms, such as penicillin-resistant *Streptococcus pneumoniae*. A similar mechanism also involves the production of

drug-resistant helicases through mutations that make *Streptococcus pneumoniae* resistant to quinolones. Although the resistance gene is located on the bacteria's chromosomes, this does not prevent its spread, as the bacteria's high mobility allows it to spread easily between people and countries.

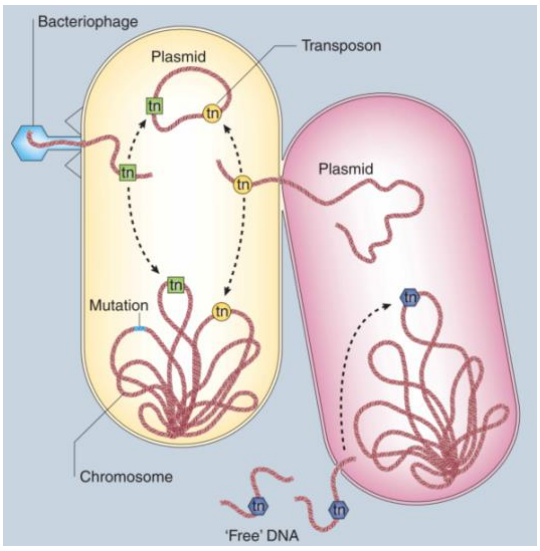


Figure 2.4 The mechanism underlying bacterial drug resistance [73].

Typically, these resistance genes target specific classes of antibiotics, but multiple resistance genes can accumulate in a single microbe, each conferring resistance to a different drug. Moreover, as shown in Figure 2.5, the diversity of resistance mechanisms is matched by the complexity of the antibiotics themselves, further increasing the difficulty of tackling resistance.

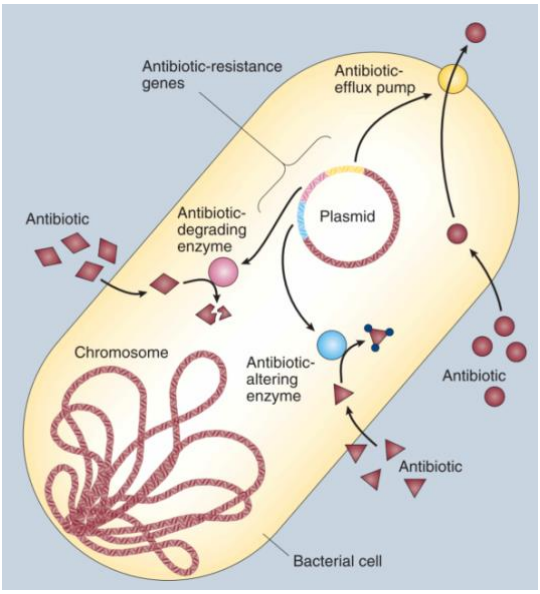


Figure 2.5 The biological mechanisms of resistance [73].

### 2.2.3 Other Antimicrobial Strategies

In addition to antibiotics, there are a variety of chemicals that can effectively kill or damage bacteria [75-78], including phenols (such as phenol, cresol, hexachlorophenol, pine oil, etc.), alcohols (such as ethanol, isopropyl alcohol, etc.), halogens (such as chlorine, iodine, bromine, common antimicrobials include sodium hypochlorite and iodine tinctum), heavy metals (such as silver, copper, mercury, zinc, etc.). Common antimicrobials include silver nitrate and mercurous chloride, surfactants (such as cationic quaternary ammonium salts, anionic sulfates, and sulfonates), acids (such as acetic acid, benzoic acid, propionic acid, often used in food preservation), bases (such as ammonia, sodium hydroxide, and sodium hydroxide). Commonly used in detergents and degreasing agents), oxidants (e.g., hydrogen peroxide, ozone, hypochlorous acid), amides (e.g., beta-lactam antimicrobials), and esters (e.g., monoglycerides). At the same time, physical antimicrobial strategies are also widely used to eliminate or inhibit the growth of microorganisms [76, 78].

Physical methods are generally more environmentally friendly and non-toxic than chemical antimicrobials [79, 80]. These strategies can be used alone or in combination to address challenges in areas such as infection control, food safety and public health. Common physical antimicrobial methods include heat treatment (such as boiling, autoclaving, dry heat or pasteurization), which sterilizes objects and surfaces by heating; Cold treatment, slowing or inhibiting the growth of microorganisms by refrigeration or freezing; Filtration, the physical removal of microorganisms from liquids or air using a filter with a pore size smaller than the microorganism, which is widely used in water treatment, air purification, and sterilization of heat-sensitive materials; Ultraviolet (UV) radiation inactivates microorganisms by damaging their DNA and RNA, and is commonly used to sterilize air, water, and surfaces [81]; Ionizing radiation, inactivation of surface microorganisms by gamma rays or high-energy electrons or sterilization of heat-sensitive materials, is commonly utilized in the food industry and sterilization of medical equipment [82, 83]. These chemical and physical antimicrobial methods complement each other and provide a variety of effective means for the control of microbial infection [84-88].

## 2.3 Contact-killing Bacteria Technologies

Contact sterilization technology realizes antibacterial effect through direct contact with the surface, such as mechanical antibacterial, silver nanoparticle antibacterial and polycationic antibacterial [89-91]. Mechanical antibacterial uses nanostructures to pierce or stretch bacterial cell membranes through physical forces, leading to their rupture and death, with non-toxic and anti-drug characteristics [92, 93]. Silver nanoparticles achieve efficient broad-spectrum sterilization by releasing silver ions or reactive oxygen species (ROS) to destroy bacterial cell membranes, DNA and proteins [94-97]. Polycationic antibacterial relies on electrostatic action to destroy the structure of bacterial membrane and inhibit its growth [98-103]. These three

technologies combine physical and chemical mechanisms to provide diverse options for antimicrobial materials.

### 2.3.1 Mechano-Bactericidal of Nanostructured Surfaces

#### 2.3.1.1 Bactericidal Properties of Cicada Wings

The remarkable characteristics of cicadas, such as non-wettability and anti-reflection (as shown in Figure 2.6), have attracted wide attention from the scientific community. These unique properties are closely related to the ordered arrangement of densely distributed "nano-protrusions" on the wing surface, a feature found in a wide variety of insects [104, 105]. Periodic nanocolumn patterns on the surface of cicada wings have been identified by various methods [106-108]. These nanocolumns exhibit different spatial arrangements, heights and diameters in different insect species, giving insect wings superior self-cleaning and superhydrophobicity [109-111].

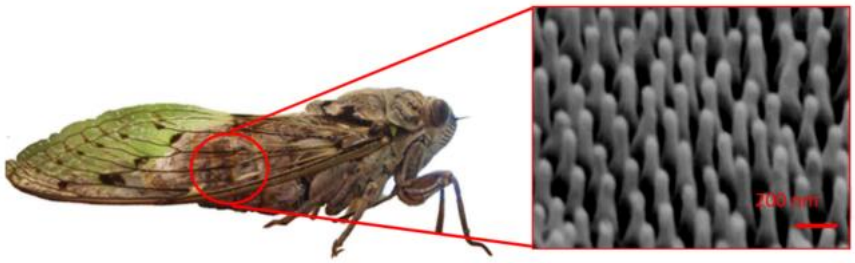


Figure 2.6 The SEM image reveals a hexagonal arrangement of densely clustered nanopillars present on the surface of cicada wings [112].

In recent studies, cicadas have demonstrated their ability to kill bacteria, especially gram-negative bacteria [113]. Studies have shown that the cicadas of the *Psaltoda claripennis* species are particularly effective at killing bacteria. In addition, studies of other insects have found that their wings have nanotopologies that can physically contact and destroy gram-positive and gram-negative cells. More interestingly, the bactericidal activity of these insects' wings is mainly due to their physical surface structure [107, 114, 115]. Changes in surface chemistry, such as gilding, did not affect its bactericidal effectiveness, highlighting the importance of physical topology in its antimicrobial properties.

2.3.1.2 Biomimetic Antibiofouling and Mechano-Bactericidal Nanostructured Surfaces

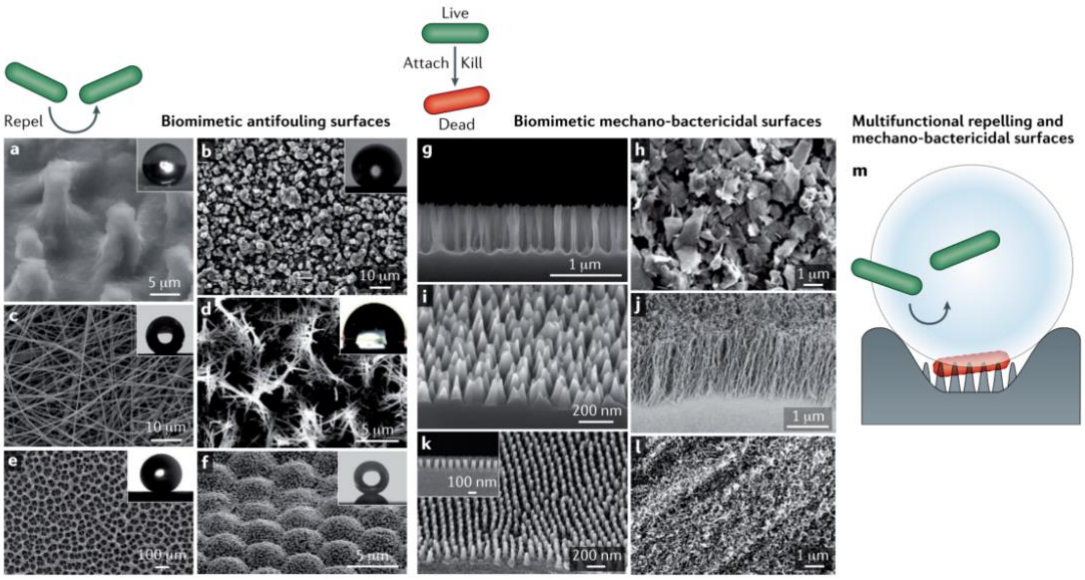


Figure 2.7 Analyzing the differences between biomimetic antibiofouling and mechano-bactericidal nanostructured surfaces [51].

Recent research has focused on material with anti-fouling properties (as shown in Figure 2.7a-f) or bactericidal properties (as shown in Figure 2.7g-l) by changing its topology. This approach

aims to improve the integration and function of mammalian cells, while inhibiting bacterial attachment, or rendering the substrate mechano-bactericidal (as shown in Figure 2.7m). Creating a bactericidal micro-nano topology through the structure design of materials can provide a safe and sustainable solution to prevent surface microbial contamination. These surfaces exert a mechanical force on the bacterial cell membrane upon contact, causing the cell to rupture and die (as shown in Figure 2.8) [112, 116, 117].

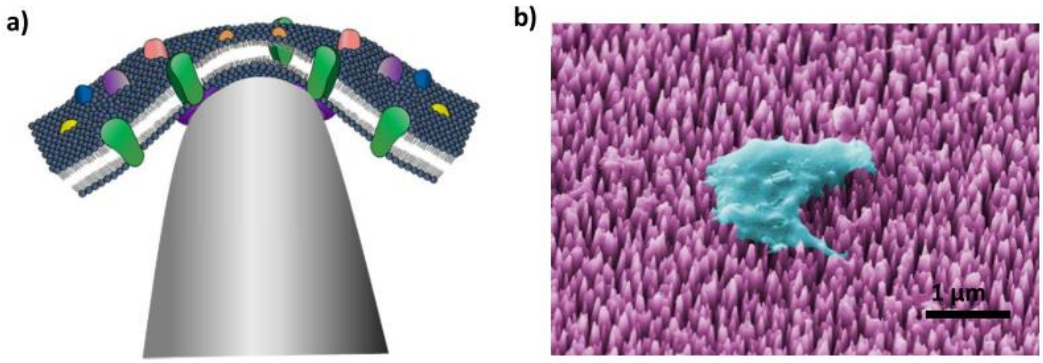


Figure 2.8 (a) Diagram illustrating the absorption of a bacterial membrane onto a nanopillar. (b) The subsequent rupturing of the cell is followed by noticeable membrane deformation, as depicted in the SEM image [112].

2.3.1.3 Mechanisms of Mechano-Bactericidal

Mechano-bactericidal actions are an effective way to kill bacteria, especially in situations where chemical disinfectants may not be effective or preferred [116, 118, 119]. However, the response of different types of bacteria to mechanical stress may vary, and the effectiveness of the mechanical sterilization process may depend on the type of bacteria, the concentration of bacteria, and the specific mechanical method used [117, 120].

The breakthrough discovery of cicada wings showed that their nanocolumns were able to damage bacterial cells, greatly advancing the application of bionics to the design of mechanically inactivated bacterial surfaces with nanotopologies [121-123]. After the first observation of cicada wing bactericidal phenomenon, many studies began to explore the internal bactericidal mechanism of the multifunctional surface of insect wings [124, 125]. However, this bactericidal activity is selective and only shows significant effects against Gram-negative bacteria. A key factor in the bactericidal efficacy of natural and man-made nanostructures is the rigidity of bacterial cells [126, 127]. When the integrity of the bacteria is significantly weakened and causes deformation, the cell is eventually destroyed. The shape stability of bacterial cells depends on turgor pressure, which results from the significant osmotic pressure difference between the inner and outer layers of the bacteria. The peptidoglycan layer in the cell wall of Gram-negative bacteria is thinner, and its turgor pressure is lower than that of Gram-positive bacteria. When bacterial cells encounter the surface of the nanostructure, the nanocolumns create indentations on the cell wall structure, placing a huge mechanical burden on it. This pressure triggers an increase in turgor pressure within the cell, causing the cell wall to stiffen over time.

There are two main types of mechanical bactericidal action on the surface of nanostructures [128, 129]: (1) Bacterial cell stretching caused by nanocolumns of different shapes and sizes (Figure 2.9a, b); (2) Cracking of bacterial cell membranes through sharp nanoedges (such as graphene nanosheets) (as shown in Figure 2.9c). With the advancement of nanomanufacturing technology, the ability to accurately control the surface size at the nanoscale has been significantly improved, greatly improving the design capability of new physical sterilization surfaces. Currently, various bactericidal nanopatterns can be integrated into a variety of surfaces, including soft materials such as polymers, fatty acids, and carbon-

based materials, as well as hard materials such as metals and alloys [5]. However, exploring the specific mechanisms that trigger the physical destruction of bacteria remains complex, largely due to the diversity and complexity of nanopatterns.

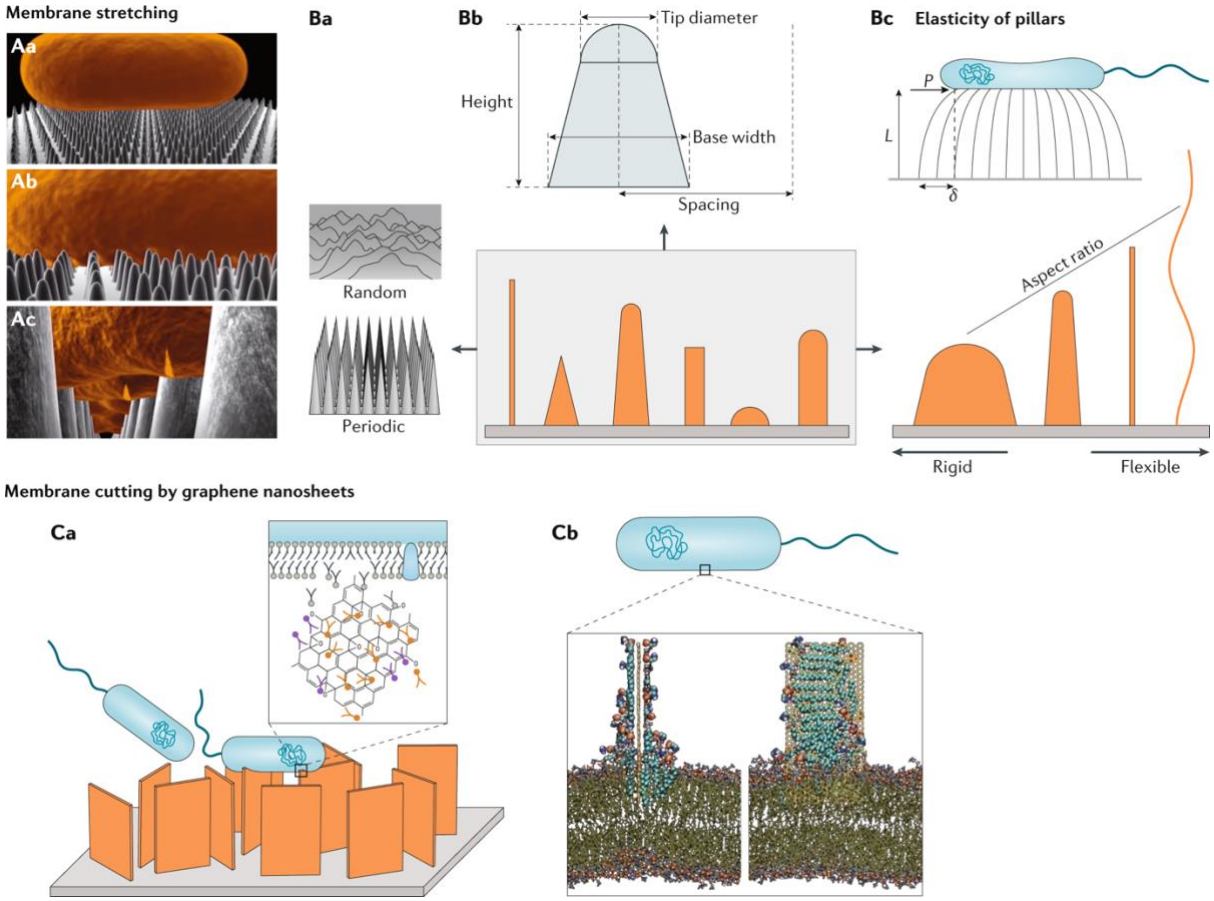


Figure 2.9 Two categories of nanostructured surfaces' bactericidal activity through mechanical means [51].

Although numerous studies have investigated the relationship between nanopattern surface structure and bactericidal activity, the effect of nanoscale topology on bacterial attachment and survival is still a controversial topic [130, 131]. The insights gained from these findings open up new possibilities for designing innovative antimicrobial surfaces and materials. By

emulating the highly effective bacterial inactivation mechanisms found in nature, scientists and engineers are expected to develop advanced solutions to curb the spread of harmful bacteria and reduce the risk of infection, thereby promoting better public health [16, 132, 133].

#### 2.3.1.4 Different Mechano-Bactericidal Surfaces and Preparation Methods

Table 2.2 Nanostructured surfaces' mechanism of bactericidal activity [51].

| Material | Nanopattern | Dimensions (height; diameter; density; period) | Wettability | Bactericidal activity[a] |
|---|---|---|---|---|
| *Mechano-bactericidal rigid nanostructures* | | | | |
| Black silicon | Nanocone | 280 nm; 62 nm; 86 $\mu m^{-2}$; 62 nm | Hydrophilic, WCA = 8° | 85% |
| | Nanopillar | NA; 150–200 nm; NA; 100–250 nm | NA | ~87% after 3 h, ~99% after 6 h |
| Titania | Nanowire | 3,000 nm; 100 nm; NA; NA | NA | 5% |
| | Nanopattern array | NA; 40 nm; NA; NA | Hydrophilic, WCA = 73° | 20% |
| | Nanopillar | 1,000 nm; 80 nm; NA; random | Hydrophilic | 76% |
| | Nanocolumn | 478 nm; NA; NA; 158 nm | Hydrophilic, WCA = 41° | 0% |
| Gold | Nanopillars | 100 nm; 50 nm; NA; NA | NA | ~99% |
| | Nanorings | 100 nm; 200 nm; NA; NA | | |
| Zeolitic imidazole framework | Nanodaggers | 1,000 nm; 2,000 nm; NA; <2,000 nm | NA | 99% |
| Polymer | Nanopillars | 250 nm; 80 nm; 60 $\mu m^{-2}$; 130 nm | NA | 31% |
| | | 200 nm; 80 nm; 68 $\mu m^{-2}$; 130 nm | | 23% |
| | | 400 nm; 80 nm; 40 $\mu m^{-2}$; 170 nm | | 100% |
| | | 200 nm; 80 nm; 40 $\mu m^{-2}$; 170 nm | | 98% |
| | | 300 nm; 80 nm; 20 $\mu m^{-2}$; 300 nm | | 26% |
| | | 150 nm; 80 nm; 20 $\mu m^{-2}$; 300 nm | | 31% |
| *Mechano-bactericidal flexible nanostructures* | | | | |
| Titania | Nanospears | 4,000 nm; 100 nm, 50 nm ($D_T$); NA; 3,000–5,000 nm | Hydrophilic, WCA = 0° | 47% |
| | Nanospike | 2,000 nm; 10–30 nm; NA; 2000 nm | Hydrophilic, WCA = 0° | 10-fold decrease in viable cells |
| Black silicon | Nanograss | 4,000 nm; 220 nm, 10–20 nm ($D_T$); NA; NA | Hydrophobic, WCA = 154° | 86% |
| Carbon nanotubes | Vertically aligned nanotube forest | 1,000 nm; 10 nm; $3 \times 10^{10}$–$5 \times 10^{10}$ $cm^{-2}$; <10 nm | Hydrophobic, WCA = 149° | 89.6% |
| | | 30,000 nm; 10 nm; $3 \times 10^{10}$–$5 \times 10^{10}$ $cm^{-2}$; <10 nm | Hydrophobic, WCA = 149° | 18% |
| | | 20,000 nm; 10 nm; $3 \times 10^{10}$–$5 \times 10^{10}$ $cm^{-2}$; <10 nm | NA | 93% |
| *Mechano-bactericidal nano-edges* | | | | |
| Graphene nanosheets | Nanoblades | Horizontal length 79.7 nm; 5 nm; 10.8 $\mu m^{-2}$; NA | NA | 77.1% |

Over the past decade, a range of physically antibacterial surfaces have emerged through a variety of artificial methods that mimic nanostructured surfaces found in nature (Table 2.2). At present, the mainstream manufacturing methods of physical antibacterial surfaces can be roughly divided into the following categories: top-down multiple etching technology, bottom-up chemical synthesis technology, surface topological coating and modification technology,

and other micro-nano surface construction technology combined with the above methods [134-138].

The research on the bionic mechano-bactericidal surface construction method not only helps to deeply understand the mechanism of surface growth and formation, but also promotes the integration of antibacterial materials in specific applications, so as to optimize the selection of construction methods. This further promotes the wide application of mechano-bactericidal surfaces. Therefore, this research field has received great attention in recent years, and both academia and industry are constantly promoting its development and progress.

2.3.1.5 Further Techniques to Improve the Antibacterial Property

Nanostructured surfaces are found in a variety of materials and have been shown to have excellent bactericidal properties, largely due to their high surface-area-to-volume ratio and unique surface topology [139, 140]. In order to further improve the bactericidal performance of these nanostructures, the following modification and implantation techniques can be used: by introducing specific functional groups or molecules (such as antimicrobial peptides, metal nanoparticles such as silver or copper, organic compounds such as quaternary ammonium salts) on the surface of the nanostructures for surface functionalization, the bactericidal performance can be enhanced; By increasing the surface roughness at the nanoscale, such as modifying the surface topology by etching, photolithography or anodic oxidation, the bacterial cell membrane can be physically damaged effectively, thus improving the bactericidal activity; Embedding antimicrobials in the surface of nanostructures and achieving continuous release (e.g. through electrospinning, sol-gel or layer assembly technologies) can provide long-lasting antibacterial effects; Combining multiple strategies, such as introducing antimicrobials and changing surface topologies or chemical properties, can create synergies that further enhance

antimicrobial activity; The application of nanostructured coatings to the surface of the implant, through techniques such as dipping, spraying or electrophoretic deposition, can effectively prevent bacterial attachment and biofilm formation, thereby reducing the risk of infection associated with the implant [51, 141-145]. By using these technologies, the antimicrobial properties of nanostructured surfaces can be significantly improved, making applications in medical devices, water treatment and food packaging more efficient. In addition, current mechanical bactericidal strategies are mainly applied in solution environments, but their effectiveness against bioaerosols is equally critical. Bioaerosols are made up of airborne particles containing bacteria, viruses and fungi that can pose a significant health risk. Therefore, the development of bactericidal or inactivation strategies for bioaerosols is critical. By studying and optimizing these strategies to inactivate bioaerosols, mechanized surfaces can be used to effectively control bacterial contamination in the air, thereby improving air quality and promoting public health.

### 2.3.2 Silver Nanoparticle and Polycation Antibacterial

In recent years, silver nanoparticles (Ag NPs) have become the focus of scientific research due to their large specific surface area, broad-spectrum antimicrobial properties and low toxicity. Ag NPs is a nanoscale silver particle prepared by physical or chemical methods with an external size of less than 100 nm. With its excellent broad-spectrum antimicrobial activity, Ag NPs has been widely used in all areas of life and is considered a strong candidate for a new generation of antimicrobials. Polycations are a class of polymers with multiple positively charged groups, because of their unique structure and biological activity in the field of antibacterial attention. Its antibacterial mechanism mainly relies on the strong electrostatic interaction between cationic groups (such as quaternary ammonium salts, guanidine, imidazolyl, etc.) and the negative charge of bacterial cell membranes, thereby destroying the integrity of cell membranes

and realizing efficient sterilization. What silver nanoparticles and polycations have in common in antimicrobial properties is that their chemical mechanisms play a central role. Ag NPs releases silver ions, reacts with bacterial cell membrane and protein, destroys cell membrane structure, inhibits enzyme activity, and eventually leads to bacterial death. However, polycations destroy the stability of the membrane chemically and inhibit the survival of bacteria through the electrostatic interaction between the cation and the bacterial membrane. Both of them destroy the basic structure and function of bacteria by chemical mechanism, showing broad spectrum and efficient antibacterial properties, and have broad application potential in medical, daily life and industrial applications.

## 2.4 Antibacterial Textiles

Antibacterial textiles play an important role in modern society and are widely used in fields such as medical treatment, food packaging, home textiles and public places [146]. Through advanced surface modification technologies such as nanotechnology, microencapsulation and electrospinning, they give textiles multi-functional properties such as waterproof, flame retardant and antibacterial, effectively controlling the spread of microorganisms and the risk of infection. At the same time, antibacterial textiles also have the potential for environmental protection, such as for biodegradable food packaging and reducing plastic pollution. These innovations provide important support for health protection and sustainable development.

### 2.4.1 The Origins and Modern Applications of Antimicrobial Fabrics

Textiles are ubiquitous and an indispensable part of human society. However, textiles can carry certain microbes, a phenomenon that has become known in recent years as “clothing microbiology,” which focuses on the interaction between textiles and the human skin

microbiome. As early as ancient times, humans have tried to give antibacterial function to textiles through natural antibacterial agents. For example, the Egyptians treated cloth with a coating of spices and herbs, which was used to make mummification shrouds; The Chinese use Bamboo fibers that contain the anti-bacterial compound bamboo-kun to build house structures. Studies have shown that bamboo fiber has antibacterial and antifungal properties because of its 2-6-dimethoxy-P-benzoquinone and bamboo.

In modern society, antibacterial textiles play an important role in hospitals and other high microbial risk environments. For example, clothing worn by patients and health care workers can harbor many microorganisms that can easily spread infections from person to person. Therefore, antibacterial textiles have broad commercial prospects in controlling the spread of microorganisms. According to functional properties, antibacterial textiles can be divided into antibacterial, antifungal and antiviral three categories, and some can even resist bacteria, fungi and viruses at the same time. In addition, certain chemical antimicrobials are collectively referred to as antimicrobials because of their broad spectrum properties. In public places such as hotels, restaurants and trains, the demand for antibacterial fabrics is particularly significant. For example, towels, curtains and carpets used to absorb fluids can be a source of infection. Microorganisms in textiles may not only spread disease, but may also cause odors, allergic reactions, fading, and degradation of textiles. Although regular cleaning is an effective way to reduce microbial load, it is difficult to achieve in scenarios such as hospitals where continuous work shifts are required. Therefore, the development of antibacterial textiles has become an important means to reduce microbial infection. This type of textile is also suitable for workers in hygiene-related jobs or in the sewage treatment industry to reduce their risk of infection.

### 2.4.2 Bacterial Growth Dynamics in Textile Fabrics

Understanding the growth mechanism of bacteria in textiles is the key to effectively inhibit their reproduction. Typically, textiles, clothing, and garments are made from synthetic or natural fibers that are mainly made up of polymers. Polymers can be made of chemical monomers or natural monomers depending on the type of fiber. These polymers provide not only a substrate for the airborne bacteria to attach to, but also nutrients for them to grow and form colonies [147]. Common bacteria that affect textiles include *Flavobacterium*, *Micrococcus* and *Pseudomonas*, of which *Pseudomonas aeruginosa* is particularly prominent [148-150].

These fibers absorb moisture from sweat and the atmosphere in general, providing a wet, ideal environment that aids bacterial growth. Bacteria consume polymers for nutrition, and during their growth process, they degrade the polymers back into monomers while producing bacterial metabolic products. These metabolites further contribute to the degradation of fiber polymers. The combined effects of the bacteria and their metabolites accelerate the breakdown of the fibres' polymers, potentially leading to fabric damage and the formation of a large bacterial colony. If pathogenic bacteria are involved in this process, it can result in irritation to human skin or trigger infections. Notably, natural fibers are more vulnerable to bacterial attack compared to synthetic fibers. This is because natural fibers provide bacteria with a rich source of carbohydrates from their polymers, while the base of most chemical-based polymers contains substances that are typically toxic to bacteria, reducing their likelihood of growth.

### 2.4.3 The Preparation and Modification Techniques

The preparation of antibacterial fabrics is of great significance, and the main preparation methods include fiber spinning addition, modification based on nanotechnology, chemical finishing and surface functionalization. These preparation technologies provide a variety of solutions for the development of highly efficient and durable antibacterial textiles to meet a wide range of needs in medical, industrial and everyday life.

Embedding antibacterial agents in the fiber spinning process can not only achieve a uniform distribution of antibacterial properties, but also significantly improve the durability and stability of the fiber. For example, nanofibers prepared using electrospinning technology have been widely used in many fields, including biomedicine (such as tissue-engineered stents, drug delivery, wound dressings, and medical implants), filtration, protective textiles, and batteries. An important function of nanofibers is to prevent the growth or infection of bacteria. Nanofibers are usually prepared using a strategy of adding antibacterial agents to the fibers, as shown in Figure 2.10, which can be achieved by: evenly mixing antibacterial agents into a polymer solution prior to electrospinning; The antibacterial agent was wrapped in the fiber core by coaxial electrospinning technology. The antibacterial agent is encapsulated in nanostructures and then dispersed into electrospinning solution; After electrospinning, the fiber is post-treated to convert the precursor substance into its active form; Or the antibacterial agent is directly attached to the fiber surface.

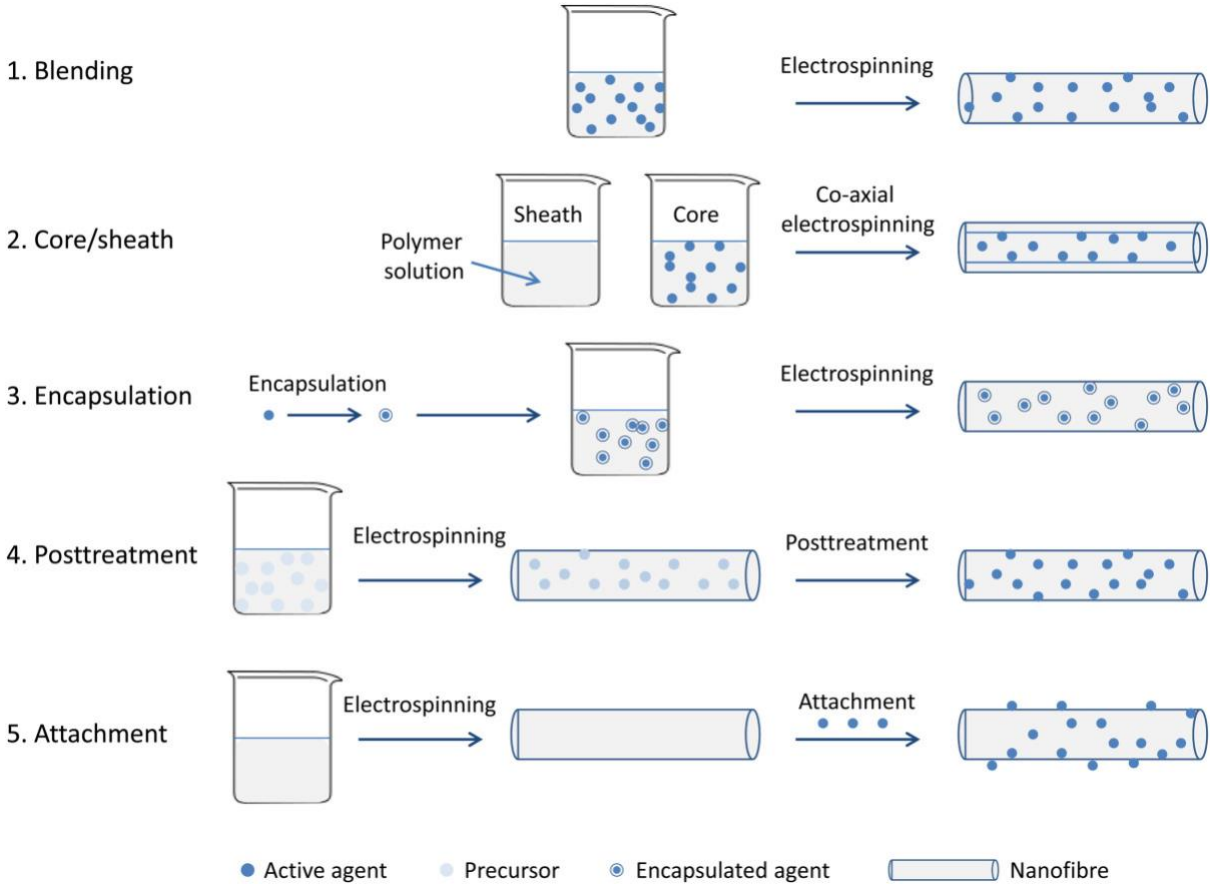


Figure 2.10 Different approaches for integrating biocides into electrospun nanofibers [151].

At present, a variety of well-known antimicrobials are widely used, including antibiotics, triclosan, chlorhexidine, quaternary ammonium compounds (QAC), biguanides, silver nanoparticles and metal oxide nanoparticles. These strategies provide a variety of technical support for the development of highly effective antibacterial textiles, helping to meet the needs of multiple antibacterial applications.

Modification based on nanotechnology has become a key means of endowing textiles with antimicrobial properties [152]. Through the introduction of nanomaterials (such as carbon

quantum dots, graphene, metal-organic frameworks (MOFs), nano-enzymes, etc.), the antibacterial properties of textiles can be significantly improved. MOFs are a class of porous crystalline solids composed of inorganic nodes and organic linkers with high structural and chemical tunability. These materials have been successfully integrated into a variety of wearable fibers to form MOF-based fiber composites to meet the needs of diverse applications. The integration of broad-spectrum bactericidal and detoxification activities into active textiles is an urgent need to address multiple threats and protect communities around the world. Cheung et al. used porous UiO-66-$NH_2$, a stable zirconium based MOF with a -$NH_2$ functional group, as a renewable carrier to introduce N-chlorine biocides into textiles (Figure 2.11) [153]. Through a simple commercial bleaching solution soaking process, the active chlorine atoms bind to the amine functionalized ligand in the frame to form the chloramine group. This active chlorine-supported MOF/ fiber composite material (UiO-66-NH-Cl/PET) has demonstrated excellent broad-spectrum antimicrobial properties, effectively inactivating pathogens including Gram-positive bacteria, Gram-negative bacteria and SARS-CoV-2 virus in just a few minutes. In addition, the active chlorine in the MOF coating carrier shows excellent stability and regeneration ability, which provides a new idea for the development of efficient antibacterial textiles.


Figure 2.11 Schematic representation of the UiO-66-$NH_2$/PET composite loaded with chlorine, showcasing its regenerable biocidal and detoxification capabilities [153].

Chemical finishing is commonly used technology in the antibacterial modification of textiles. By coating the textile surface with antibacterial agents (such as silver ions, quaternary ammonium salts or natural extracts), it can give durable antibacterial properties of textiles, and is widely used in medical, daily life and industrial fields [154]. Common chemical finishing techniques include dipping, coating and cross-linking. According to different fiber materials, chemical finishing methods have their own characteristics. For synthetic fibers, for example, antibacterial agents (such as silver particles) can be embedded in the polymer at the spinning stage, ensuring a uniform distribution of antimicrobial properties and long-term durability; Antibacterial agents (such as silver nanoparticles) can also be introduced in the electrospinning process for the manufacture of nanofibers with antibacterial properties [155]. Natural fibers, on the other hand, are usually treated with metal at the finishing stage, with special strategies to enhance the adsorbability and durability of metal ions. For example, cotton fibers can be pretreated with succinic anhydride, a compound that acts as a ligand for metal ions,

significantly improving the adsorption capacity of metal salts such as $Ag^{+}$ and $Cu^{2+}$, thus achieving high antibacterial properties; Aspartic acid and glutamate residues in wool fibers provide metal-binding sites, and these binding capacities can be further enhanced by pretreatment with tannic acid or EDTA. In addition, Quaternary ammonium compounds (QACs), as an important antibacterial agent, are mainly dependent on the ionic interaction between the cation and the anion on the fiber surface [156]. For polyester fibers, QAC can be directly adsorbed under near-boiling conditions, while in wool, carboxylic groups of glutamyl and aspartate residues provide binding sites that allow QAC-treated wool fibers to withstand multiple washes. Through these chemical finishing technologies, not only can achieve the efficient antibacterial properties of textiles, but also ensure their durability and performance stability after repeated cleaning, showing a wide range of application potential. For the antibacterial finishing of textiles made of natural or synthetic fibers, in addition to the above-mentioned dip - dry - cure technology, several advanced antibacterial finishing methods have also been studied, such as sol-gel technology and layer by layer deposition technology. Sol-gel technology is a way of impregnating the fabric in sol (a colloidal solution that gradually turns into a gel) and then going through a dipping and drying - washing system. Layer-by-layer deposition is a technique in which fabric is first immersed in a cationic polymer solution, followed by immersion in an anionic polymer solution, depositing polymer layers in sequence. In this technique, the fabric needs to be rinsed and dried between dipping operations.

Surface functionalization treatment is an important means to improve the antibacterial properties of textiles. Common techniques include plasma treatment, coating and surface polymerization. Plasma treatment is a unique and efficient method in textile finishing, with the significant advantage that it does not require the use of water or drying, thus significantly reducing water and energy consumption [157]. By plasma-assisted antibacterial finishing,

antimicrobial properties can be conferred by polymer deposition or grafting polymerization. Among them, polymer deposition is to uniformly cover the surface of the textile substrate, while graft polymerization is to directly bind the antibacterial finishing agent to the textile surface. What's more, plasma technology is utilised as a pre-treatment process before finishing, it can significantly improve the basic functional characteristics of the textile (such as absorption rate) and achieve excellent results like traditional finishing methods with less water and time investment. This green finishing method shows a wide range of application prospects.

### 2.4.4 Application of Antibacterial Textiles

#### 2.4.4.1 Application in Fashion Design

In recent years, antibacterial textiles have attracted great attention due to their wide range of application scenarios. These textiles find extensive use in healthcare, hygiene products, medical equipment, sportswear, underwear, food packaging and storage, as well as thermal and mechanical protection. They are also employed in automotive textiles, HVAC systems, air filters, and water purification systems. They also play an important role in protecting functional clothing for health care workers and household everyday items.

Antibacterial textiles are particularly popular in sportswear and active fashion. In the global market, the popularity of sportswear and active wear is rapidly increasing. The impetus for this trend may come from people's interest in personalized athletic looks, a trend often influenced by celebrities. These sportswear are typically designed with special fibers and yarns combined with a variety of chemical finishing processes to meet the needs of moisture management and heat control during sports. In addition, the demand for antibacterial textiles in active sportswear has increased significantly due to the COVID-19 outbreak. Some brands even claim that their

products are innovative in their antiviral properties. Lululemon's "Silverescent" series achieves antibacterial properties through X-Static technology embedded in 99.9% sterling silver. Similarly, companies such as Microban, Lululemon, and Under Armour, Dow Microbial Control have developed products that protect against sweat stains and bacteria. The rapid development of antibacterial textiles not only meets the market demand after the epidemic, but also promotes innovation in textile technology, bringing new possibilities to the fields of healthcare and fashion design.

#### 2.4.4.2 Application in Healthcare

Antibacterial textiles have been widely used in the medical field, providing important support for preventing infection, promoting healing, and improving patient care. Its main functions include inhibiting the growth of bacteria, viruses and fungi and reducing the risk of pathogen transmission and infection. For example, antibacterial fabrics can be used to make chronic wound dressings that prevent wound infections and promote tissue healing by incorporating antibacterial agents such as silver nanoparticles. In addition, antibacterial fabrics are widely used in surgical sutures, medical uniforms, bed sheets and pillowcases to provide additional hygiene protection. In recent years, antibacterial textile technology has been particularly important in mask manufacturing, especially in global health events, antibacterial and antiviral masks can effectively reduce the spread of pathogens in the air, protecting the health of healthcare workers and the public. These masks typically use a multi-layer structure, combined with electrospinning nanofiber technology and an antibacterial coating, to efficiently filter microbial particles while ensuring breathability. In the treatment of chronic wounds and periodontitis, dressings containing chitosan nanofibers and silver alginate nanoparticles with antimicrobial properties have been shown to accelerate wound healing and reduce scarring. By combining advanced electrospinning technology and bioactive materials, antibacterial textiles

are providing innovative solutions for the medical industry to further improve patient outcomes and quality of care.

## 2.5 Summary of Current Research Potentials

In summary, bioaerosols pose a severe challenge in the field of public health. Traditional antibacterial strategies are insufficient in dealing with highly pathogenic and drug-resistant microorganisms. There is an urgent need to develop new, efficient and environmentally friendly antibacterial materials. Nanostructured surfaces have become a research hotspot due to their excellent contact bactericidal properties, especially in terms of biomimetic structural design and physical and mechanical bactericidal mechanisms. At the same time, chemical bactericidal components such as silver nanoparticles and polycationic polymers have also attracted widespread attention due to their broad-spectrum antibacterial ability. Existing studies have shown that the multi-mechanism synergistic antibacterial strategy combining physical structure and chemical function can significantly improve the comprehensive antibacterial properties of materials and break through the limitations of a single mechanism. In addition, functional antibacterial textiles have good application transformation potential due to their flexibility, wearability and scalable preparation, and have broad prospects in medical protection, air purification and personal protection. In current research, a variety of antibacterial factors have been successfully introduced into textile material systems, including MOFs, plant-extracted essential oils, nano-metal particles, etc., which have improved the antibacterial properties of materials. However, there are still challenges in terms of material antibacterial properties, antibacterial stability and sustainability. Therefore, further in-depth research from the dimensions of material structure design, bactericidal mechanism regulation and actual textile adaptability will provide a solid foundation for the realization of efficient, sustainable and low-risk antibacterial materials.

# 3 Superhydrophilic AgNPs-Cellulose Nanofiber Layer for Airborne Bacterial Killing: Synthesis, Characterization, and Application

## 3.1 Introduction

With the increasing global health awareness and the increasing demand for the prevention and control of infectious diseases, the research and development of bioaerosol (such as bacteria and viruses) barrier materials have been paid more and more attention. As a key barrier to bioaerosols, masks and air filtration membranes need to be antimicrobial, breathable and durable. In this context, metal nanomaterials have become ideal antibacterial agents because of their unique physical, chemical and biological properties [158-161]. Among them, Ag NPs stands out for its broad-spectrum antibacterial properties, heat resistance and safety, especially in inhibiting the growth of pathogenic bacteria and delaying the development of drug resistance [162-164].

Silver nanoparticles achieve antibacterial action through multiple mechanisms, including adhesion to cell walls, penetration of cell membranes, release of silver ions to attack key biomolecules, and induction of bacterial metabolic disorders through reactive oxygen species (ROS) and inhibition of DNA replication, thus effectively killing bacteria [165, 166]. Electrospinning is an efficient and flexible method to prepare antibacterial fibers containing silver nanoparticles. The technique uses a high voltage electric field to stretch the polymer solution to form nanoscale fibers and deposit it into a non-woven fiber film. By incorporating silver nanoparticles into the spinning solution or surface modification of the fibers, the

materials with excellent antibacterial properties and bioaerosol barrier ability can be prepared. These silver-containing nanofiber materials not only efficiently kill microorganisms in the air, but also maintain good breathability and flexibility, making them ideal for use in masks and air filtration membranes.

However, traditional masks face some key challenges in practical use, including skin irritation and respiratory discomfort caused by moisture and sweat accumulation, as well as microbial growth in humid environments; The antibacterial property is limited, and it is difficult to effectively inhibit the propagation of pathogenic microorganisms. And PP melt-blown fabrics rely on static electricity to enhance the filtration performance, but the accumulation of moisture will cause the static charge to gradually weaken, thus weakening the filtration effect.

To solve these problems, this chapter uses electrospinning technology to prepare an antibacterial cellulose nanofiber layer containing silver nanoparticles. Cellulose acetate nanofibers, possess desirable properties for antibacterial materials. It has biocompatibility, biodegradability, extensively suitable for antibacterial applications. Cellulose acetate can be hydrolysed in an alkaline solution to regenerate cellulose, endowing the nanofiber layer with superhydrophilic properties. The following goals are achieved: superhydrophilic nanofibers ensure the high filtration performance of the mask during the whole life cycle by reducing water accumulation [167]; Its super-hydrophilicity combined with the antibacterial property of silver nanoparticles can capture and inactivate microorganisms, while keeping the inside of the mask dry, reducing the risk of microbial breeding and improving hygiene performance; In addition, it can improve wearing comfort, reduce respiratory burden, and effectively reduce skin discomfort. This innovative silver-containing superhydrophilic nanofiber layer helps to overcome the shortcomings of traditional masks and provides a new solution for improving protective performance and optimizing user experience. Its development is of great

significance in improving the performance of masks and air filtration membranes and lays a solid foundation for technological progress in the field of public health protection.

## 3.2 Experimental Section

### 3.2.1 Materials

Silver nitrate ($AgNO_3$) and cellulose acetate (average $M_n$ ~50,000 by GPC, 39.7 wt% acetyl) were purchased from Sigma-Aldrich Co., Ltd. Acetone ($C_3H_6O$, ≥99.5%) and N, N-Dimethylacetamide (DMAc) was purchased from Duksan reagents Co., Ltd. Potassium Hydroxide (KOH, ACS) was purchased from Shanghai Aladdin Biochemical Technology Co., Ltd. All chemicals were used as received without further purification. Bacteria (*E. coli.*, CMCC 44102) was purchased from JINGBIO Co., Ltd. PP melting blown cloth was purchased from DOCTOR MASK. The PP melt-blown nonwoven cloth has a basis weight of about 25 g/m² and consists of fibers with diameters ranging from 1 to 5 μm.

### 3.2.2 Preparation of Superhydrophilic Nanofiber Layer

#### 3.2.2.1 Fabrication of Electrospun Nanofibers

Cellulose acetate spinning solution. DMAc is less corrosive, less toxic, and not easily hydrolyzed, while acetone is a good solvent for cellulose acetate. Both solvents are common and widely used solvents and are often used in cellulose acetate electrospinning. Firstly, as shown in Table 3.1, a mixture of acetone/DMAc (2/1 w/w) solvent was prepared, and then a certain amount of cellulose acetate, the mass fraction of cellulose acetate was 15 wt%, was dissolved in the above prepared solvent, and stirred at room temperature for 3~4 h until

completely dissolved to obtain a transparent clarified spinning solution. Different ratios of acetone/DMAc have been tried previously, of which a 2/1 acetone/DMAc ratio proved to be the most versatile as it could produce bead-free, continuous cellulose acetate fibers in the concentration range of 12.5~17 wt% [168]. The spinning solution was left to rest overnight to allow the solvent and solute to fully function before it can be used for electrospinning.

Cellulose acetate nanofibers. An electrospinning device made in the laboratory was used. During electrospinning, the process parameters were selected based on the previous work and initial experiments [168-170]. The voltage was set as 20 kV. The feed rate was employed as 1 mL/h. A stable jet was formed, the needle did not clog, and the collected fibers were uniform and free of beaded structures. Use a 10 mL syringe to extract an appropriate amount of the above-mentioned prepared cellulose acetate spinning solution, fix the syringe on the injection pump, then add high pressure to the needle, and ground the collection device, injection pump and high-pressure generator to avoid electric leakage and ensure safety. The syringe needle had an outer diameter of 0.8 mm, and the receiving distance was 13 cm. At the same time, the high voltage static electricity on the injection pump was diverted to prevent damage to the injection pump. Cellulose acetate nanofibers layer was obtained, noted as N0.

Table 3.1 Composition of electrospinning solutions with different $AgNO_3$ concentrations for nanofiber layers (N0, N1, N2).

| Nanofibers layer | Cellulose acetate | $AgNO_3$ | Solvent |
|---|---|---|---|
| N0 | 15 wt% | 0 | Acetone/DMAc |
| N1 | 10 wt% | 0.1 wt% | Acetone/DMAc/Water |
| N2 | 10 wt% | 0.5 wt% | Acetone/DMAc/Water |

$AgNO_3$/cellulose acetate spinning solution. As shown in Table 3.1, a mixture of acetone /DMAc (2/1 w/w) was prepared. A certain amount of cellulose acetate (the mass fraction: 10 wt%) was added to the solvent and stirred for 3~4 h until completely dissolved to obtain a clarified solution. 0.04 g of $AgNO_3$ was weighed and dissolved in 40 g of deionized water to prepare a 0.1 wt% $AgNO_3$ aqueous solution. Then, 0.8 g of the above $AgNO_3$ solution was weighed and added to 8 g of 10 wt% cellulose acetate solution. The solution was stirred thoroughly at room temperature until mixed evenly and a homogeneous silver-containing solution was obtained. Currently, the mass ratio of $AgNO_3$ to cellulose acetate was 0.1 wt%. Similarly, 10 wt% cellulose acetate solution 0.5 wt% $AgNO_3$ was prepared. The solutions were left to rest overnight before electrospinning.

AgNPs/cellulose acetate nanofibers. The $AgNO_3$/cellulose acetate precursor spinning solution prepared by the method was electrospun at room temperature and the relative humidity was less than 50%, and the fibers were received on the collector. Then the obtained electrostatic spinning fibers were dried at a temperature of 60 °C and under vacuum conditions for 24 h. Finally, the dried fiber was irradiated under UV light for 3 h, and the $Ag^+$ is reduced to Ag by ultraviolet reduction technology, to obtain AgNPs/cellulose acetate nanofibers layer, noted as N1 and N2.

3.2.2.2 Fabrication of Superhydrophilic Nanofiber Layer

At room temperature, cellulose acetate and AgNPs/ cellulose acetate nanofibers were hydrolyzed/deacetylated in 0.5 M KOH ethanol solution for 3 h to obtain cellulose layers. Finally, the cellulose films were washed with ethanol several times to remove residual KOH and dried under vacuum at 80℃ for 12 h, marked as M0, M1, M2.

### 3.2.3 Characterization and Measurements

#### 3.2.3.1 Scanning Electron Microscopy

SEM uses electron beams to image the surface of the sample at micro/nano scale resolution and perform trace element analysis. Using gold as evaporation source, the sample was evaporated through high vacuum with a working current of 40 mA. After 10 s of gold plating, the sample was coated with conductive layer. The surface morphologies of sample fibers, nanocomposites and films were evaluated by Tescan MIRA Field Emission Scanning Electron Microscope (FESEM) with an accelerated voltage of 5.0 kV.

#### 3.2.3.2 Transmission Electron Microscopy

TEM provides high-resolution images and sample information based on mass thickness contrast, diffraction contrast and phase contrast. The structure of silver nanoparticles is easy to distinguish due to the obvious contrast between the mass density of metal materials and polymer materials. In the process of electrospinning, TEM samples were made directly from the receiving fibers of ultra-thin carbon films supported on copper meshes for 10-20s, and the JEM-2100 TEM produced by JEOL, Japan was used with an accelerated voltage of 200kV. It was used to analyse the microstructure of nanofibers and the dispersion of AgNPs.

#### 3.2.3.3 X-ray Photoelectron Spectroscopy

XPS is a surface analysis technique used to study the chemical composition and electronic state of a material's surface. By measuring the kinetic energy and distribution of these photoelectrons, it is possible to calculate their binding energy, which is closely related to the

chemical state and environment of the atoms in the sample. Thermo Scientific Nexsa X-ray photoelectron spectrometer was used to analyse the element composition of the nanofibers modified with silver nanoparticles.

#### 3.2.3.4 Fourier Transform Infrared Spectroscopy

FTIR is a simple technique to detect the different functional groups of a material, which can obtain the absorption infrared spectrum of the material in the solid, liquid and gas states. The FTIR spectra of textile materials were recorded by Thermo Fisher Scientific Nicolet iN10 spectrometer.

#### 3.2.3.5 Static Water Contact Angle

CA measurements were performed using OCA20 machine (Data-Physics, Germany) at ambient temperature. The water droplet volume was set as 2 μL. The optical images were captured after equilibrium. The data for each contact angle was calculated from the average of five repeated measurements.

#### 3.2.3.6 Aerosol Evaporation Rate Test

The appropriate amount of deionized water was added to the atomizer and sprayed onto the textile surface for 2 minutes. In the constant temperature and humidity environment, the balance (Shanghai Precision Instrument Co., LTD.) was used to record the change of textile weight over time and calculate the evaporation rate.

#### 3.2.3.7 Air Permeability

Air permeability tester is an instrument used to measure the breathability of textiles, fabrics and other porous materials. It evaluates the ability of the fabric to allow air to pass through the flow of air under specific pressure conditions. This is important for applications that require breathability and ventilation properties, such as clothing, industrial filtration materials, and medical textiles. The air permeability tester (KES-F8-AP1) was used to measure the breathability of textiles.

3.2.3.8 Antibacterial Test

Gram-negative *E. coli* (CMCC 44102) was cultured to prepare a bacterial solution. Individual colonies on solid Luria-Bertani (LB) agar were transferred to 10 mL of LB broth and cultured at 37°C for 24 hours. Subsequently, the bacteria were cleaned with a PBS solution and the bacterial precipitate was collected by centrifugation (Thermo Fisher Scientific, centrifuge Pico 17). The bacterial precipitates were suspended with PBS for further experiments. The bacterial concentration was determined by continuous dilution method and colony forming unit (CFU) counting method. 5 mL bacterial solution with a concentration of $10^7$ CFU/mL was added to a compression atomizer (XBK, MCN-S600MF) to generate bioaerosol. Using this aerosol ($10^7$ CFU/mL), spray the surface of the test sample for 30 seconds to bring the sample into full contact with *E. coli*. The bacteria on the surface of the sample were then transferred to agar medium by ultrasonic elution and incubated at 37°C for 24 hours to assess the antibacterial properties of the sample. The results of the experiment were quantitatively evaluated by analysing the formation of colonies.

3.3 Results and Discussion

3.3.1 Characterization and Morphology

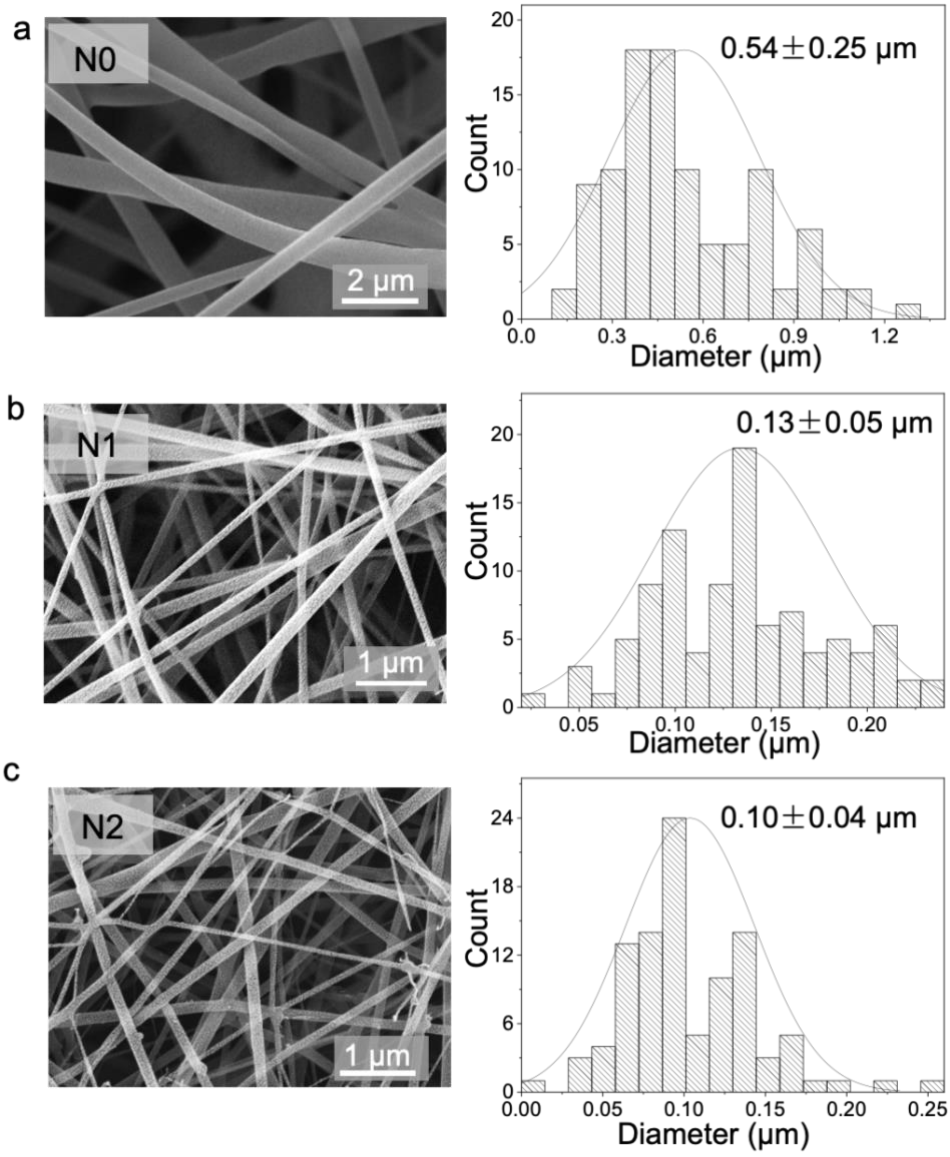


Figure 3.1 SEM and diameter distribution of three kinds of nanofiber layers (N0, N1, N2).

The spinning solution was firstly prepared according to the formula in Table 3.1, and the nanofiber layers (N0, N1, N2) were prepared by electrospinning combined with ultraviolet light

technology. The corresponding microscopic morphology and size distribution are shown in the SEM diagram in Figure 3.1. Through the analysis and statistics of nanofiber diameter size, it can be known that the average diameter of N0, N1 and N2 nanofibers is about 540 nm, 130 nm and 100 nm respectively. When $AgNO_3$ was added into the spinning solution, the jet formed by the polymer solution showed obvious instability. Under the action of electric field force, the droplet is directly thrown out without being fully stretched, and it is difficult to form continuous nanofibers. The few fibers received showed uneven thickness and were accompanied by beads. Due to the poor solubility of $AgNO_3$ in DMAc, $AgNO_3$ was unevenly dispersed in the spinning solution, resulting in an uneven charge distribution of the solution jet during electrostatic spinning and unable to achieve normal spinning. To address this problem, $AgNO_3$ takes advantage of its good solubility in water and chooses a mixed solution of acetone /DMAc/ water as the solvent system to significantly improve the spinning performance. The average diameter of the fiber is reduced, the thickness is more uniform, and the problem of nozzle blockage is effectively alleviated.

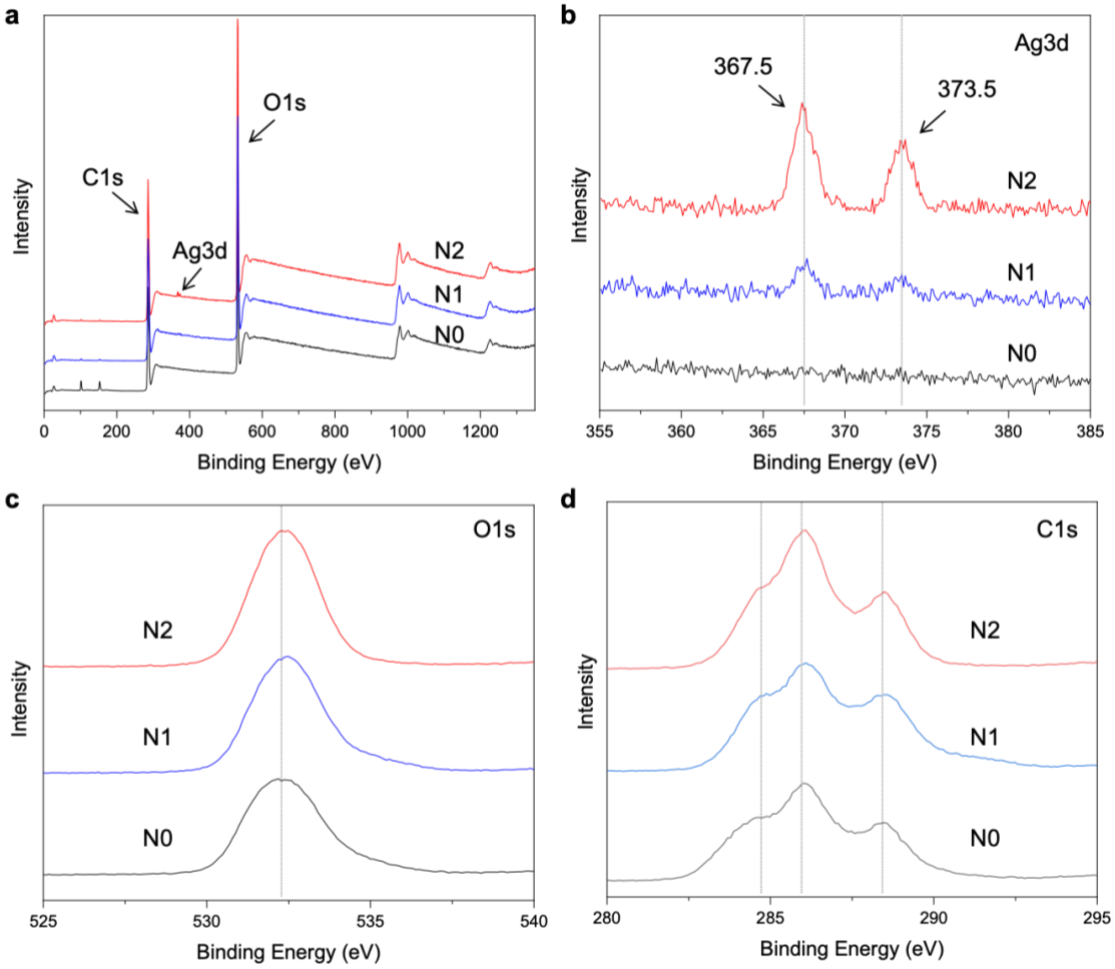


Figure 3.2 XPS spectra of three nanofiber layers.

Figure 3.2 shows the comparison of XPS spectra between pure cellulose acetate nanofibers (N0) and AgNPs/cellulose acetate nanocomposite fibers (N1, N2). Figure 3.2a is the full spectrum of XPS, in which it can be observed that N0 only has characteristic peaks of C and O, while N1 and N2 mainly contain three elements: C, O and Ag. Figure 3.2b shows the high-resolution XPS pattern of Ag3d, indicating that the two characteristic peaks of Ag in the composite nanofibers are located at BE = 367.5eV ($Ag3d_{5/2}$) and BE = 373.5eV ($Ag3d_{3/2}$), and the distance between them is 6.0 eV. The position of XPS peak is consistent with that of metal elemental Ag. However, when compared with the $Ag3d_{5/2}$ (368 eV) and $Ag3d_{3/2}$ (374 eV), these peaks were offset by 0.5 eV in the low energy direction, indicating that there was a

chemical binding between Ag and cellulose acetate rather than a simple physical adsorption. It also further proves the existence of AgNPs. Figure 3.2c shows the high-resolution XPS map of O1s. Compared with pure cellulose acetate nanofibers, the position of O1s peak in AgNPs/cellulose acetate composite fibers moved towards high energy. The O1s peak of cellulose acetate is usually divided into three parts, corresponding to the C=O bond in the acetic acid group, the oxygen atom in the ether bond, and the C-O single bond in the acetic acid group. When AgNPs is incorporated into cellulose acetate, due to the interaction between carbon-based oxygen atoms in cellulose acetate and Ag, the charge density of O is reduced, and the chemical environment of part of O is changed, resulting in chemical shift. Figure 3.2d shows the high-resolution XPS map of the C1s. The C1s peak of cellulose acetate is divided into three parts: 286.5eV corresponds to the carbon atoms of C-O-H and C-O-C in cellulose acetate, 288.8eV corresponds to the carbon atoms of O-C=O and O-C-O, and 284.7eV corresponds to the $-CH_3$ carbon atoms of hydrocarbons and acetyl groups in cellulose acetate. It can be seen from the figure that the C1s peak of cellulose acetate in this experiment is consistent with the characteristic peak of pure cellulose acetate, and the C1s pattern of AgNPs/ cellulose acetate composite fiber does not show significant chemical shift, which indicates that AgNPs has no significant effect on the carbon atoms of cellulose acetate.

While DMAc may exhibit mild reducing ability under elevated temperature or alkaline conditions [171, 172], its contribution is considered negligible in this UV-assisted process. The formation of AgNPs in this study was primarily driven by photoreduction under UV irradiation. Cellulose acetate nanofibers containing $AgNO_3$ take on a yellowish color after ultraviolet irradiation, indicating that $Ag^+$ has successfully reduced AgNPs. It can be observed from Figure 3.3 that the silver nanoparticles formed are spherical and have good dispersion. The measurements show that the average diameter of AgNPs is about 3.46 nm. In the HRTEM

image (Figure 3.4), the crystal faces of silver nanoparticles can be clearly seen, and the crystal face spacing of 0.23 nm is measured, which is consistent with the lattice spacing of silver (111) crystal faces.

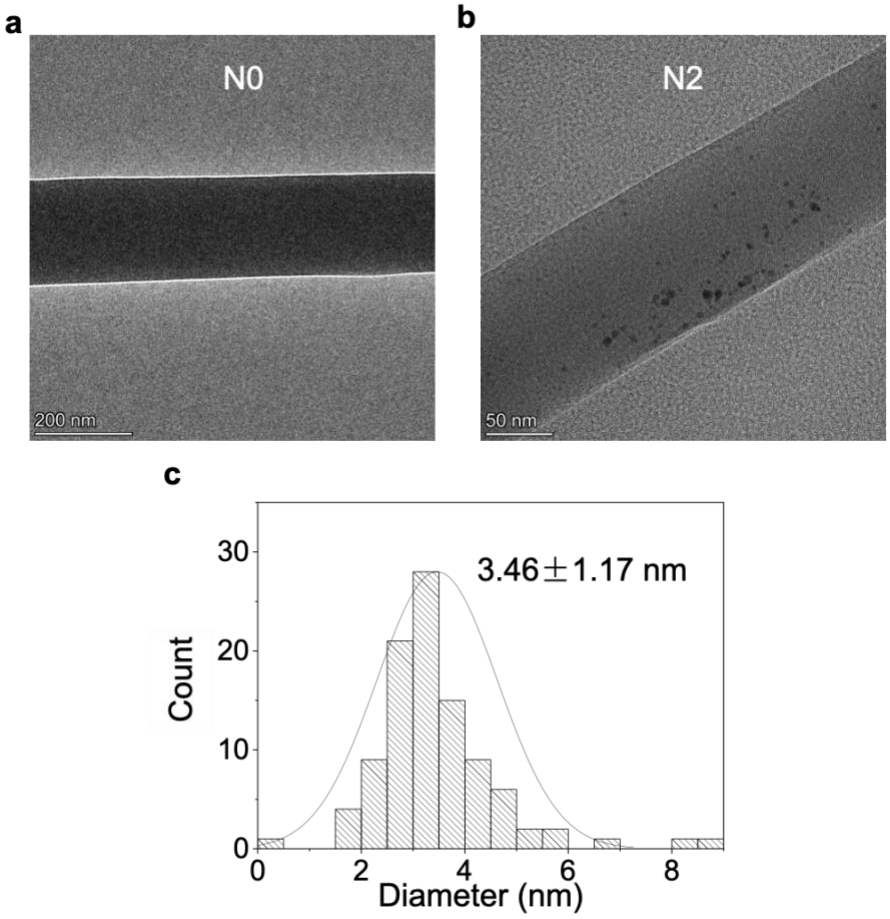


Figure 3.3 TEM of N0 (a) and N2 (b) nanofiber. c, Diameter distribution of the AgNPs.

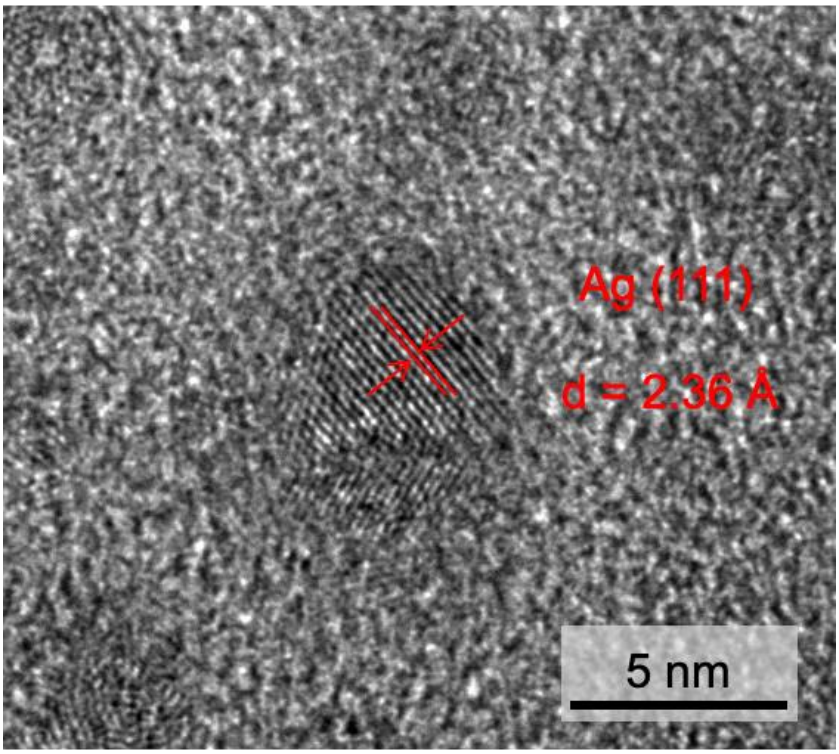


Figure 3.4 HRTEM image of AgNPs.

Table 3.2 Composition of electrospinning solutions with different $AgNO_3$ concentrations for superhydrophilic nanofiber layers (M0, M1, M2).

| | Cellulose acetate | $AgNO_3$ | Solvent | KOH Immersing time (h) |
|---|---|---|---|---|
| M0 | 15wt% | 0 | Acetone/DMAc | 3 |
| M1 | 10wt% | 0.1wt% | Acetone/DMAc/Water | 3 |
| M2 | 10wt% | 0.5wt% | Acetone/DMAc/Water | 3 |

Electrospinning technology is used to prepare cellulose acetate nanofiber layers and convert them into cellulose films by alkaline hydrolysis. The specific composition and treatment conditions of the spinning solution are shown in Table 3.2. The molecular structure changes of

fiber materials before and after hydrolysis are shown in Figure 3.5, which clearly shows the chemical process of conversion of cellulose acetate into cellulose after deacetylation.

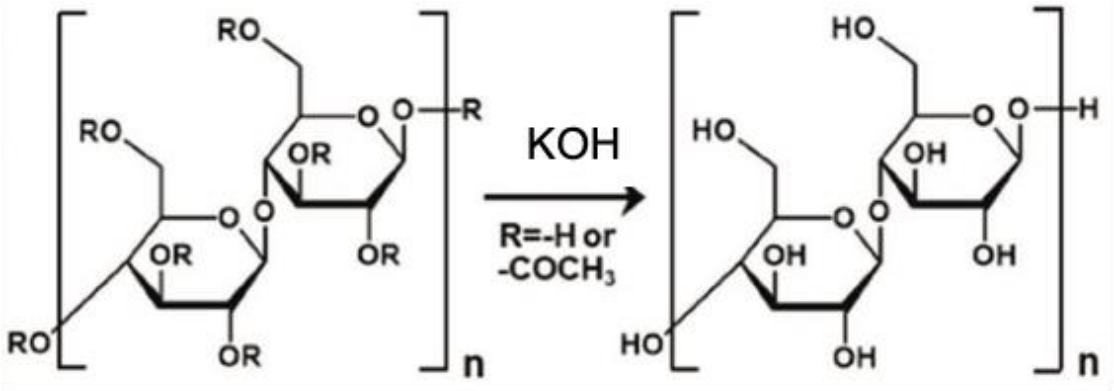


Figure 3.5 Schematic illustration of the hydrolysis reaction of cellulose acetate to cellulose.

Infrared spectroscopic analysis (Figure 3.6) further verifies the success of this conversion process. In the infrared spectrum of cellulose acetate, the characteristic peaks at 1734 $cm^{-1}$ and 1230 $cm^{-1}$ correspond to the tensile vibration of C=O and the characteristic absorption of ester base C-O-C, respectively. These characteristic peaks disappeared completely after hydrolysis, indicating that the acetyl group in cellulose acetate was removed under alkaline conditions and cellulose molecules were successfully formed. In addition, samples M0, M1, and M2 show stronger and wider absorption bands in the range of 3200-3500 $cm^{-1}$, which is caused by hydrogen bond formation, further confirming the success of the hydrolysis reaction. This result clearly shows the successful preparation of cellulose membrane from two aspects of molecular structure and chemical composition.

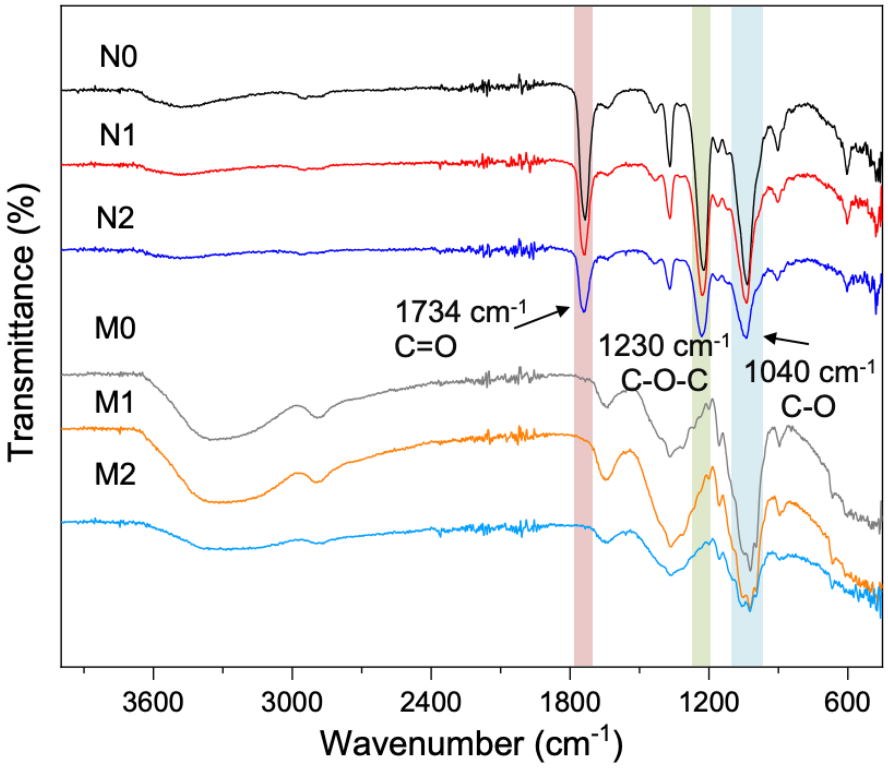


Figure 3.6 FTIR spectroscopy of different nanofiber layers (N0, N1, N2, M0, M1, M2).

In terms of microstructure, Figure 3.7 shows the significant influence of hydrolysis treatment on the morphology of nanofibers. The hydrolyzed nanofibers showed a more curved shape, and their flexibility was significantly enhanced compared with the linear fibers before hydrolysis. At the same time, the stacking between fibers is more obvious, which may be attributed to the enhancement of hydrogen bonding between cellulose molecular chains.

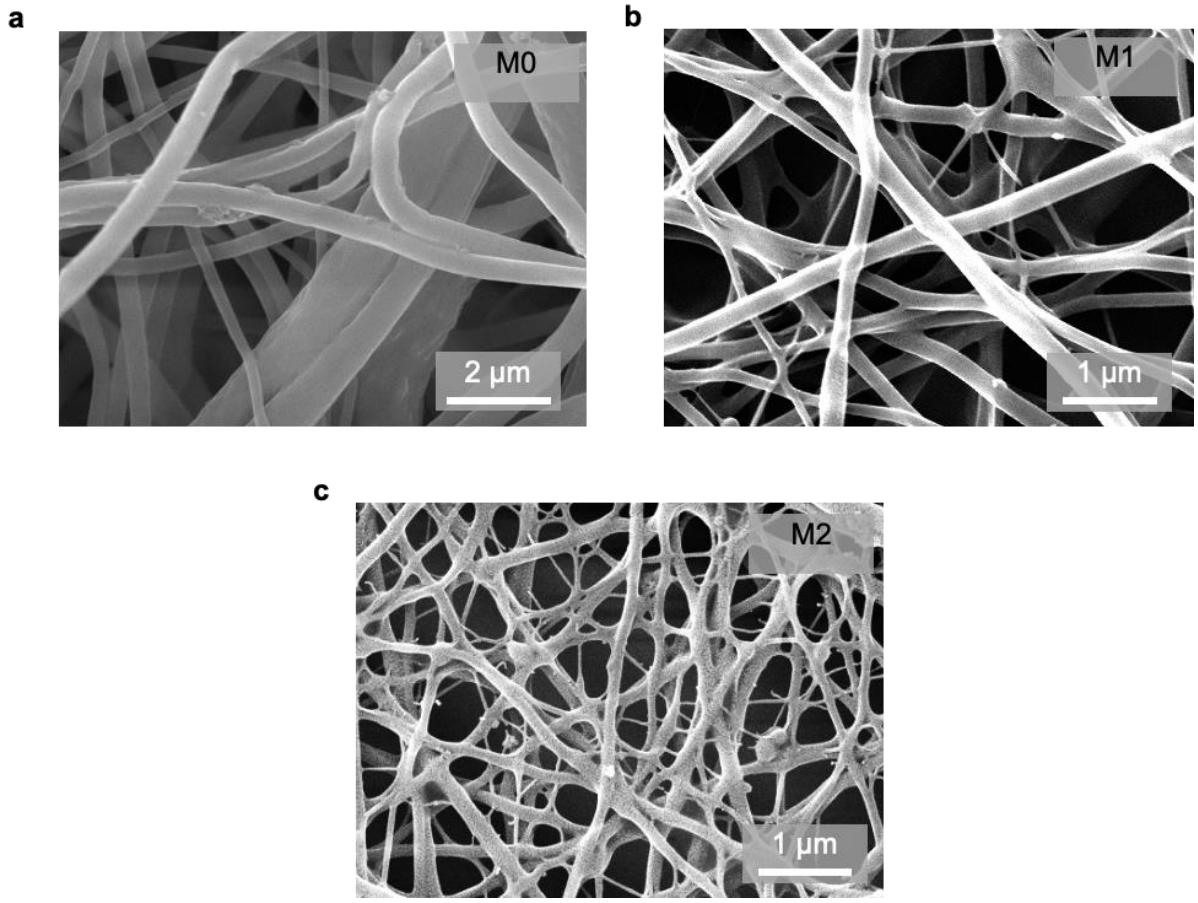


Figure 3.7 SEM of three kinds of nanofiber layers (M0, M1, M2).

3.3.2 Performance Evaluation for Functional Textile Properties

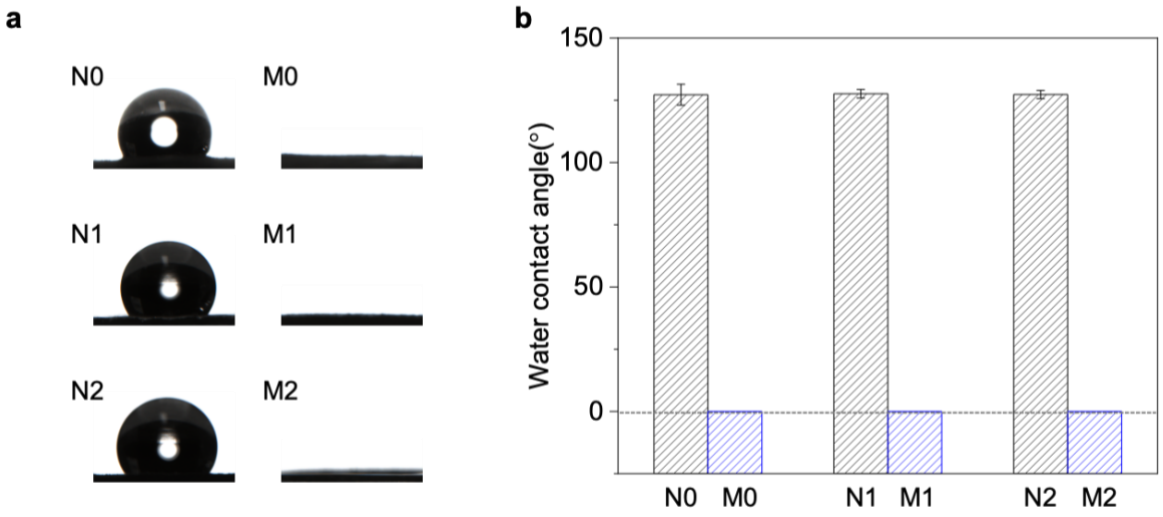


Figure 3.8 Water contact angle of different nanofiber layers (N0, N1, N2, M0, M1, M2).

The hydrophilicity of cellulose membrane was also significantly improved. As shown in Figure 3.8, the contact Angle of the surface of the hydrolyzed fiber film decreased significantly from the high value before hydrolysis to close to 0°, showing complete hydrophilicity. This remarkable hydrophilicity further validates the successful preparation of cellulose membranes and lays a good foundation for their potential value in a variety of applications.

I compared the dynamic process of water drop spreading on the surface of PP and M2, and the results were shown in Figure 3.9. It can be clearly seen from the figure that there are significant differences in the behaviour of PP and M2 after contact with water droplets. For the PP surface, when the water droplets contact the surface, from the initial moment to 7893 milliseconds (ms), the water droplets always maintain a large spherical shape, and the contact Angle is stable at about 138°. This phenomenon shows that the surface of PP has strong hydrophobicity to water,

and water droplets are difficult to spread or penetrate on its surface, showing typical characteristics of hydrophobic materials.

In contrast, M2 surfaces exhibit completely different behaviour. The same volume of water droplets spread rapidly after touching the M2 surface, and the overspreading process was completed in only about 332 ms, and the contact angle quickly dropped to nearly 0°. This super-fast spreading phenomenon shows that M2 surface exhibits strong hydrophilicity to water, can quickly absorb or diffuse water droplets, and shows excellent wettability. This difference may be closely related to the chemical composition and microstructure of the surface of the two materials. The hydrophobicity of PP is due to its low polarity and low surface energy, while the high hydrophilicity of M2 is related to the improvement of surface hydroxyl group and surface energy.

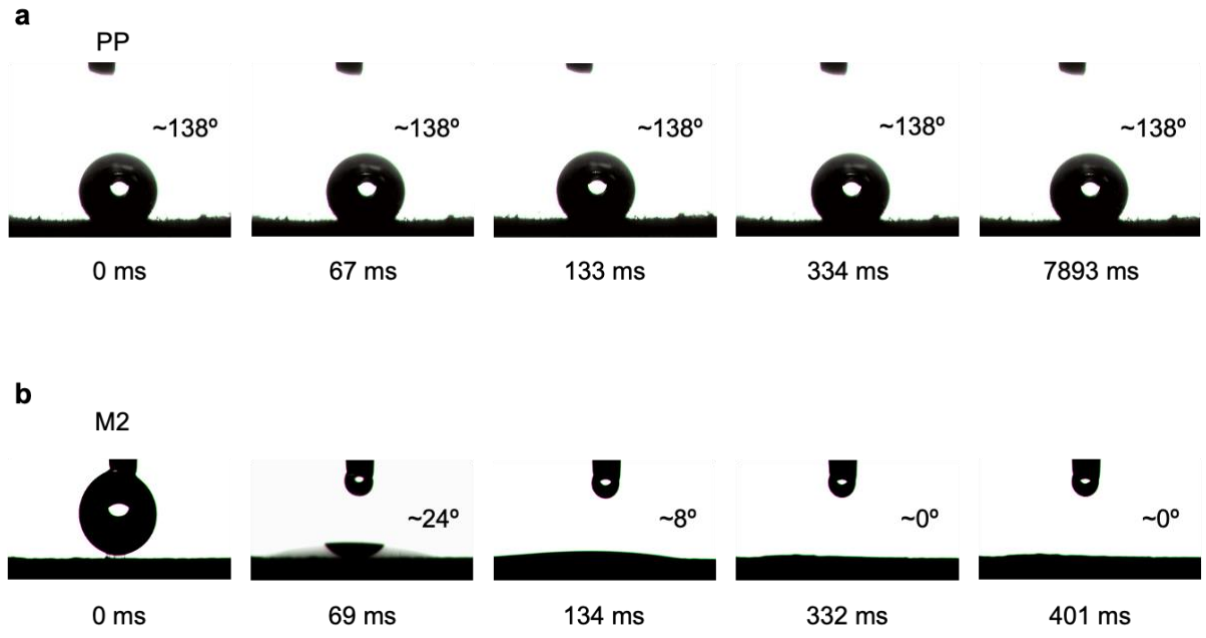


Figure 3.9 The snapshots of water droplet over time on PP (a) and M2 (b), recorded using a camera.

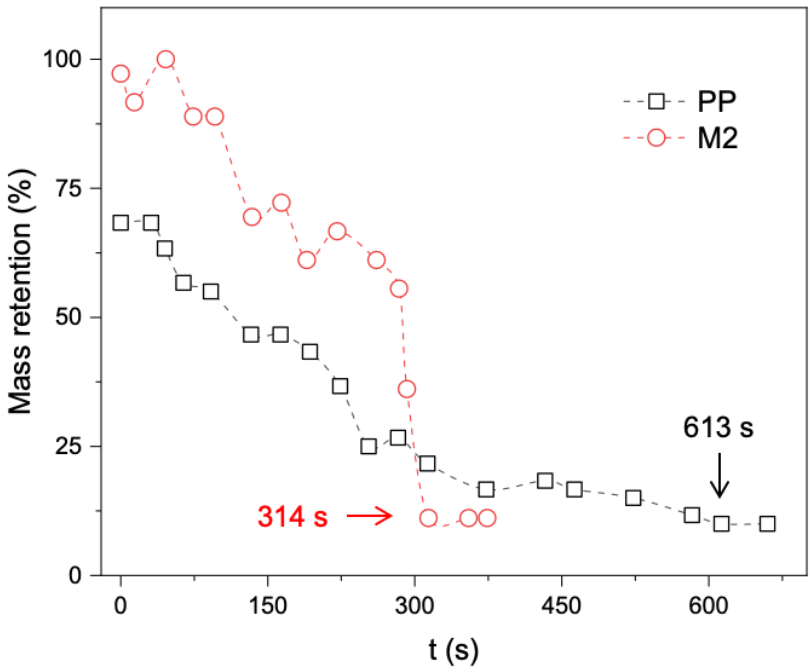


Figure 3.10 Time-dependent mass retention (%) on PP and M2 during aerosol evaporation.

The Figure 3.10 shows the change of PP sample mass fraction with time during water evaporation. In the initial stage (0 s), almost all water was retained, and evaporation had not begun, or only weak evaporation occurred. Over time, the sample entered a rapid evaporation stage. In the early stage (0 ~ 350 s), the mass fraction decreased rapidly, and the decline of the curve was large, indicating that the water evaporation rate was high. This may be due to the sample surface exposed to more water, evaporation conditions were more adequate. When the time exceeded 350 s, the decline rate of mass fraction slowed down significantly, and the curve gradually flattened out. This stage indicated that the water on the surface of the sample had evaporated, and the remaining water may be adsorbed inside the sample or take longer to evaporate slowly. At the later stage (after about 600 s), the mass fraction stabilized, and the curve was almost horizontal, marking the entry of a stable stage of evaporation. At this time,

the water in the sample had basically evaporated, and the evaporation process was basically over.

As can be seen from the Figure 3.10, in the initial stage (when the time is close to 0 s), the mass fraction was close to 1, indicating that the sample contains almost all water, and the water was mainly concentrated on the surface of the sample. Between 0 s and about 300 s, the mass fraction gradually decreased, reflecting the evaporation process of surface water. When the time was close to 300 s, the decline rate of mass fraction was obviously accelerated, the curvature of the curve was increased, and the accelerated evaporation stage was entered. Subsequently, after 300 s, the mass fraction stabilized and the curve became horizontal, indicating that the water in the sample had evaporated and the evaporation process was over. Compared with PP, M2 exhibited a higher initial mass percentage (~100% vs. 75%), indicating improved aerosol uptake likely due to its greater water affinity. Despite the difference in starting values, both materials showed a similar decreasing trend over time. M2 showed a faster dynamic process of water evaporation (314 s), and its total evaporation time was reduced by half, further demonstrating M2's excellent evaporation performance.

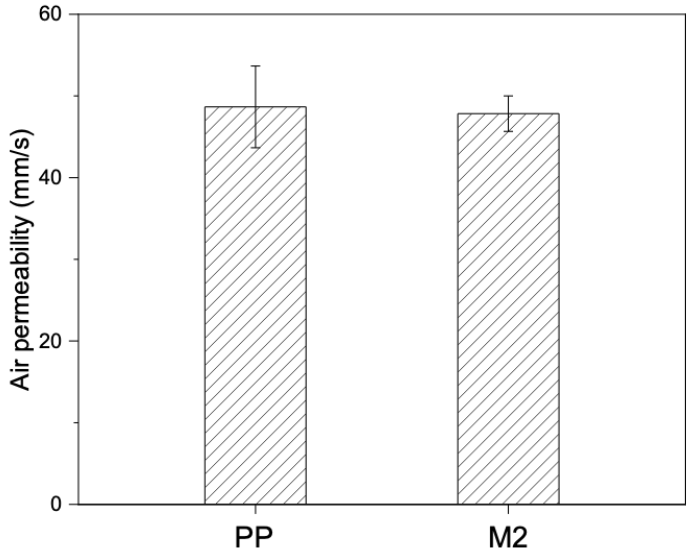

Figure 3.11 The air permeability of PP and M2.

It can be seen from the Figure 3.11 that the air permeability of PP and M2 is very close, and the histogram shows that the two materials have little difference in air permeability. PP samples showed high air permeability, indicating that it has a suitable pore structure, which can effectively allow air to pass through under a certain pressure, showing better ventilation performance. The air permeability of M2 samples is similar to that of PP samples, and the resistance of air passing between the two samples is similar. This result shows that both PP and M2 have good air permeability.

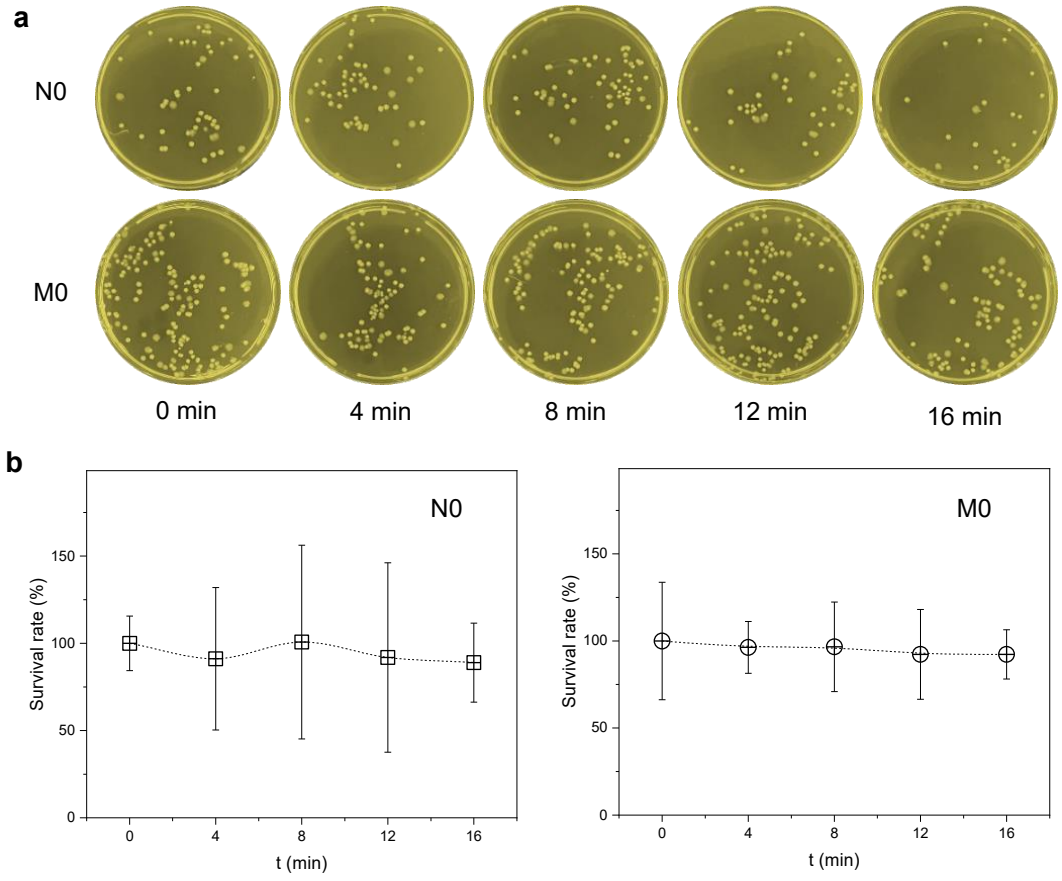

Figure 3.12 The antibacterial performance of N0 and M0. a, Optical images of representative agar plates of transferred airborne *E. coli* after exposure to surfaces. b, Time-dependent *E. coli* survival rate on surfaces.

In order to further evaluate the antibacterial activity of the nanofiber layer, I conducted contact sterilization experiments and verified its antibacterial effect by agar plate counting method. As shown in Figure 3.12a, agar plates of colonies of N0 and M0 at different contact times showed that the number of colonies remained basically unchanged over time. At the same time, the survival rate of the material against *E. coli* were calculated under different contact times (see Figure 3.12b), and the results showed that the survival rate was always close to 100%. The above results clearly indicate that N0 and M0 do not have significant bactericidal activity. This is mainly because cellulose acetate and cellulose themselves do not have antibacterial properties.

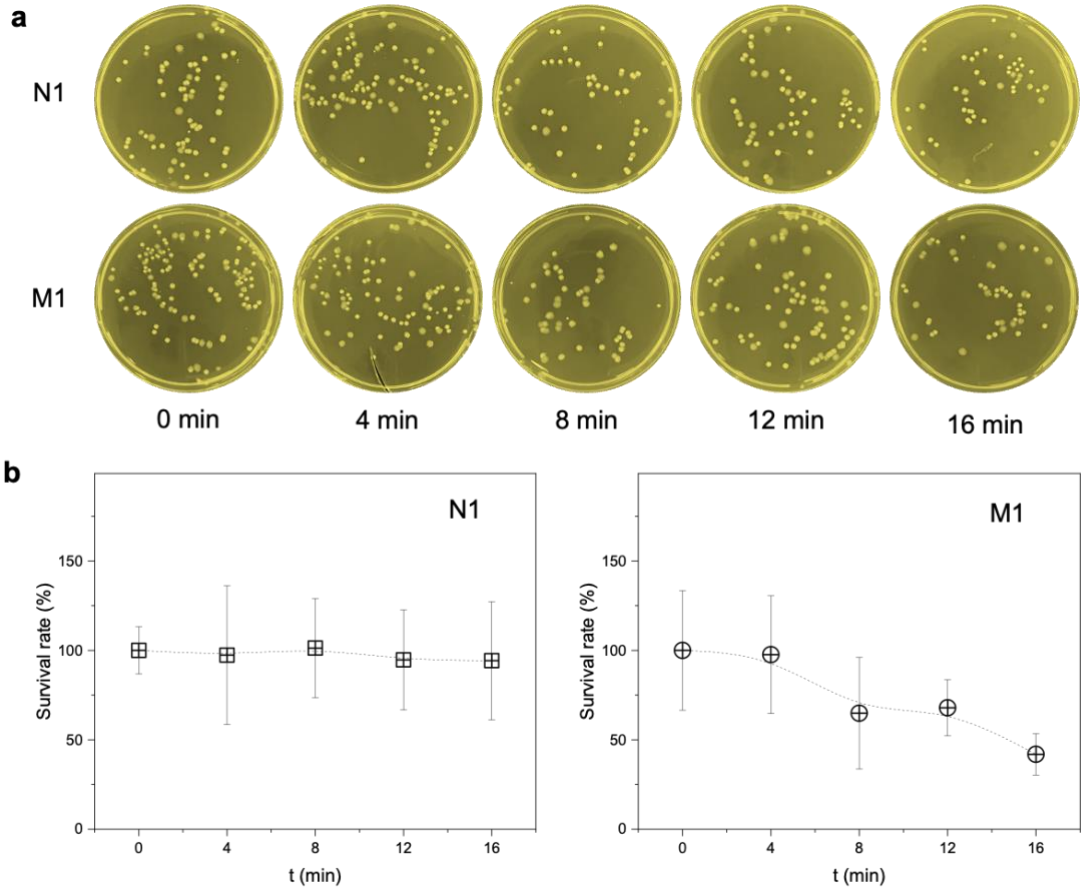


Figure 3.13 The antibacterial performance of N1 and M1. a, Optical images of representative agar plates of transferred airborne *E. coli* after exposure to surfaces. b, Time-dependent *E. coli* survival rate on surfaces.

Similarly, bioaerosol contact killing experiments were performed on N1 and M1. As shown in Figure 3.13a, agar plates of the colonies of N1 under different contact times showed that the number of colonies changed little with time. M1, however, exhibits different behavior. By calculating the survival rate of N1 and M1 against *E. coli* at different contact times (see Figure 3.13b), the results show that the survival rate of N1 is always close to 100%, while the bacterial survival rate of M1 gradually decreases with the increase of time, from 100% to 50%, showing obvious antibacterial activity. These results indicate that M1 has higher bactericidal activity

than N1. This is mainly due to its super-hydrophilic properties, which allow the surface of the material to capture more bioaerosols, thereby increasing the chance of contact with bacteria and enhancing the antibacterial effect.

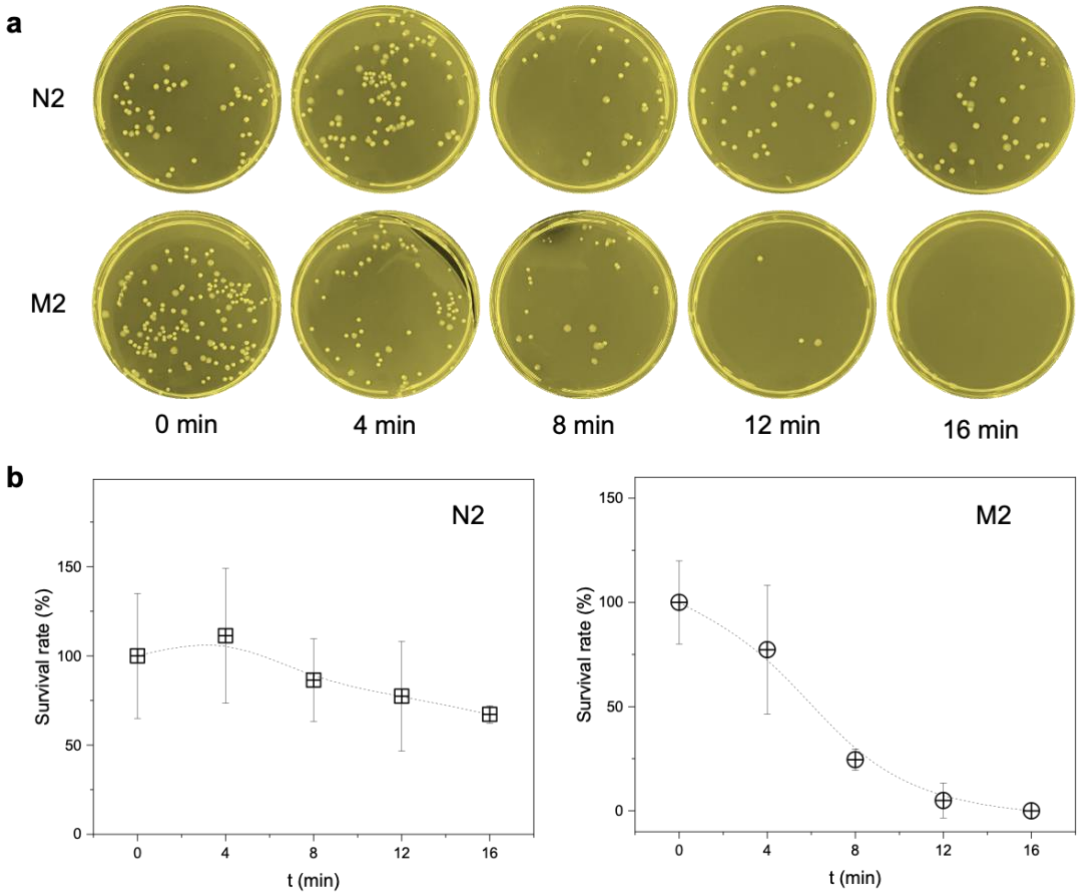


Figure 3.14 The antibacterial performance of N2 and M2. a, Optical images of representative agar plates of transferred airborne *E. coli* after exposure to surfaces. b, Time-dependent *E. coli* survival rate on surfaces.

Finally, N2 and M2 were tested for contact killing. As shown in Figure 3.14a, agar plates of N2 and M2 colonies at different contact times show that the number of colonies gradually decreases with time. The survival rates of N2 and M2 against *E. coli* at different contact times were further calculated (see Figure 3.14b). The results show that N2 survival rate decreases

from 100% to 70% after 16 minutes of exposure to bacteria in aerosols. In contrast, the bacterial survival rate of M2 decreases rapidly over time, from 100% to 0%, showing significantly better antibacterial activity than N2. The above results clearly indicate that M2 has a stronger bactericidal capacity than N2. This is mainly due to its superhydrophilic properties, which further validates that the superhydrophilic surface can effectively capture more bioaerosols and increase the chance of contact with bacteria, thus significantly enhancing the antibacterial effect.

## 3.4 Conclusions

In this study, a kind of superhydrophilic antibacterial nanofiber membrane containing AgNPs was successfully prepared by electrospinning technology, and its properties were systematically studied. By adding $AgNO_3$ into the spinning solution and optimizing the spinning process conditions, a nanofiber layer (N0, N1, N2) with uniform fiber diameter and good dispersion was prepared, and a superhydrophilic cellulose membrane (M0, M1, M2) was prepared by alkaline hydrolysis. The results showed that the introduction of AgNPs and its combination with superhydrophilic properties significantly improved the antibacterial properties of the materials.

FTIR and XPS analysis confirmed the successful transformation of cellulose film and the chemical bonding between AgNPs and substrate. Water contact angle test showed that hydrolytic treatment significantly enhanced the hydrophilicity of the membrane, and the water contact angle of M2 was close to 0°, fully demonstrating its superhydrophilic properties. Compared to traditional PP materials, M2 not only exhibits a faster rate of water evaporation, but also maintains an air permeability comparable to PP.

Antimicrobial performance tests show that M0 and N0 lacked significant bactericidal activity, while M1 and M2 show significantly enhanced antibacterial performance. Among them, M1 reduces the survival rate of *E. coli* from 100% to 50% within 16 minutes; M2 went a step further, reducing the survival rate to 0% at the same time, showing excellent bactericidal effect. This superior antibacterial ability is mainly attributed to M2's superhydrophilic surface, which can effectively trap bioaerosols and significantly increase the chance of contact with bacteria, thus enhancing antibacterial properties.

In summary, the silver nanoparticle superhydrophilic nanofiber membrane developed in this study shows excellent antibacterial performance and multi-functional properties, providing a new idea to solve the shortcomings of traditional antibacterial materials, and has broad application prospects, laying a solid foundation for technological innovation in the field of public health protection.

# 4 Capillary Condensation-Driven Mechano-Bactericidal Superhydrophilic Textiles for Rapid Airborne Bacteria Inactivation: Synthesis, Characterization, and Application

## 4.1 Introduction

Bacterial colonization, especially when using medical devices in a medical setting, is a very important cause of infection [173]. A number of solutions have been proposed to deal with the problem, including the development of efficient sterilization protocols and materials/coatings with antimicrobial properties. However, these methods still show some limitations; thus, a more promising alternative strategy is the use of mechanically bactericidal surfaces [174-176]. Designed geometric textures and patterns at certain microscopic and nanoscale sizes on its surface are the prime weapons, because a surface enables physical destruction to bacterial geometrical structures, thus injuring them [15, 177, 178]. Interaction between bacteria coming in contact with the surface makes their cells elicit obvious physical mechanical destruction, hence results in killing [179]. Mechanical bactericidal surfaces have the extra beneficial feature than traditional chemical-based active approaches in respect that they could ensure the required action by physically deterring bacteria from becoming antimicrobially resistant. Therefore, such a surface is effective in combat against bacterial infection and helps in reducing healthcare-associated infections.

Capillary condensation occurs when water vapor condensates into confined geometries [180, 181], such as soil particles and sugar powders, at a partial pressure ($P$) below the saturation vapor pressure ($P_0$), as described within Kelvin equation [182, 183]:

$$\ln\frac{P}{P_0} = -\frac{2\gamma V_m \cos\theta}{r_1 RT} \qquad \text{Equation 4.1}$$

where $r_1$ is the meniscus curvature radius of the condensed water; $\gamma$ is the surface tension; $V_m$ is molar volume of the condensate; $\theta$ is the contact angle of the water against the solid wall. Capillary condensation typically results in a dynamic liquid bridge that forms a saddle-shaped volume liquid between wetting surfaces and induces a strong attraction based on air relative humidity (RH) and surface wettability.

In this study, the capillary condensation can significantly enhance mechanical bactericidal activity by inducing significant mechanical strain and deformation between superhydrophilic nanostructures and bacteria. This mechanism of action provides a new perspective on the antimicrobial properties of mechanical bactericidal surfaces. Specifically, the representative aerosol bacteria had significantly lower survival rates on superhydrophilic nanorods (S-NRs) surfaces compared to unmodified nanorods (NRs). For example, at about 30% relative humidity, the bacterial survival rate of S-NRs is 0%, while the bacterial survival rate of NRs is still as high as 40.8%.

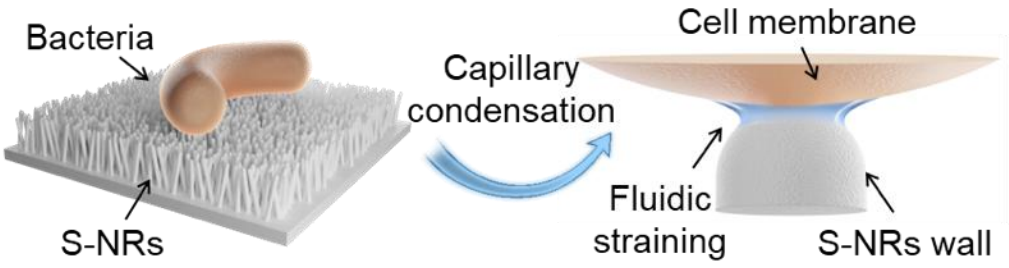


Figure 4.1 Capillary condensation driven fluid stretching mechanism and its application in bioaerosol disinfection conceptual design. When the humidity of the air between the cell

membrane and the S-NRs (modified nanorods) wall is lower than the saturated vapor pressure, spontaneous condensation occurs, forming a saddle-like liquid structure. The formation of a liquid meniscus induces the capillary tensile effect, which is driven by the combined action of surface tension and Laplacian pressure.

In addition, this mechanical bactericidal mechanism avoids the problem of antimicrobial resistance that can be caused by traditional chemical bactericidal methods. The formation of strain induced by capillary condensation in mechanical bactericidal systems can effectively enhance the antimicrobial properties and achieve a more environmentally friendly bactericidal strategy. This discovery provides a significant scientific foundation for the development of new antibacterial materials and coatings, and also provides a broad prospect for antibacterial technology innovation in the fields of medical devices, air filtration and food packaging.

## 4.2 Experimental Section

### 4.2.1 Materials

Zinc acetate was purchased from Sinopharm. Ethanolamine (AR, 99%) and 2-Methoxyethanol (AR) were purchased from Aladdin. Zinc nitrate hexahydrate (98%) was purchased from Alfa Aesar. Hexamethylenetetramine (99%) was purchased from international laboratory USA. 3-Methacryloxy propyl trimethoxy silane (KH570, 97%) was purchased from Alfa Aesar. Benzophenone (BP, 99%) was purchased from J&K Scientific. N-Vinylpyrrolidone (NVP, 99%) and glutaraldehyde (50% aq. soln. 50% aq) were purchased from Alfa Aesar. Phosphate-buffered Saline (PBS, pH 7.4) was purchased from Sigma. Nutrient agar (022021) and nutrient broth (022010) were purchased from HKM. SYTO 9 (3.34 mM in dimethylsulfoxide) and Prodium iodide (PI, 20 mM in dimethylsulfoxide) were purchased from Thermo Fisher

Scientific. Potassium nitrate ($KNO_3$, AR) was purchased from DAMAO. Lithium bromide (LiBr, 99%), potassium acetate ($CH_3COOK$, 99%), magnesium chloride ($MgCl_2$, 99%) and potassium carbonate ($K_2CO_3$, 99%) were purchased from Aladdin. Magnesium nitrate hexahydrate ($Mg(NO_3)_2 \cdot 6\ H_2O$, 99%) was purchased from Sigma-Aldrich. Potassium iodide (KI, 99%), potassium chloride (KCl, 99%) and sodium chloride (NaCl, 99%) were purchased from Aladdin. Ethanol (AR) was purchased from UNI-CHEM. Deionized water was produced from Thermo Scientific. PP melting blown cloth was purchased from DOCTOR MASK. The PP melt-blown nonwoven cloth has a basis weight of about 25 g/m² and consists of fibers with diameters ranging from 1 to 5 μm. Polyethylene Terephthalate (PET) fabric was provided by China Dyeing Holdings Ltd., Hong Kong. The woven PET fabric has a basis weight of about 110 g/m² and consists of fibers with diameters about 10 μm. Nylon fabric was provided by China Dyeing Holdings Ltd., Hong Kong. The woven Nylon fabric has a basis weight of about 140 g/m² and consists of fibers with diameters about 10 μm.

### 4.2.2 Preparation of Nanorods (NRs) and Superhydrophilic Nanorods (S-NRs)

#### 4.2.2.1 Fabrication of NRs and S-NRs on Glass Slide

Zinc oxide (ZnO) is widely used in many biomedical fields because of its excellent biocompatibility, safety, and long-lasting stability. A classical hydrothermal method was used to prepare ZnO NRs as typical nanostructures for evaluating strategy performance. To achieve capillary condensation between the tip of NRs and bacterial cell membranes, S-NRs were designed by grafting highly hydrophilic PVP onto the surface of NRs. PVP was chosen not only for its excellent hydrophilicity, but also for its non-toxicity, chemical stability, and ease of fixation on solid surfaces [184, 185].

First, the ZnO seed solution was prepared: 3.3 g of zinc acetate and 0.915 g of ethanolamine were dissolved in 30 g of ethylene glycol methyl ether, and ultrasonic treatment was performed to ensure that there was no longer any sediment in the solution. Then, ZnO growth solution was prepared: 2.975 g of zinc nitrate hexahydrate and 1.4 g of hexamethylenetetramine were dissolved in 1 L of distilled water, and the transparent solution was obtained after ultrasonic treatment. In the preparation of ZnO nanorods (NRs) by hydrothermal method, glass sheets were first immersed in distilled water and ethanol respectively, and ultrasonic cleaning was carried out for 15 minutes each to remove surface impurities. Subsequently, the glass sheets were uniformly coated with ZnO seed solution through a spinning coating device (KW-4A, Institute of Microelectronics, Chinese Academy of Sciences) and heated on a 230 °C heating plate (Heidolph) for 15 minutes to form a stable seed layer. Next, the glass sheets were immersed in ZnO growth solution and heated at 85 °C for 9 hours to promote the growth of the nanorods. When finished, rinse the glass sheet with deionized water and dry it in the air.


Figure 4.2 Fabrication process of S-NRs.

In this work, the surface of NRs was modified through $O_2$ plasma pre-treatment and UV-induced graft polymerization of NVP, to fabricate S-NRs (Figure 4.2). The NRs was first placed in an inductively coupled plasma (ICP) etcher (Trion, Phantom RIE ICP) and treated in an oxygen atmosphere of about 10 mT for 180 seconds. In this step, the surface was uniformly modified by polar groups [186]. This change improved the wettability of hydrophilic NVP and BP solution on the surface. KH570, as a silane coupling agent, acts as a molecular bridge

between the inorganic surface of the NRs and the organic monomer NVP. It can enhance the grafting efficiency and adhesion stability of the polymer [187]. NRs was then immersed in KH570 solution for 4 hours and dried successively, and then immersed in BP solution (initiator) for 15 minutes before drying. Finally, the NRs was immersed in the NVP monomer solution and subjected to ultraviolet irradiation for 1.5 hours for polymerization, and finally the S-NRs was obtained.

#### 4.2.2.2 Growth of the NRs and S-NRs on Cloth

First, the cloth was soaked in ZnO seed solution for 30 minutes to fully adsorb it. The fabric was then placed on a heating plate and heated at 100°C for 15 minutes for drying and fixing. Next, the cloth was immersed in ZnO growth solution and heated at 85°C for 12 hours to promote the growth of ZnO nanostructures. When done, rinse the fabric with deionized water and let dry in the air. Finally, the fabric surface was treated according to the same modification steps as the glass sheet, and the functional fabric based on S-NRs was successfully prepared.

### 4.2.3 Characterization

The morphologies of NRs and S-NRs were observed by obtaining SEM images on a Tescan MAIA3 at an acceleration voltage of 5 kV. Energy dispersive X-ray spectroscopy was carried out to analyze the elemental composition of NRs and S-NRs. Besides, the chemical differences between NRs and S-NRs were characterized by XPS and FT-IR.

### 4.2.4 Validation of Ultrasonic Rinsing for Bacterial Cell Recovery

The fluorescence microscopy imaging of *E. coli* and *S. aureus* before and after ultrasonic cleaning was performed. Images before and after the ultrasonic cleaning were compared in order to systematically evaluate the performance of the ultrasonic cleaning in the process of bacterial removal. Imaging was performed to visually record the changes in the distribution of bacteria across the sample surface during the entire experiment, and the changes both before and after cleaning to provide a key observation for verifying the effect of the ultrasonic cleaning.

### 4.2.5 Antibacterial Tests

To prepare bacterial aerosols, *S. aureus* (ATCC 6538) and *E. coli* (CMCC 44102) were selected. First, a single colony on a solid LB agar plate was inoculated into a 10 mL broth and cultured at 37 °C for 24 hours. The cultured bacterial solution is cleaned with PBS (phosphate buffer), and the bacterial precipitate is collected using a Centrifuge (Thermo Fisher Scientific, Centrifuge Pico 17). Subsequently, the bacterial precipitation was re-suspended in PBS to obtain the bacterial suspension for the experiment, and its concentration was determined by gradient dilution method and colony forming unit (CFU) counting method. 5 mL bacterial solution with a concentration of $10^7$ CFU/mL was added to a compression atomizer (XBK, MCN-S600MF) to produce bioaerosol. Prior to this, a microscope (Nikon, SMZ1270) was used to observe the deposition of water droplets generated by the spray on the glass sheet to determine the optimal spray distance. In the antimicrobial performance test, I sprayed a bacterial aerosol with a concentration of $10^7$ CFU/mL from 25 cm from the surface of the sample for 30 seconds, exposing it to *E. coli* for 6 minutes and *S. aureus* for 20 minutes or more. The bacteria on the surface of the sample were then transferred to an agar plate by ultrasonic cleaning and cultured at 37 °C for 24 hours to assess the antibacterial properties of

the sample. To further characterize the living state of the bacteria, I used green fluorescent dye SYTO 9 and red fluorescent dye PI to stain the bacterial suspension. After 20 minutes of dyeing, wash and dilute the suspension with PBS. Subsequently, the fluorescence signatures of the bacteria were observed and recorded using a fluorescence microscope (Nikon Eclipse Ti2) to distinguish between living and dead cells. In addition, to study the influence of humidity on antibacterial performance, the humidity conditions were adjusted by saturated solution method, and antibacterial experiments were carried out under different humidity to systematically evaluate the antibacterial performance of samples.

### 4.2.6 Determination of Spray Distance

Droplets generated by the aerosol generator at different spray distances (5 cm, 15 cm, and 25 cm) were observed under a microscope, and the characteristics of their distribution on the surface of the glass sheet were analyzed in detail. Meanwhile, the number of newly formed water droplets per second was accurately recorded to evaluate the influence of spray distance on the deposition behavior of water droplets.

### 4.2.7 SEM Characterization of Bacteria Deposited

The bacteria were extracted from the sample by ultrasound treatment and washed three times with PBS solution to remove impurities. The bacterial samples were then immobilized in a PBS solution containing 2 wt% glutaraldehyde and kept overnight at 4°C. The fixed sample was cleaned three times with deionized water (DI water). For dehydration, the samples were successively dehydrated with gradient ethanol/aqueous solution at each concentration (30%, 50%, 70%, 90%, 95%, 100%) for 1 hour. Finally, a layer of gold film was uniformly coated on the surface of bacterial cells for easy scanning electron microscopy (SEM) observation.

### 4.2.8 Water Contact Angle Measurements of Bacterial Surface

After 24 hours of culture, *E. coli* cells were collected by centrifugation (8000×g, 15 minutes) and rinsed twice with 0.1 M potassium nitrate ($KNO_3$) solution before being re-suspended. Subsequently, 10 mL of bacterial suspension was filtered through a 0.45 μm cellulose acetate filter membrane. Under the effect of negative pressure filtration, a dense bacterial layer was formed on the filter membrane with a cell density of $10^8$ cells /$mm^2$. The wet membrane is then placed on a glass sheet and allowed to dry naturally for 90 minutes. Finally, the water contact angle was measured using the hanging drop method to provide parameters to support subsequent simulation studies.

### 4.2.9 Simulation Method

In this study, molecular dynamics (MD) simulation was used to investigate the formation of liquid bridge tensile process and the interaction between S-NR (modified nanorods) and bacteria in a wet environment. By simplifying the model, S-NR was simplified as a spherical column shape and bacteria as a cylinder shape, and the simulation region was set to 80 nm × 80 nm × 40 nm. The surface tension of water molecules (66 mN/m) can be accurately reproduced using the classical mW model. The interaction between the solid and water molecules is described by a 12-6 Lennard-Jones potential function, with the desired wettability achieved by adjusting the parameter $\varepsilon_{s\text{-}w}$.

Eight humidity conditions were simulated by gradually generating water molecules to reflect humidity levels. The static method is used to measure the bonding force of liquid bridge, which avoids the error caused by the velocity dependence in the traditional dynamic method. The motion of atoms and molecules is updated by the velocity Verlet algorithm, the simulation

platform is LAMMPS, and the trajectory visualization tool is OVITO. This study provides theoretical support for understanding the formation mechanism of liquid bridging force in humid environment and its effect on antibacterial properties.

## 4.3 Results and Discussion

### 4.3.1 Characterization NRs and S-NRs

The morphology of NRs and S-NRs were firstly observed by SEM imaging, as shown in figures 4.3 a and b. The height of S-NRs is about 1.2 μm, the centre distance is about 176 nm, and the diameter of S-NRS is increased from 58.8 nm to 60.9 nm (Figures 4.3 c-f). Further testing showed that the contact angle of S-NRs dropped to 0°, significantly lower than that of NRs (about 8°), which is visually demonstrated in Figure 4.4, reflecting the significant difference in wettability between the two.

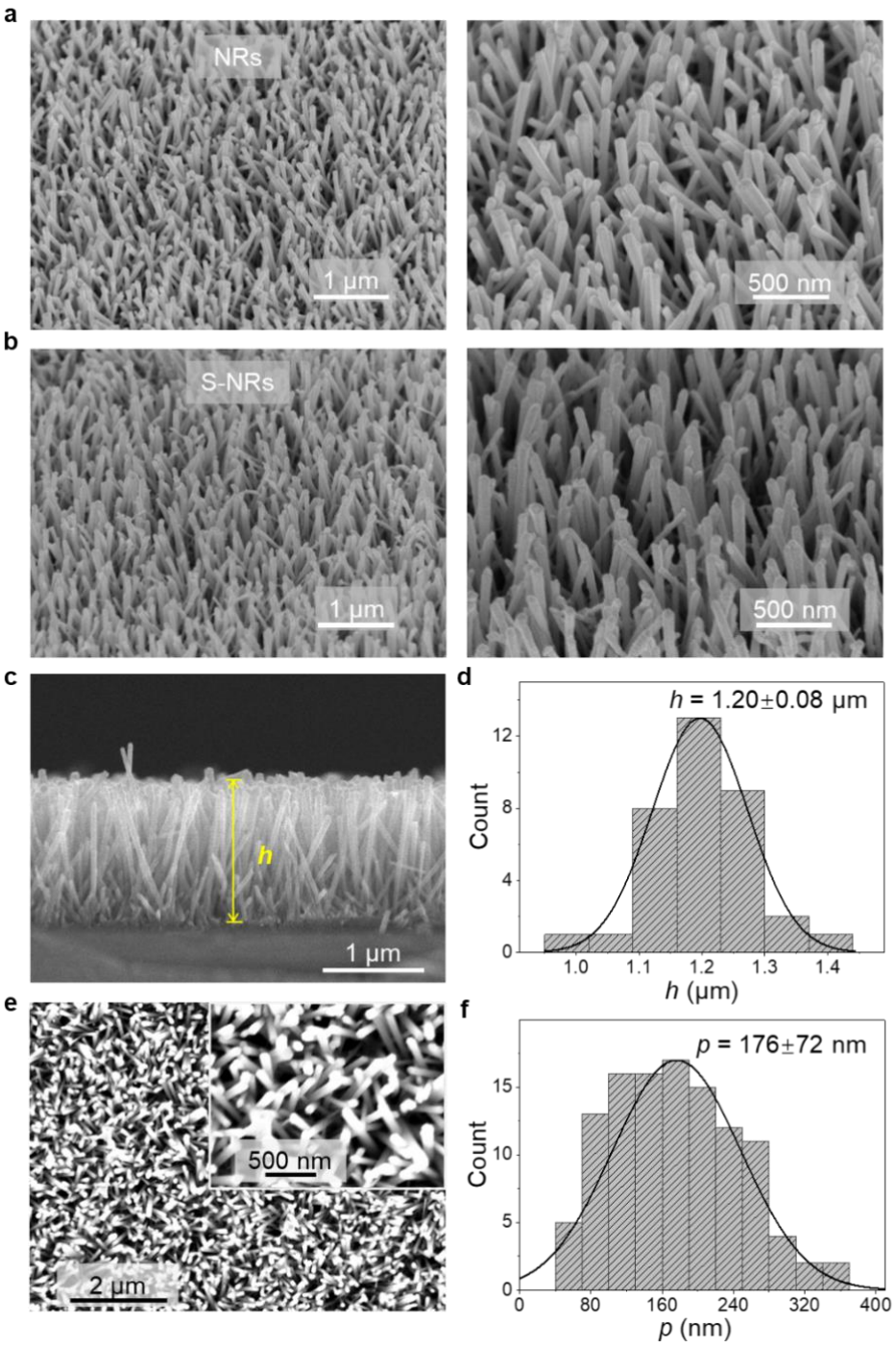


Figure 4.3 Morphology characterization of NRs and S-NRs. a, SEM image of NRs at 45° tilt angle. b, SEM image of S-NRs at 45° tilt angle. c, cross-sectional view of S-NRs. d, S-NRs height (*h*) distribution map. e, top view of S-NRs. f, S-NRs centre distance (*p*) distribution.

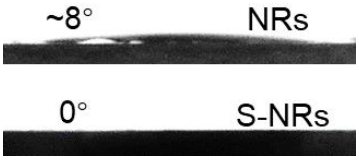


Figure 4.4 Water contact angle optical images of NRs and S-NRs.

Subsequently, the chemical composition of the surface was characterized using XPS, as shown in Figure 4.5. The results show that the 399.8 eV peak corresponds to the N 1s signal in the pyrrole ring. In PVP modified NRs, the C1s peak showed two distinct carbon components, namely aliphatic carbon (284.8eV) and amide (288.4eV).

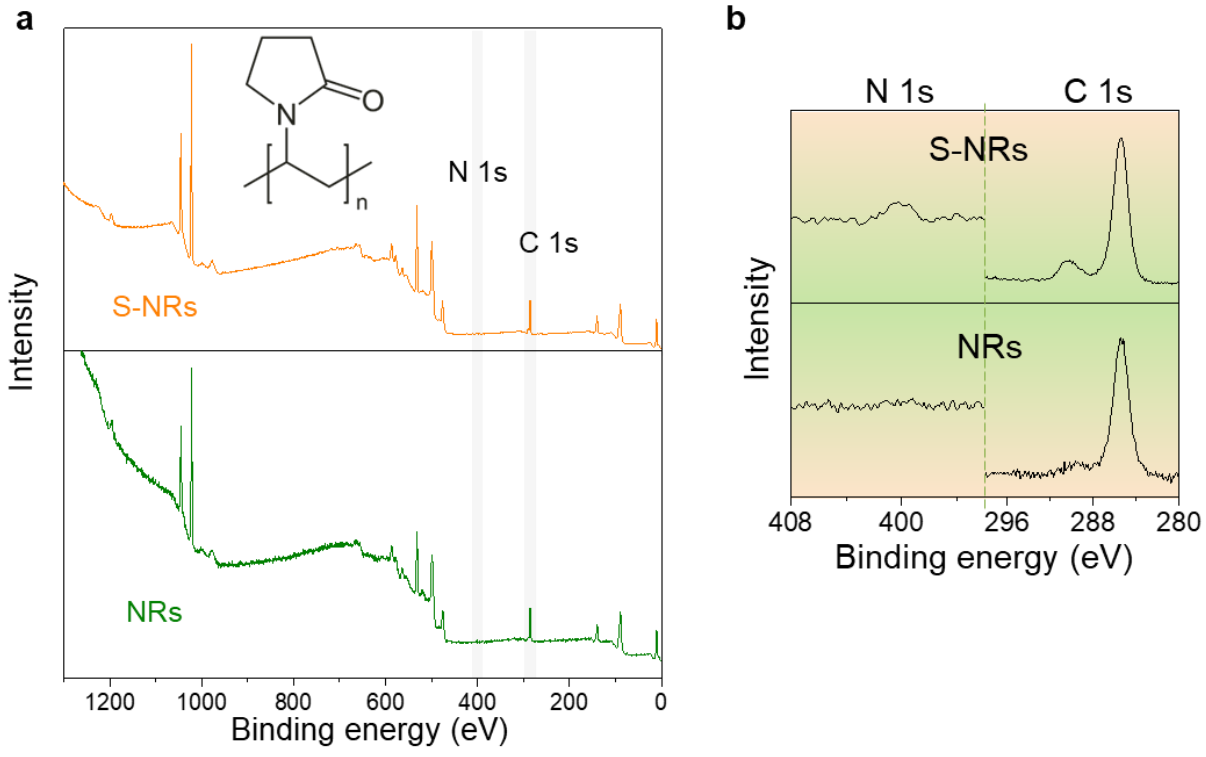


Figure 4.5 a, XPS spectrum of NRs and S-NRs. Inset in a is the chemical structure of PVP. b, High-resolution XPS of C 1s and N 1s peaks of NRs and S-NRs.

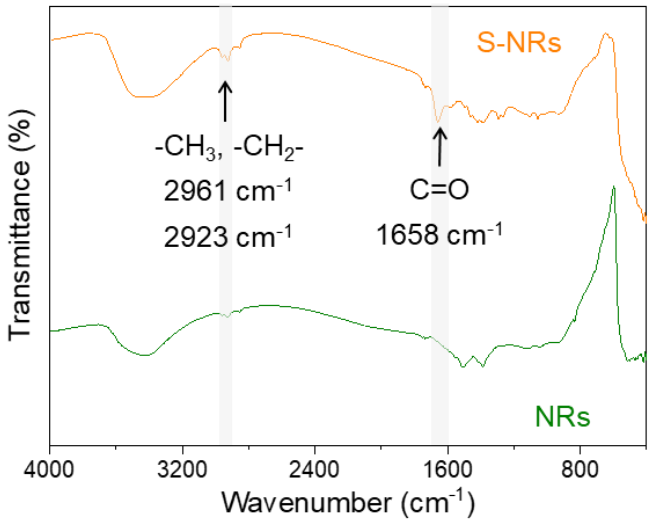


Figure 4.6 FTIR spectrum of NRs and S-NRs.

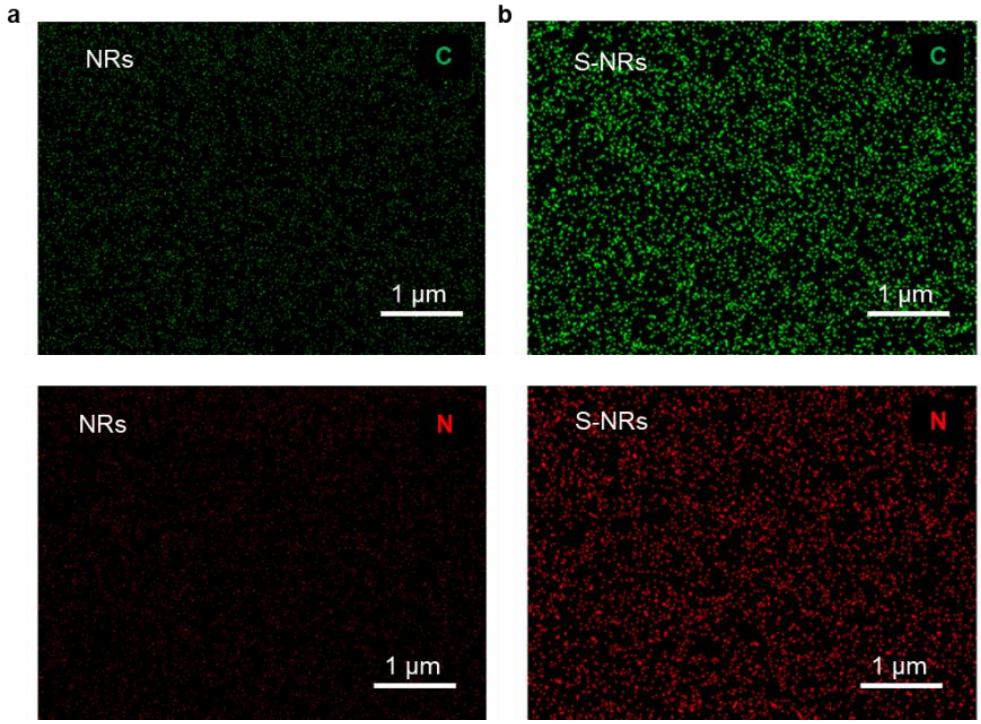


Figure 4.7 Elemental analysis of carbon and nitrogen in NRs and S-NRs. EDX mapping illustrates the elemental composition of NRs (a) and S-NRs (b), highlighting variations in element content.

The chemical properties of NRs and S-NRs were further analysed using Fourier transform infrared spectroscopy (FTIR) (Figure 4.6). The results show that in the infrared spectrum of S-NRs, there is a clear C-O absorption peak from the PVP amide group at 1658 $cm^{-1}$. In addition, absorption peaks of $-CH_3$ (2961 $cm^{-1}$) and $-CH_2-$ (2923 $cm^{-1}$) were observed in PVP. For NRs, the spectra show the presence of hydroxyl and water molecules on the surface, which may be in the form of chemisorption or physical adsorption and appear as a wide absorption band at about 3440 $cm^{-1}$. Due to the excellent water absorption properties of S-NRs, this absorption band is significantly enhanced in S-NRs. At the same time, a compositional analysis of NRs and S-NRs using energy dispersive X-ray (EDX) element distribution maps (Figure 4.7) confirmed significant differences in carbon and nitrogen content between the two. The above results fully verify the successful preparation of S-NRs.

### 4.3.2 Antibacterial Efficacy of S-NRs

The antimicrobial performance of S-NRs against bacteria-containing aerosols was evaluated at a relative humidity (RH) of 70%, focusing on *E. coli* and *S. aureus*. By observing the morphological changes of bacteria after contact with different surfaces, the antibacterial mechanism was discussed. In order to exclude the interference of light-induced reactive oxygen species, all antibacterial experiments were carried out under light conditions to highlight the study of mechanical mechanisms. In the experiment, bare glass (as control), NRs and S-NRs were selected as test samples. Notably, the ultrasonic device used in the experiment was able to effectively remove bacteria from flat glass surfaces without affecting their survival rate (see Figure 4.8).

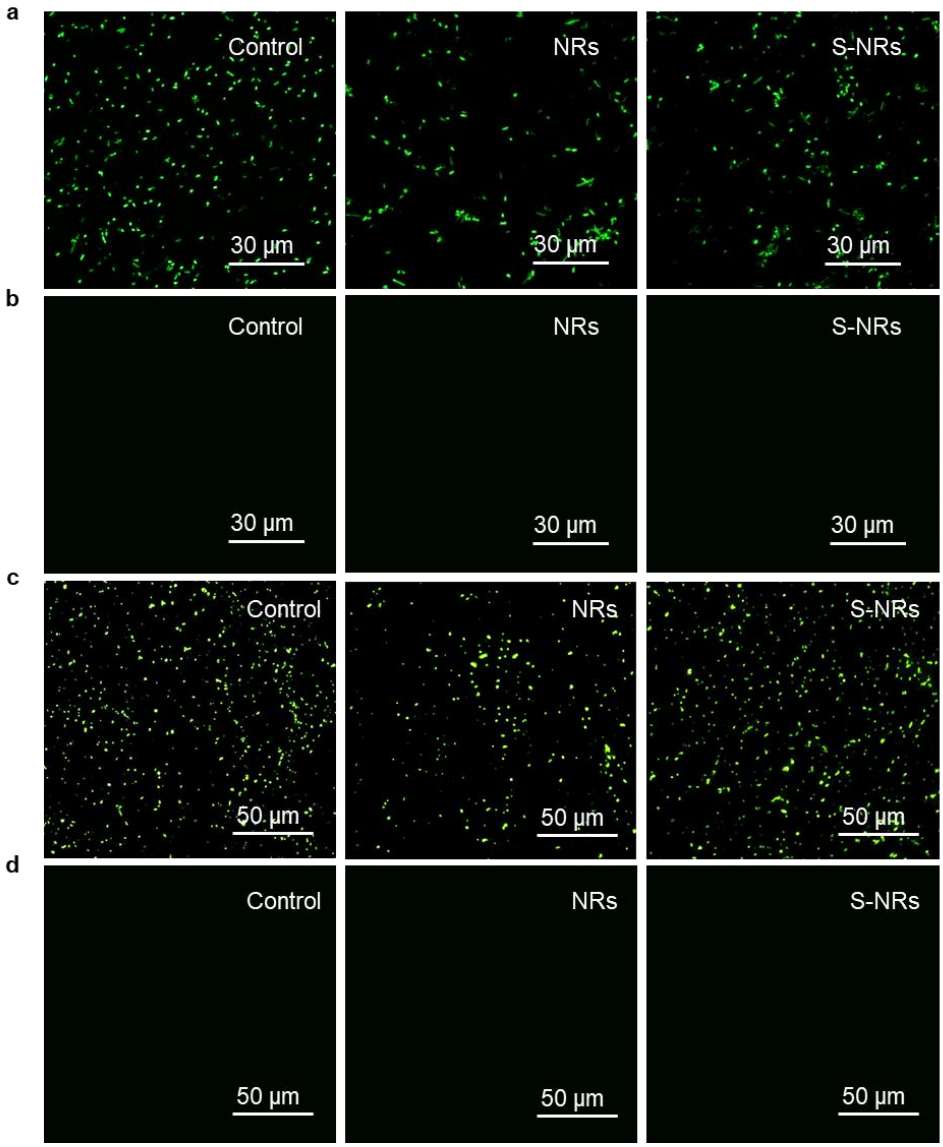


Figure 4.8 Assessment of the ultrasonic rinsing method for bacterial cells. Fluorescent microscope images captured before (a, c) and after (b, d) ultrasonic rinsing demonstrate the effective removal of *E. coli* (a, b) and *S. aureus* (c, d) from control, NRs, and S-NRs surfaces.

Through microscope observation, the distribution of water droplets formed on the glass surface of the aerosol generator was analysed at different spray distances (5 cm, 15 cm and 25 cm), and recorded the number of new water droplets formed per second. As shown in Figure 4.9,

when the spray distance is 25 cm, almost no new water droplets are generated on the surface of the glass sheet, which indicates that 25 cm is the optimal spray distance for the experiment.

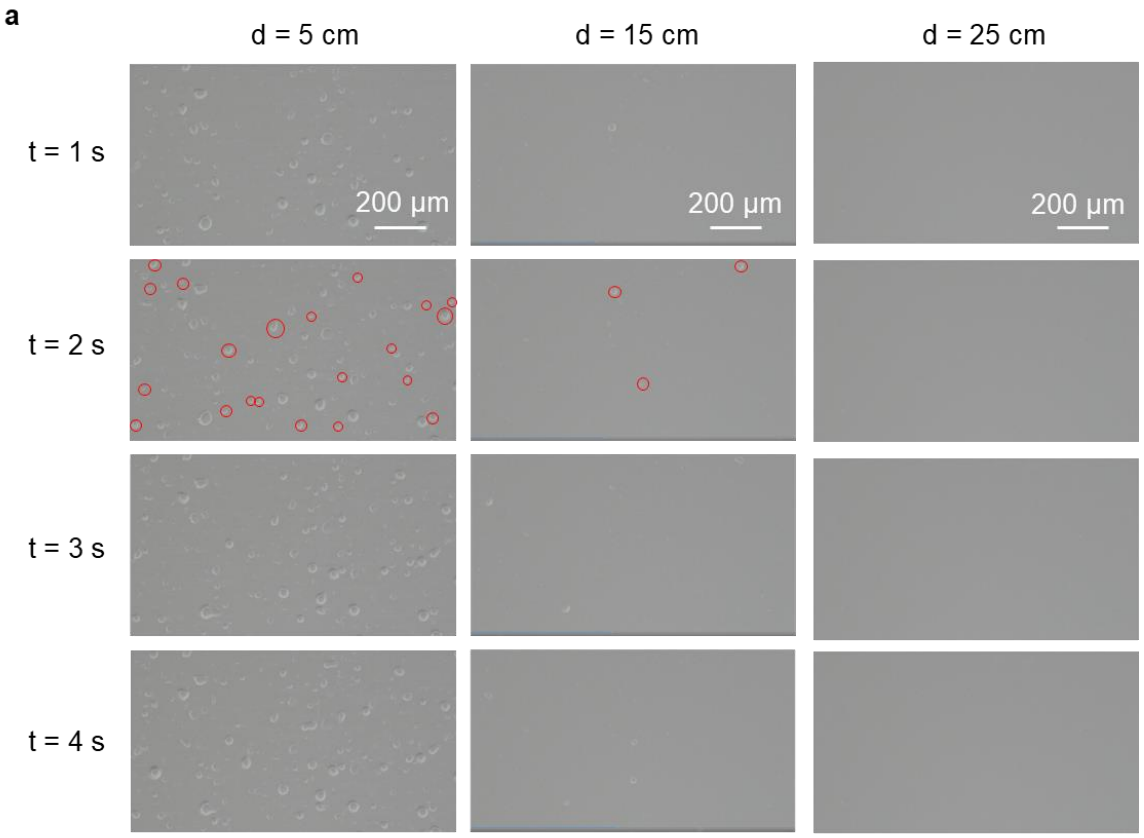


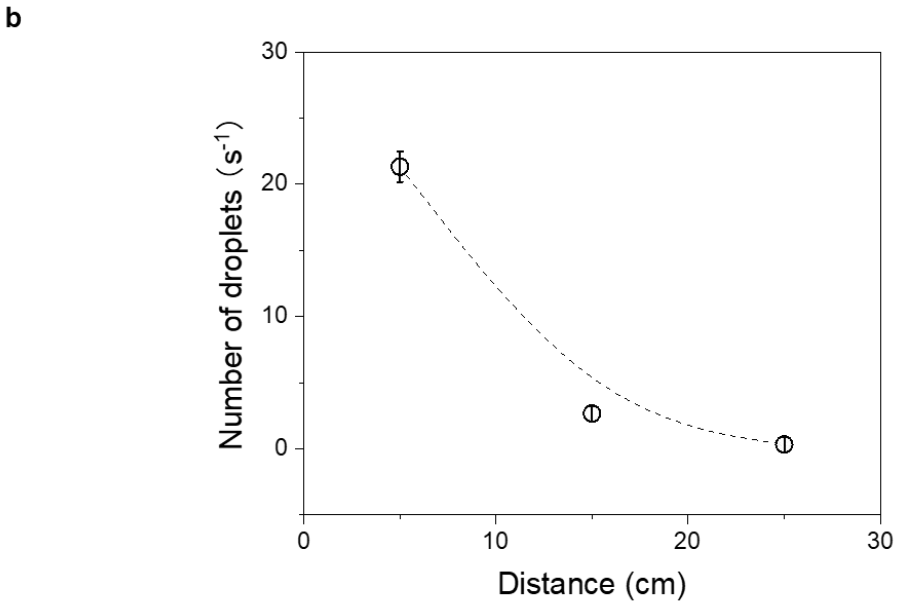

Figure 4.9 Determination of spray distance. a. Use a microscope to observe the distribution process of water droplets formed on the surface of the glass sheet by the aerosol generator at different spray distances. b. Record the number of new water droplets formed on the glass sheet per second by the aerosol generator at different spray distances. The error bar represents the standard deviation, and the experiment is repeated 5 times per data point (n = 5).

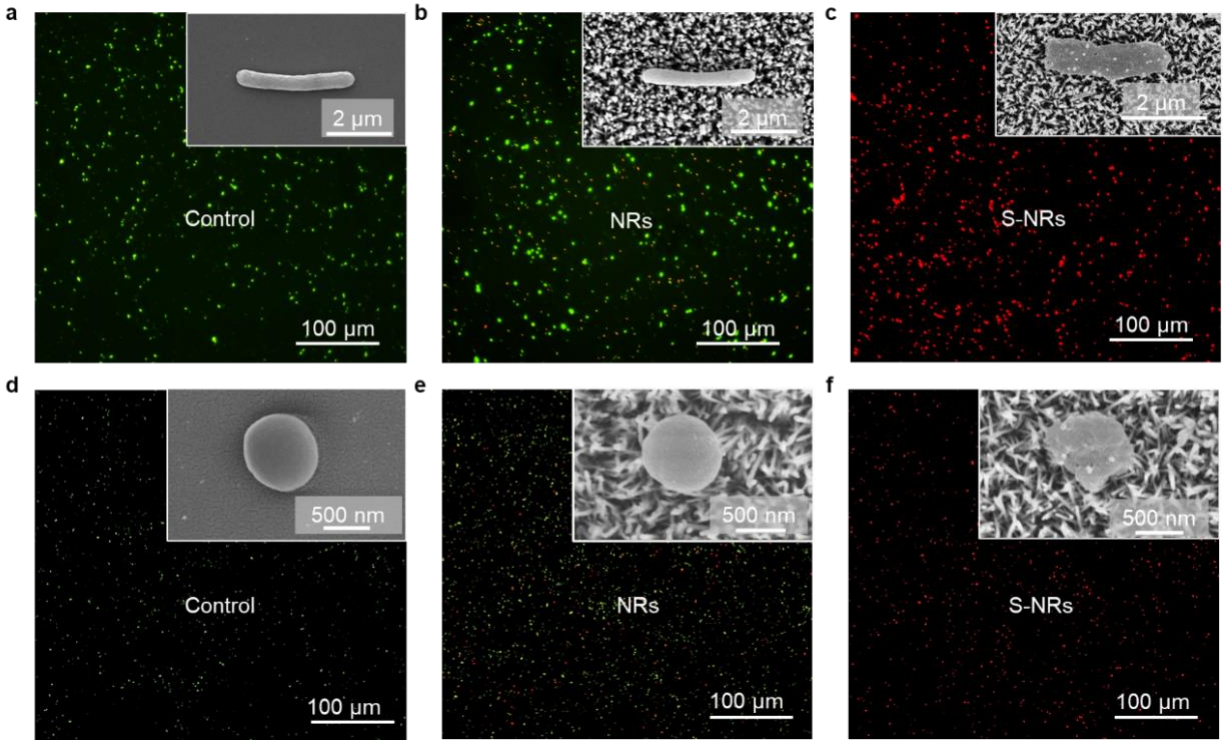


Figure 4.10 Representative fluorescent microscopy images showing dead (red) and live (green) *E. coli* (a-c) and *S. aureus* (d-f) after deposition on control surfaces (a, d), NRs (b, e), and S-NRs (c, f). Insets display SEM images of individual bacterial cells.

In the antibacterial experiment, the bacteria that came into contact with the three surfaces were firstly cleaned and stained them with the cell impermeable red dye propyl iodide (PI). PI can only enter cells with damaged cell membranes. This was followed by contrast staining with the permeable green dye SYTO 9, which can label nucleic acids in living cells. As shown in Figure

4.10 a-c, a large number of live cells (green) were observed in *E. coli* exposed to both the control group and the NRs, while some dead cells were also present, indicating that the NRs had some antimicrobial capacity. However, after contact with S-NRs, the green fluorescence signal almost completely disappeared, indicating that the bacterial cell membrane was damaged or lysed. This observation was further confirmed in the accompanying SEM images: *E. coli* cells in contact with the control group and the NRs retained a smooth surface and intact cell membrane, while cells in contact with the S-NRs showed significant membrane deformation and collapse. Similarly, the S-NRs surface showed significant bactericidal properties when treated with *S. aureus* (Figure 4.10 d-f). Survival was assessed by live/dead bacterial activity assays (Figure 4.11), and S-NRs exhibited superior antimicrobial performance compared to control groups and NRs.

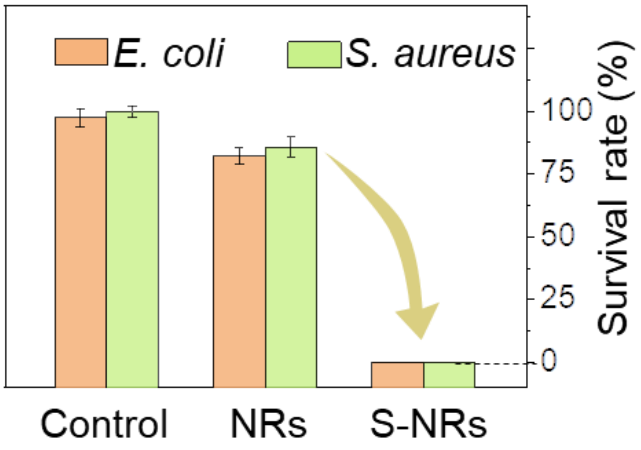


Figure 4.11 Survival rates of *E. coli* and *S. aureus* on control surfaces, NRs, and S-NRs, highlighting the significantly enhanced antibacterial efficacy of S-NRs.

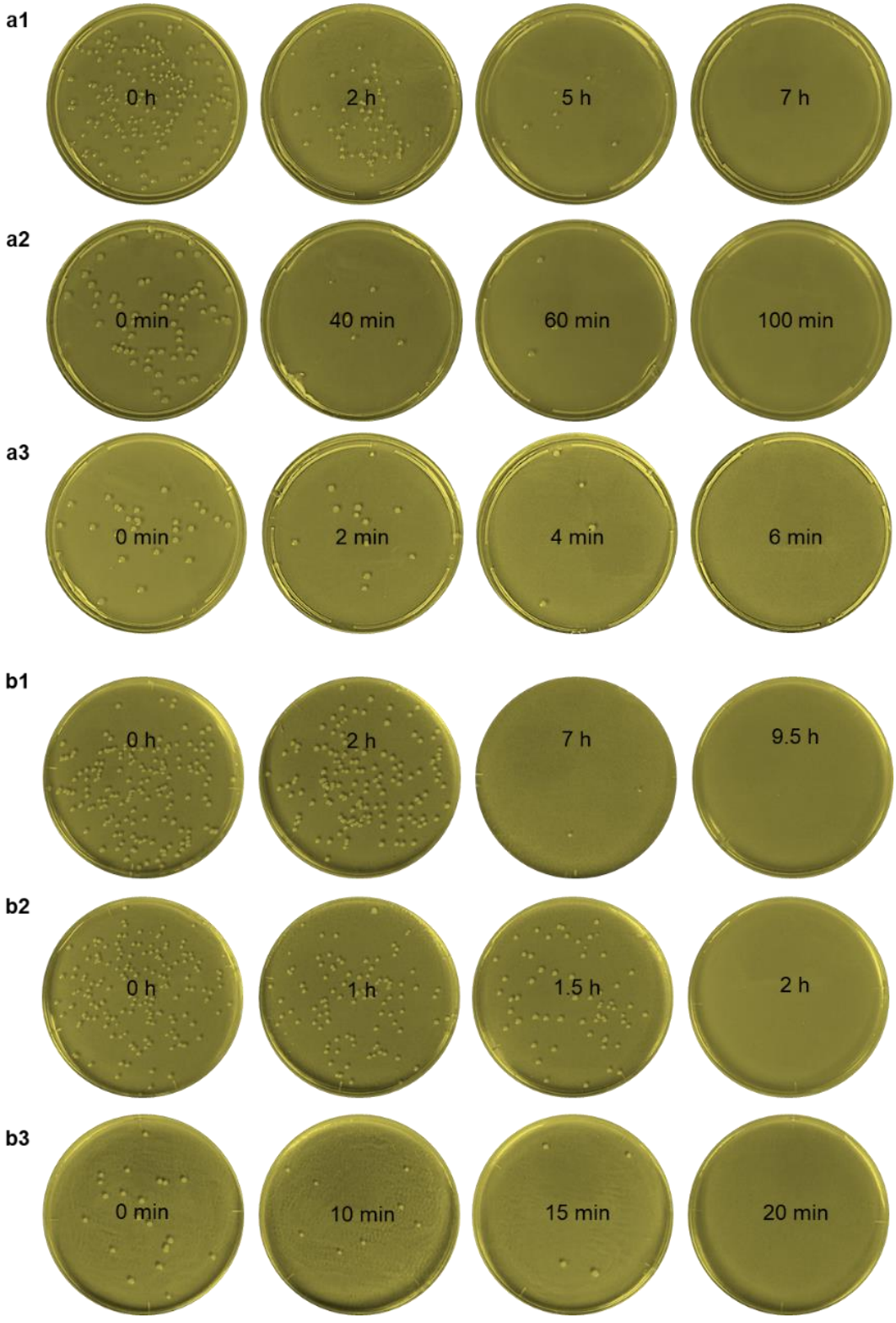


Figure 4.12 Optical images of representative agar plates showing transferred airborne *E. coli* (a) and *S. aureus* (b) after exposure to control surfaces (a1, b1), NRs (a2, b2), and S-NRs (a3, b3).

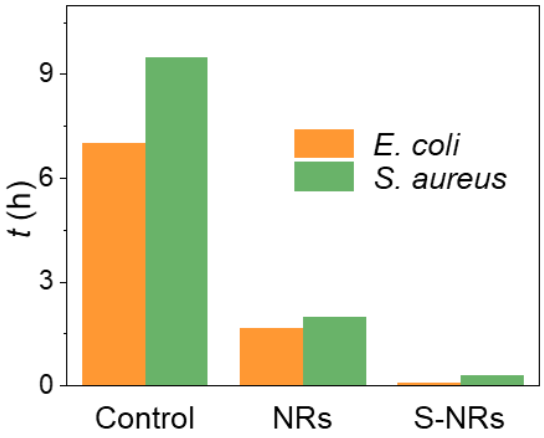


Figure 4.13 Time needed to eliminate all airborne bacteria deposited on control surfaces, NRs, and S-NRs.

In order to evaluate the antibacterial properties of S-NRs, contact sterilization experiments were carried out under the conditions of relative humidity of 70% to test the antibacterial effect under different contact times, and analysed by agar plate counting method. Figure 4.12 and Figure 4.13 show the growth of bacterial colonies in the control group, NRs and S-NRs on the agar plate at different times. The results showed that the control group required 7 hours and 9.5 hours for complete elimination of *E. coli* and *S. aureus*, respectively, while NRs significantly shortened the disinfection time by 1.7 hours and 2 hours, respectively. Notably, S-NRs demonstrated excellent antimicrobial ability, sterilizing airborne *E. coli* and *S. aureus* in just 6 minutes and 20 minutes, respectively. In addition, the survival rates of *E. coli* and *S. aureus* on three surfaces at different exposure times were assessed (Figure 4.14). The results further verified the enhanced bactericidal activity of S-NRs.

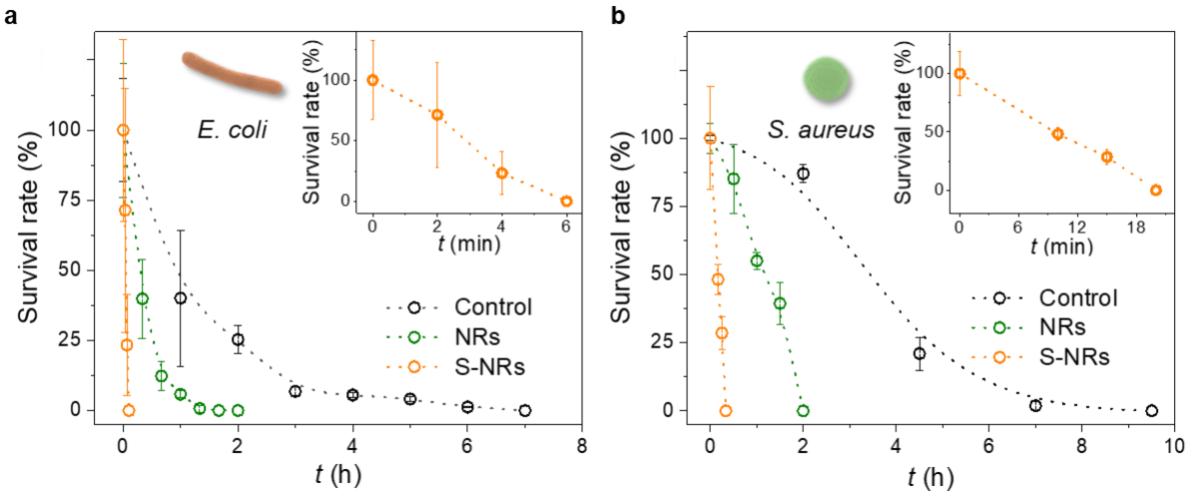


Figure 4.14 Time-dependent survival rates of *E. coli* (a) and *S. aureus* (b) on the tested surfaces, demonstrating the superior antimicrobial performance of S-NRs.

### 4.3.3 Mechanism of Capillary Straining in S-NRs

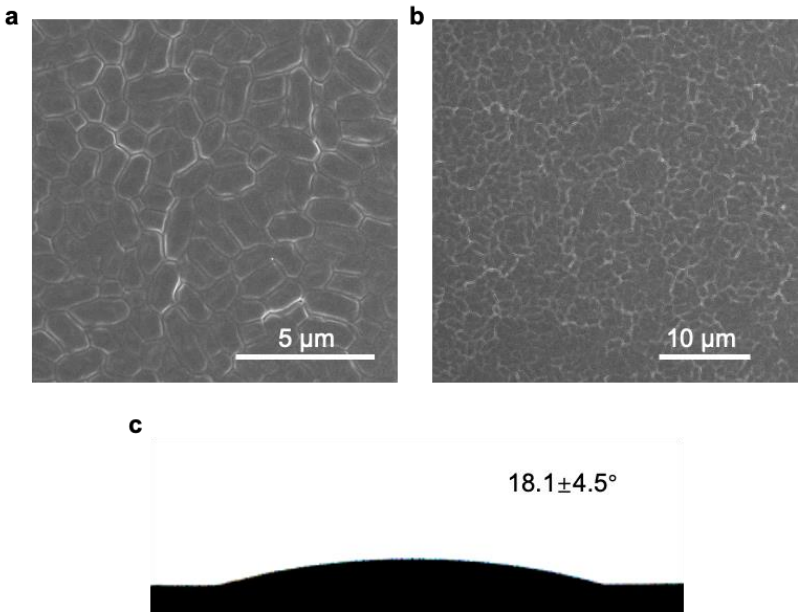


Figure 4.15 SEM (a and b) and water contact (c) angle of *E. coli* cells deposited on a cellulose triacetate filter.

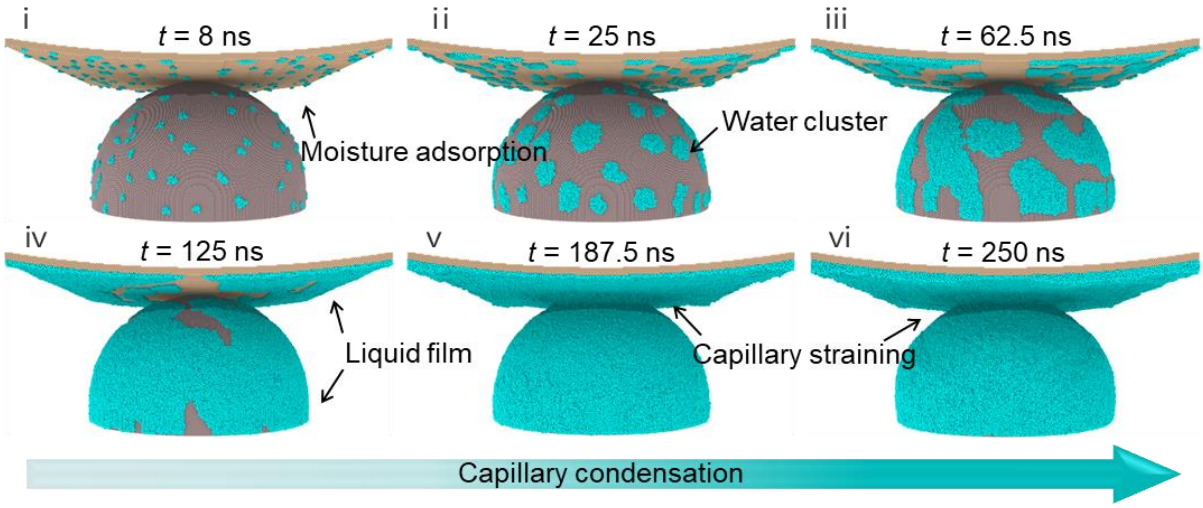


Figure 4.16 Simulated capillary straining process between S-NR and bacteria, excluding vapor molecules for clarity.

Molecular dynamics (MD) simulations were used to delve into the mechanism of condensation formation between S-NR and bacteria. The experimentally measured equilibrium contact angles of water droplets on S-NR and bacteria surfaces were 0° and 18°, respectively (Figures 4.4 and 4.15), which were important in the determination of potential parameters [187]. Figure 4.16 shows six time series snapshots of a typical condensation process. The simulation results showed that in the initial stage of condensation, vapor molecules adsorbed on the surfaces of S-NR and bacteria and gathered into randomly distributed clusters consisting of several to dozens of water molecules through intermolecular interactions (Figure 4.16 i). Over time, these clusters gradually expand into droplets by adsorbing more vapor molecules, and the droplets take on a film-like morphology due to the strong hydrophilicity of S-NR and the bacterial surface (Figure 4.16 ii). As condensation progresses further, water droplets continue to grow and fuse with each other, eventually forming a complete liquid film on the surface of S-NR and bacteria (Figures 4.16 iii and iv). In addition, the simulation results showed that most vapor molecules preferentially adsorbed to S-NR and other parts of the bacterial surface before

reaching the contact region, so no significant liquid bridge phenomenon was observed during the initial condensation period. When the liquid film on S-NR was fused with the liquid film on bacteria, the size of the meniscus increased rapidly. In the subsequent simulation process, the thickness of the liquid film and the size of the meniscus further increased with the adsorption of more vapor molecules (Figure 4.16 v and vi).

The effect of humidity on the capillary tensile force between S-NRs and bacteria was quantified through simulation studies at different relative humidity (RH) levels. RH levels were characterized by the number of water molecules in the simulated domain. When the simulation system reaches an equilibrium state, the tensile force value acting on the bacteria was obtained. As shown in Figure 4.17, the tensile force is highly correlated with the number of water molecules (i.e. RH) in the simulated domain. Specifically, when the number of water molecules increases from 0 to 500,000, the tensile force increases rapidly. At higher humidity, the tensile force decreases slightly, which is consistent with the existing experimental results. The dependence of tensile force on RH is closely related to the formation and size of liquid condensates. Under low humidity conditions, most of the water vapor molecules adsorbed on the surfaces of S-NRs and bacteria, forming small cluster-like structures that may further expand into larger droplets or films. In this case, however, no significant capillary condensation has yet formed, so the capillary tensile force is small (such as in the case of 125,000 water molecules). As RH increases, enough water vapor molecules in the environment encourage the formation of significant liquid Bridges that connect S-NRs and bacteria, resulting in a significant increase in tensile forces (such as in the case of 375,000 to 875,000 water molecules). Additionally, it is worth noting that the enlargement of the condensates size leads to an increase in the radius of curvature $r_1$, which in turn reduces the corresponding forces $F_c$ (as seen in cases with 50,000 to 875,000 water molecules).

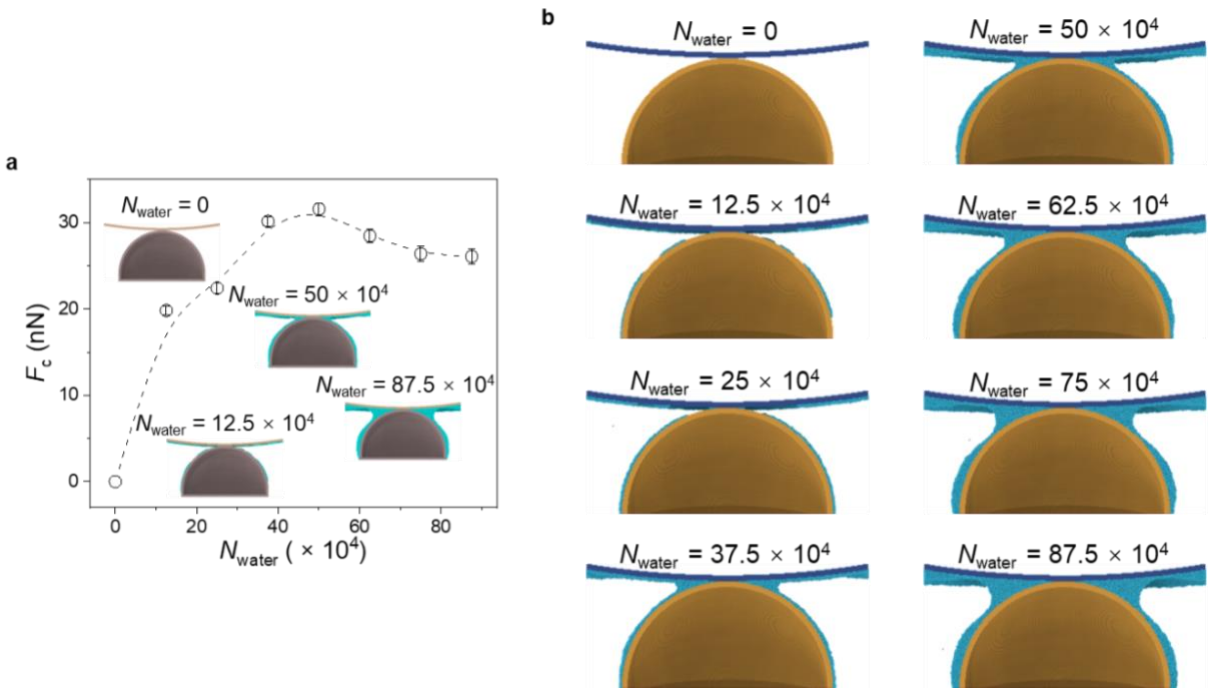


Figure 4.17 a, Relationship between capillary straining force $F_c$ and the number of water molecules $N_{water}$ present in the simulation system. b, Water molecules adsorption equilibrium state under eight RH levels, corresponding to 0, 125,000, 250,000, 375,000, 500,000, 625,000, 755,000, and 875,000 water molecules within the simulation domain, respectively.

$$F_c = 2\pi\gamma R \sin\Phi \sin(\Phi + \theta) + \frac{\gamma}{r_1}\pi R^2 \sin^2\Phi \qquad \text{Equation 4.2}$$

where $R$ is radius of the bacteria sphere; $\Phi$ is filling angle; $\gamma$ is the surface tension of the liquid; $\theta$ is the contact angle, shown in Figure 4.18. Notably, the calculated pressure is about 40 MPa, much higher than the ultimate tensile stress 13 MPa.

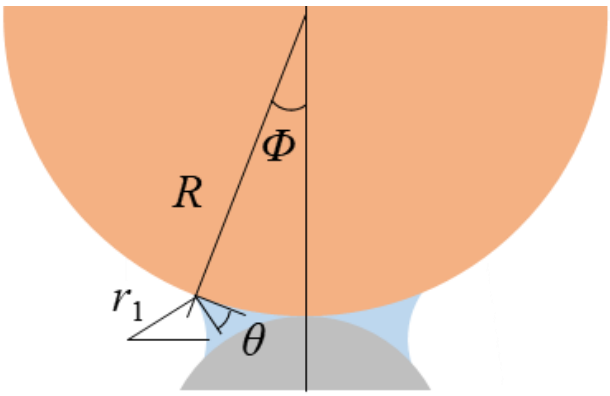


Figure 4.18 Schematic illustration of fluidic straining (blue region) occurring between bacteria (orange region) and S-NR (grey region).

As shown in Figure 4.19, with the increase of RH, the survival rate of bacteria on the surface of S-NR rapidly decreases to about 0% over a wide humidity range (RH ≥30%). This phenomenon is in stark contrast to ordinary NRs, which are only effective at killing most bacteria at RH > 90%. These results are highly consistent with experimental and theoretical data from previous studies.

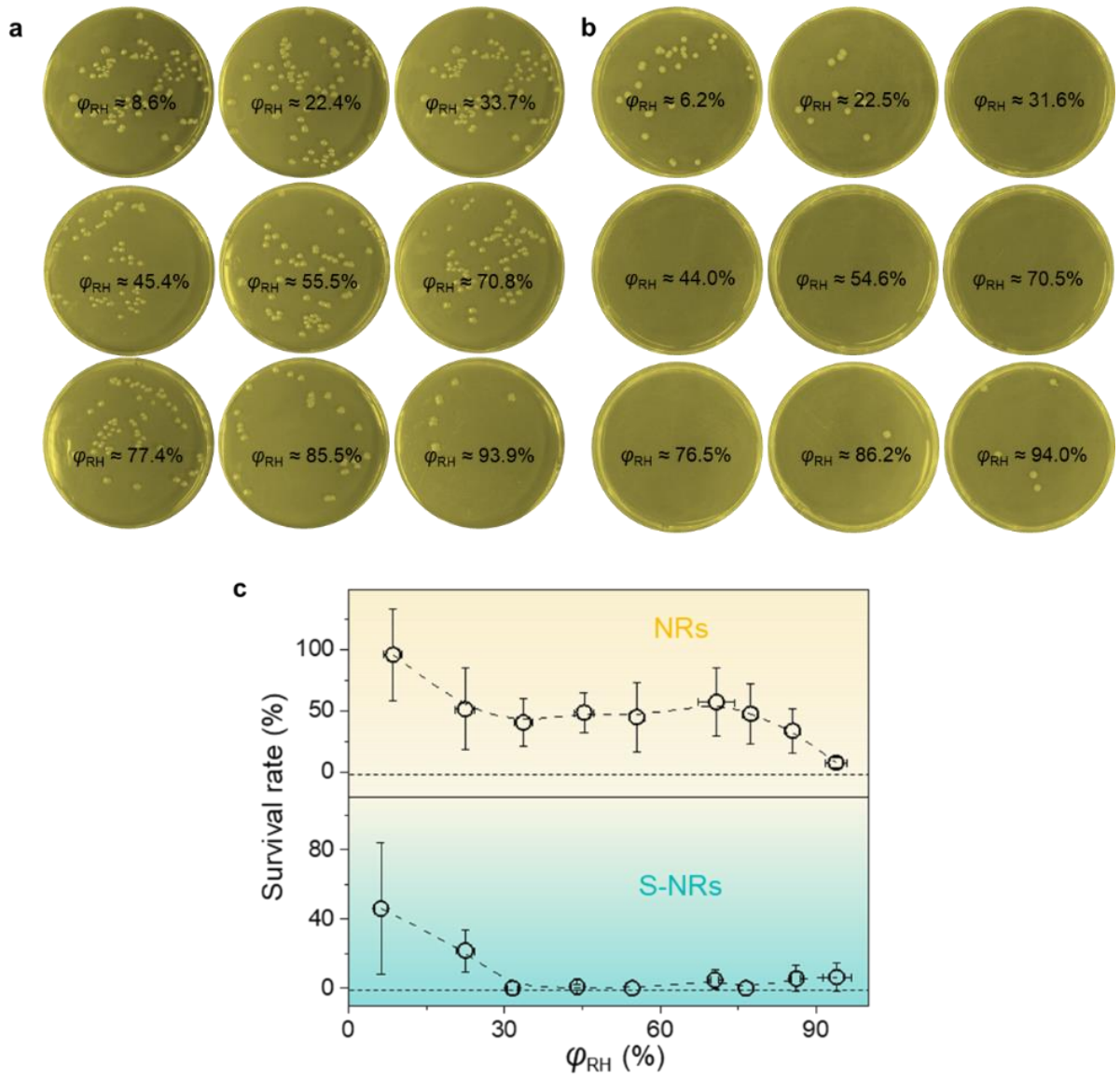


Figure 4.19 Representative agar plate images of antibacterial test results on NRs (a) and S-NRs (b) under different humidity. c, Dependence of bacterial survival rate on varying levels of RH ($\varphi_{RH}$).

4.3.4 Antibacterial Textiles

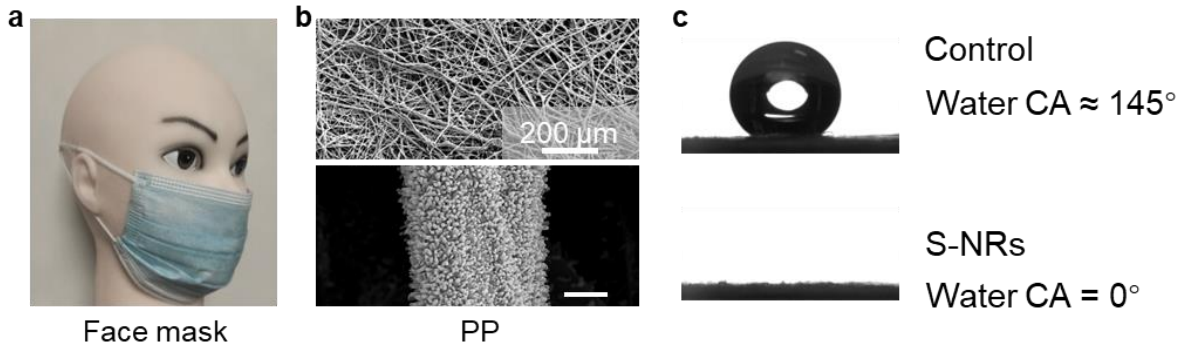


Figure 4.20 a,b, Optical image and SEM images of S-NRs on PP melt-blown fabric for medical masks. c, Water contact angle comparison between control and S-NRs-modified PP melt-blown fabric.

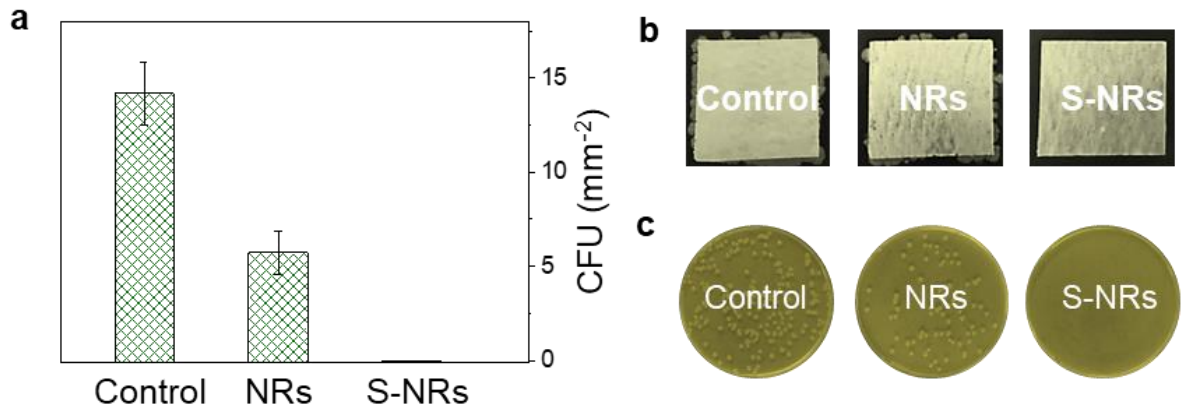


Figure 4.21 a, CFU count of *E. coli* on various PP fabrics. b, Representative photographs of the respective samples (2 × 2 cm²). c, Optical images of typical agar plates showing *E. coli* colonies from control, NRs, and S-NRs-modified PP fabrics.

S-NRs showed the potential application in personal protective equipment. Similar to the treatment of glass, polypropylene (PP) fiber cloths can be simply modified to combine with S-

NRs to become an antibacterial layer in masks (see Figure 4.20). Subsequently, its biological protection against *E. coli* was evaluated. After loading the bacteria-containing aerosol onto the PP cloth and touching it for 6 minutes (as shown in Figure 4.21), the S-NRs modified cloth showed high contact bactericidal effect, and the colony forming unit (CFU) was reduced to 0. In addition, the S-NRs modified PP cloth maintained excellent antimicrobial properties for up to six weeks (see Figure 4.22).

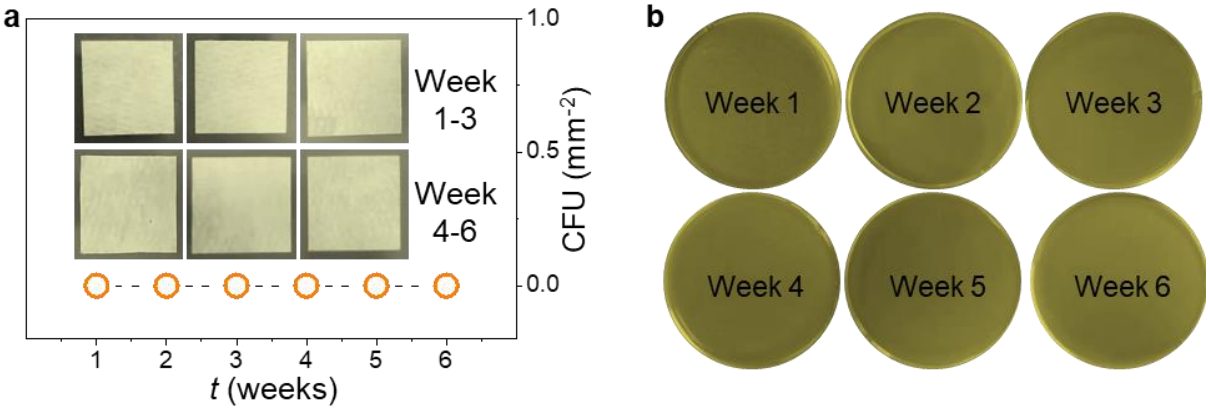


Figure 4.22 a, Colony formation assay showcasing the outstanding long-term antibacterial performance of S-NRs-modified PP cloth over a six-week period, with no CFUs observed (as shown in the inset images). b, Optical images of typical agar plates displaying *E. coli* colonies after a six-week antibacterial test with S-NRs-modified PP cloth.

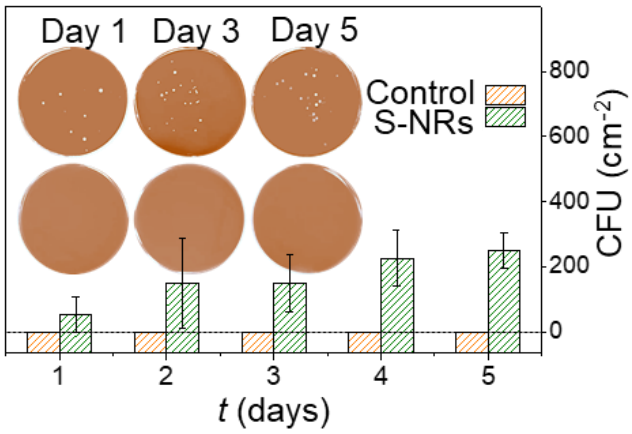

Figure 4.23 An untreated medical mask and a medical mask with S-NRs modified PP cloth as a filter layer were worn for five consecutive days to evaluate their antimicrobial properties.

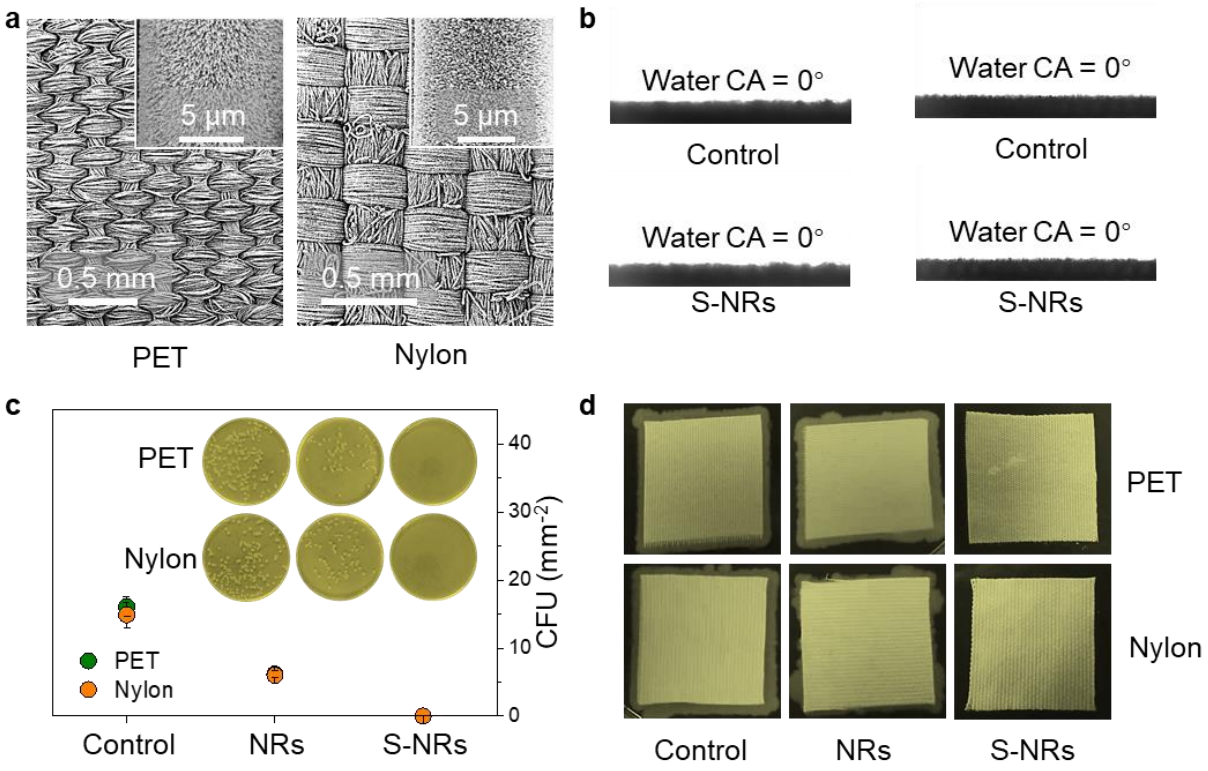


Figure 4.24 a, SEM images of S-NRs modified PET fabric (left) and nylon fabric (right). b, Water contact angle measurements of S-NRs modified PET and nylon fabrics. c, *E. coli* colony count (CFU) to demonstrate the difference in antimicrobial performance between the control group and S-NRs modified cloth.

The antibacterial properties of common commercial masks and commercial masks integrated with S-NRs modified melt-blown PP cloth were further studied. As shown in Figure 4.23, the modified mask maintained no detectable live bacterial residue for 5 days, compared to the gradually increasing levels of bacterial residue in normal commercial masks. In addition, the application of S-NRs is not limited to masks but can also be extended to other fabrics. Similar to its application on glass sheets and PP fabrics, S-NRs has been successfully introduced into

polyethylene terephthalate (PET) and nylon fabrics (Figures 4.24 a and b), fully demonstrating the wide applicability and practical value of the method. PET and nylon fabrics modified with S-NRs exhibit excellent bactericidal properties, as shown in Figures 4.24 c and d. These results indicate that S-NRs has great potential in protecting airborne pathogens by regulating the capillary condensation effect on fabric surfaces.

## 4.4 Conclusions

These results confirm the hypothesis that in the narrow space between bacteria and carefully designed nanostructures, the capillary condensation of liquid bridges can generate mechanical tensile forces that spontaneously destroy and kill microorganisms such as *E. coli* and *S. aureus*. This mechanism is based on the liquid bridge effect triggered by environmental humidity, using nanoscale surface tension to produce mechanical stretching, fundamentally destroying the bacterial cell structure, and achieving efficient sterilization. This discovery not only deepens the understanding of the mechanism of capillary cohesion and mechanical bactericidal theoretically, but also further validates the feasibility of its practical application through experiments and computational models.

In the study of superhydrophilic nanorods, the environmental humidity has a significant effect on the capillary condensation process and its antibacterial effect. This method is unique in that it does not rely on traditional chemical antimicrobials but achieves sterilization through natural physical effects. Compared with chemical antibacterial agents, this mechanical bactericidal method can not only reduce environmental pollution, but also effectively avoid the problem of bacterial resistance caused using chemical agents. This green antibacterial technology shows great application potential in killing bacteria in the air, providing a new way to develop antibacterial strategies based on natural environmental factors.

In addition, this study further extends the antimicrobial strategy of hydrostatics to the field of biological contamination resistance of biomedical devices and materials. For example, this technology can effectively prevent bacterial attachment and biofilm formation on the surface of medical devices. In terms of medical protective equipment, its ability to rapidly kill bacteria, long-term stability over a wide humidity range, and the characteristics of no side effects on the human body make it extremely valuable in practical applications. For example, surgical masks modified with S-NRs maintain excellent antimicrobial properties even in environments with fluctuating humidity. This not only significantly reduces the risk of pathogen transmission during surgery, but also provides an important basis for the future development of a new generation of antimicrobial protective equipment.

# 5 Polycationic Oligomer-Modified Superhydrophobic Textiles for Fast Elimination of Aerosolized Bacteria: Synthesis, Characterization, and Application

## 5.1 Introduction

Cell membrane binding refers to the interaction between molecules or nanomaterials (such as proteins, lipids, or drugs) and the cell membrane [188-190]. As a selective barrier, the cell membrane not only protects the cell, but also plays a key role in signal transmission, material transport and cell integrity maintenance [191]. This combination determines how cells communicate with their environment and other cells to perform important functions such as nutrient uptake, immune response, and signalling [192].

The adsorption of bacterial cell membranes to nanomaterials is a typical case, in which the specific interaction between nanomaterials and bacterial outer membranes is particularly significant [15, 193-195]. Using unique properties of bacterial surfaces, nanoparticles can be designed to target binding bacterial cell membranes [4, 196-199]. Such nanomaterials provide an effective tool in the fight against antibiotic-resistant bacteria, while helping to develop new diagnostic techniques for bacterial infections [200-205]. The study of the manipulation of cell membrane binding is of great significance, and its implications are widely involved in many fields of science and medicine.

In this study, the polycationic oligomers were introduced to enhance the interaction between cell membranes and nanostructures [206]. Carboxy-terminated polycationic oligomers were synthesized by RAFT polymerization and modified to zinc oxide nanorods (NR). RAFT

polymerization is a controlled radical polymerization technique that allows precise regulation of molecular weight and architecture. The accumulated polycations significantly enhance the binding effect locally through the electrostatic interaction between the positive charge cluster and the negative charge of the bacteria. In addition, the hydrophobic chain can destroy the phospholipid bilayer of cells, resulting in membrane structure disorder, disintegration, and cytoplasmic leakage, and finally lead to cell wall destruction and lysis [207, 208].

The experimental results showed that the modified polycationic zinc oxide nanorods (PCaNR) exhibited far better antibacterial properties than the unmodified nanorods (NR). Compared with the unmodified nanorods, the survival rate of *E. coli* decreased from 86.5% to 0% after 3 minutes of exposure. The study further proves that the contact bactericidal ability of nanomaterials can be significantly improved by the long-distance electrostatic attraction and short distance van der Waals force generated by the accumulation of good multi-cations. In addition, PCaNR were applied to textile functionalization for use in the field of biological protection. The experiment verifies the potential feasibility of PCaNR as an antibacterial surface layer, which provides strong support for the development of new functional textiles and efficient biological protection materials.

## 5.2 Experimental Section

### 5.2.1 Materials

2-mercaptoethanol, carbon disulfide ($CS_2$), benzyl bromide and deuterated Dimethyl Sulfoxide (DMSO) were purchased from Adamas. Tripotassium phosphate ($K_3PO_4$) and azobisisobutyronitrile (AIBN) were purchased from Sinopharm Chemical Reagent Co., Ltd. 1-octyl-3-vinylimidazolium bromide was purchased from Zhuoyan Chemical Technology Co.,

Ltd. Zinc acetate was purchased from Sinopharm Chemical Reagent Co.,Ltd. Ethanolamine (AR, 99%) and 2-methoxyethanol (AR) were purchased from Aladdin. Zinc nitrate hexahydrate (98%) was purchased from Alfa Aesar. Hexamethylenetetramine (99%) was purchased from international laboratory USA. Glutaraldehyde (50% aq. soln. 50% aq) was purchased from Alfa Aesar. Phosphate-buffered Saline (PBS, pH 7.4, Sigma). Nutrient agar (022021) and nutrient broth (022010) were purchased from HKM. SYTO 9 (3.34 mM in dimethylsulfoxide) and prodium iodide (PI, 20 mM in dimethylsulfoxide) were purchased from Thermo Fisher Scientific. Lithium bromide (LiBr, 99%), potassium acetate ($CH_3COOK$, 99%), magnesium chloride ($MgCl_2$, 99%) and potassium carbonate ($K_2CO_3$, 99%) were purchased from Aladdin. Magnesium nitrate hexahydrate ($Mg(NO_3)_2 \cdot 6\ H_2O$, 99%) was purchased from Sigma-Aldrich. Potassium iodide (KI, 99%), sodium chloride (NaCl, 99%) and potassium chloride (KCl, 99%) were purchased from Aladdin. Ethanol (AR) was purchased from UNI-CHEM. Acetone and dimethylformamide were purchased from Sinopharm Chemical Reagent Co.,Ltd. Methanol was purchased from Sinopharm Chemical Reagent Co.,Ltd). PP melting blown cloth was purchased from DOCTOR MASK. The PP melt-blown nonwoven cloth has a basis weight of about 25 g/m² and consists of fibers with diameters ranging from 1 to 5 μm. Polyethylene Terephthalate (PET) fabric was provided by China Dyeing Holdings Ltd., Hong Kong. The woven PET fabric has a basis weight of about 110 g/m² and consists of fibers with diameters about 10 μm. Nylon fabric was provided by China Dyeing Holdings Ltd., Hong Kong. The woven Nylon fabric has a basis weight of about 140 g/m² and consists of fibers with diameters about 10 μm.

### 5.2.2 Design Principles and Material Selection of Ionic Liquids and Polycation

Ionic liquids (ILs) have the advantages of efficient binding to bacterial membranes and rapid destruction of bacterial membranes. As a green, safe and difficult to produce drug resistance

antibacterial strategy, ILs provide a practical and effective alternative for the prevention and treatment of multi-drug resistant bacteria. Therefore, this study selected ILs as the basis of antibacterial functional components to achieve efficient bactericidal effects. To enhance the mechanical bactericidal properties of nanostructures, a polycationic oligomer containing imidazole rings and alkyl chains was designed. The imidazole ring achieves the concentration of positive charges through π-π stacking, which strengthens the electrostatic attraction with the bacterial membrane; the alkyl chain improves the compatibility with the cell membrane and promotes the close contact between the molecule and the bacterial membrane [209]. The polycationic oligomer was efficiently grafted onto the surface of ZnO nanorods using carboxyl-modified RAFT agents to construct a surface with excellent targeting and bactericidal ability [210]. The polycation (PCa) consists of two functional parts: one is the carboxyl anchoring group, which ensures stable binding with ZnO nanorods; the other is the cationic part, which imparts strong antibacterial activity. This design achieves the synergistic effect of chemical and physical mechanisms, significantly improving the antibacterial properties of the nanostructured surface.

### 5.2.3 Synthesis of RAFT reagent and PCa

RAFT reagent refers to the chain transfer agent (CTA) used in RAFT polymerization, and it is an important component of the RAFT polymerization process. 2-Mercaptoethanol (β-Mercaptoethanol, $K_3PO_4$ (1.35 g) and acetone (10 mL) were added to a round-bottled flask, stirred well, and reacted for 10 min. Then, $CS_2$ (1.46 g) was added, and the mixture continued until the yellow solution was formed. After another 10 minutes, benzyl bromide (1.10 g) was added. After the mixture reacts for another 30 min, the solid was removed by filtration, the solvent was removed by decompression, and further concentrated from the organic filtrate. The crude product was purified by column chromatography to obtain a yellow oily liquid (RAFT

reagent, CTA). AIBN was a commonly used free radical initiator. Appropriate amount of 1-octyl-3-vinylimidazole bromide monomer, CTA and AIBN were added into 25 mL pressure-resistant reaction tube according to proportion [Monomer: CTA: AIBN = 100:2:1], dissolved with 5 mL DMF, and stirred well. The reaction system was fully degassed after three freezing-vacuum-thawing cycles and was stirred at 60 °C for 20 h after returning to room temperature. Quench quickly with liquid nitrogen after the reaction. The resulting polymer was dissolved in acetone and gradually precipitated in ethanol. After repeated three times, the light-yellow solid product was obtained. The solid product was vacuum-dried overnight at room temperature, collected and stored properly. Finally, an appropriate amount of the product was dissolved in deuterated DMSO and the structure was confirmed by nuclear magnetic resonance (NMR) analysis. Figure 5.1 shows the fabrication process of CTA and PCa.

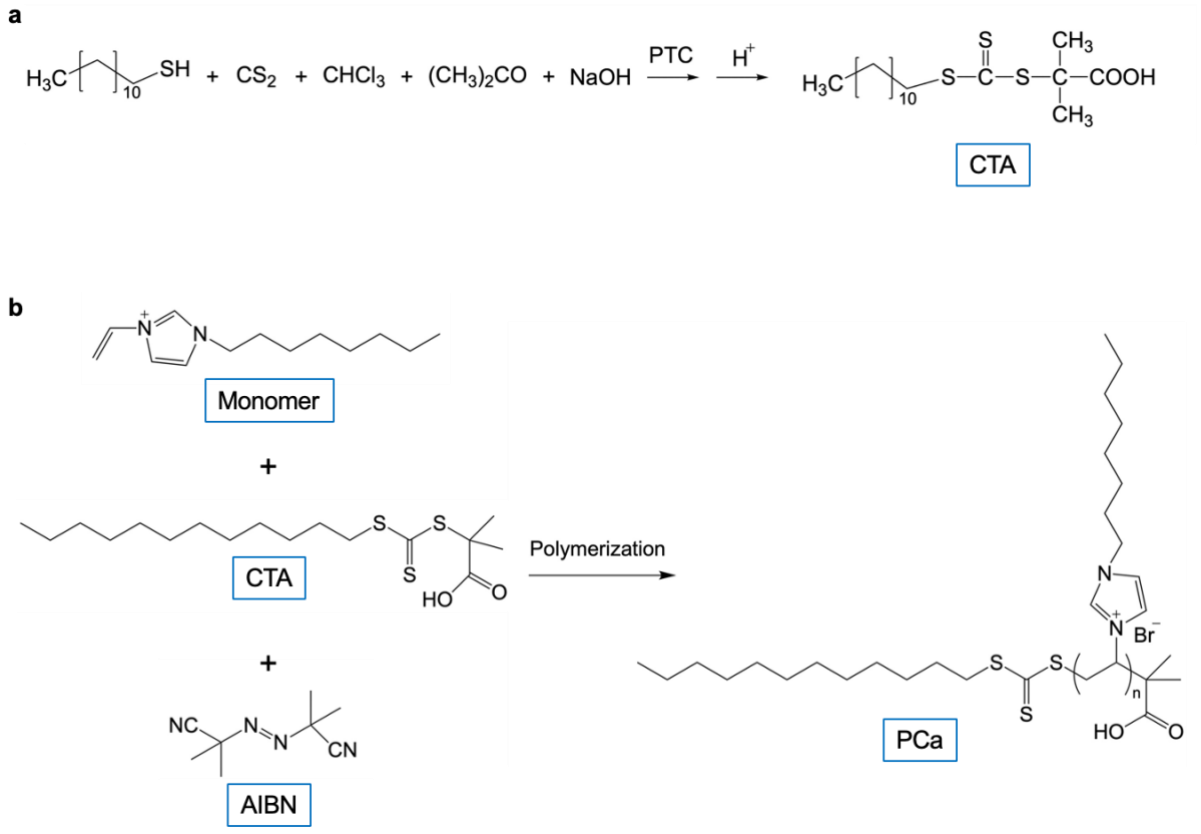


Figure 5.1 Schematic illustration of the fabrication of RAFT agent (a) and PCa (b).

### 5.2.4 Fabrication of NR and PCaNR

NR and PCaNR were synthesized by hydrothermal method. First, zinc acetate and ethanolamine are dissolved in ethylene glycol methyl ether, and the mixture is ultrasonic treated until a uniform precipitation-free solution is formed, called ZnO seed solution. Then zinc nitrate hexahydrate and hexamethylenetetramine were dissolved in distilled water to prepare ZnO growth solution. Both the seed solution and the growth solution were transparent after ultrasonic treatment. In the preparation process of the glass substrate, the glass sheets are first immersed in distilled water and ethanol for 5 min each time, and ultrasonic cleaning was performed after each soak. After cleaning, a small amount of ZnO seed solution was added to the glass sheet, and the solution was evenly distributed by spinning coating method. The coated glass sheet is heated on a hot plate preheated to 230°C for 15 min. Then, the glass sheet was immersed in ZnO growth solution and the hydrothermal synthesis was completed at 85°C for 9 h. After growth, NR was rinsed with deionized water and dried naturally. Then, NR was immersed in a PCa solution prepared with methanol for 20 min, then rinsed with methanol and dried, and finally PCaNR was obtained. For the fabric base, a similar method is used, but with appropriate adjustments: the fabric was soaked in a ZnO seed solution for 30 min and then heated on a hot plate at 100°C for 15 min, which was the only difference from the glass base method. The other steps remained consistent, resulting in NR and PCaNR samples with good properties.

### 5.2.5 Characterization

SEM (Tescan MAIA3) was utilised to observe the morphology. EDX was employed to map the element composition. FT-IR spectra meter (Thermo Nicolet iS50) were used to analyse NR, PCa, and PCaNR. NMR spectroscopy (Bruker Avance III 600 MHz) was applied to test PCa

with functional groups. Water contact angle was tested via SDC-100Standard contact angle instrument. XPS (Thermo Scientific Nexsa) was used to identify the surface elemental composition. TEM (FEI Talos F200x) was utilized to observe the morphology of nanoclusters. Small-Angle X-ray Scattering (SAXS, Anton Paar SAXSess mc2) was used to analyze the nanostructure of PCa.

### 5.2.6 Antimicrobial Assay

Antibacterial tests were performed using the *E. coli* strain CMCC 44102. *E. coli* colonies on the surface of the agar plate were selected into 10 mL of nutrient broth and cultured at 37°C for 24 hours. Subsequently, the bacterial suspension was washed with PBS and concentrated by Thermo Fisher Scientific Centrifuge Pico 17. The resulting bacterial precipitates were redispersed in a PBS solution and the bacterial concentrations obtained were verified by continuous dilution and colony forming unit (CFU) counting by plate coating method. In the antibacterial experiment, a compression atomizer was used to spray aerosols containing bacteria onto the surface of the sample. Firstly, a bacterial suspension with a concentration of $10^7$ CFU/mL was prepared, and 3 mL was sprayed at 25 cm from the sample for 30 seconds through the atomizer, so that it could contact the sample for a certain time. After that, the bacteria on the sample were extracted using ultrasonic cleaning and coated on the agar plate. The plates were cultured at 37°C for 24 hours to evaluate the antibacterial effect. In the SEM study, the bacteria on the sample were removed with ultrasonic treatment and cleaned three times with PBS. The bacteria were then immobilized with 2% glutaraldehyde solution (PBS preparation) and incubated overnight at 4°C. The fixed bacteria were washed several times with deionized water and then dehydrated with a series of gradient ethanol/water mixtures (ethanol concentrations of 30%, 50%, 70%, 90%, 95%, and 100%, respectively, for 1 hour at each gradient). Finally, the bacterial samples are treated with gold coating to make them

suitable for SEM analysis. In live/dead bacterial fluorescence staining, bacterial suspensions were stained with SYTO 9 green fluorescent dye and propyl iodide (PI) red fluorescent dye for 20 minutes. After dyeing, wash with PBS and re-suspend. Fluorescence images were observed and recorded using a fluorescence microscope. The antimicrobial tests were carried out under different humidity conditions, and the humidity was controlled by saturated aqueous solution.

## 5.3 Results and Discussion

Biomimetic nanostructured surfaces have been widely demonstrated to have mechano-bactericidal effects on a wide variety of bacteria. Take *E. coli*, a typical Gram-negative bacterium and a commonly used model organism in research. Its structural characteristics are shown in Figure 5.2. From the outside to the inside, there are cell wall, cell membrane, cytoplasm, nucleoid and various intracellular structures. To further improve the mechanical sterilization performance of the nanostructures, a polycationic oligomer with cationic imidazole ring and alkyl chain was designed and synthesized. In particular, the carboxyl modified RAFT reagent not only realizes the polymerization of antibacterial cation molecules, but also promotes the efficient assembly of cationic oligomers and zinc oxide nanorods as surface engineered ligands [211]. The imidazole rings can form ordered molecular stacks through π-π interactions, as shown in Figure 5.2b. This ordered arrangement will significantly concentrate the cationic charge distribution, resulting in a stronger attraction to the bacterial cell membrane, further enhancing the antibacterial effect [209]. In addition, the introduction of alkyl chains is believed to effectively improve the compatibility of nanostructures with cell membranes. This compatibility promotes the close contact between the nanostructure and the bacterial cells, thereby enhancing the synergistic effect on the destruction and killing of bacteria, as shown in Figure 5.2c. The combined effect of the above design is expected to greatly improve the efficiency of nanostructures in targeted elimination of pathogenic bacteria

and open up new directions and application prospects for the development of new efficient antibacterial materials.

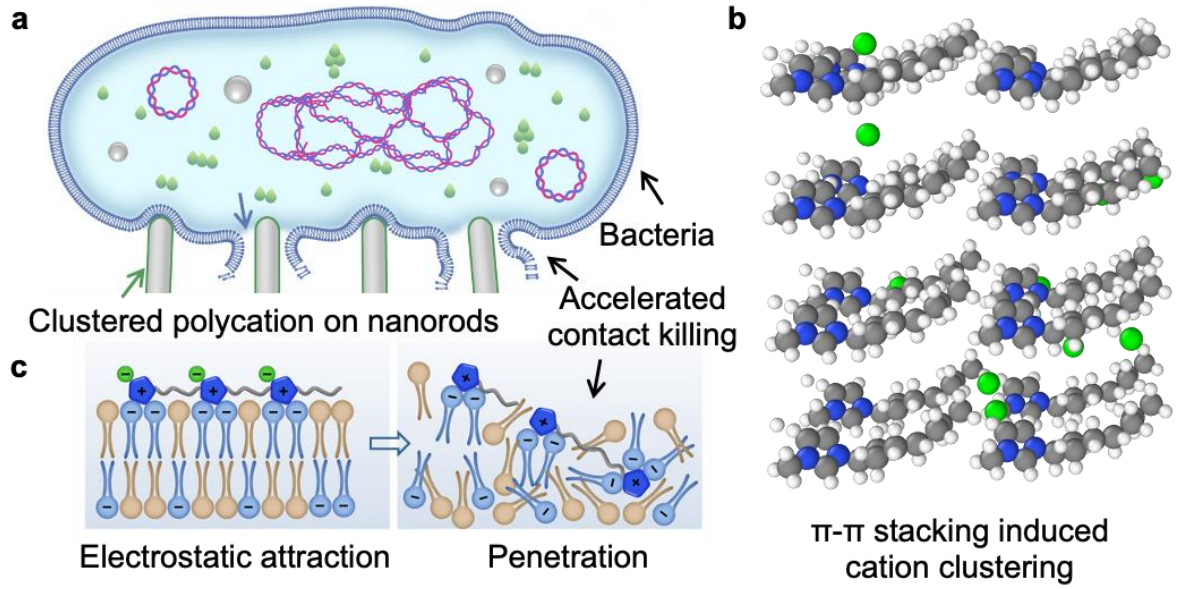


Figure 5.2 Mechanism and properties of oligomer arrangement enhancing bacterial cell binding. a, Polycationic clusters cause cell membrane destruction and achieve high antibacterial performance through enhanced contact bactericidal action. b, Molecular dynamics (MD) simulations reveal how π-π stacking induces cationic aggregation. The grey, blue, green and white spheres represent carbon, nitrogen, bromine and hydrogen atoms, respectively. c, Schematic diagram of the mechanism of PCa leading to bacterial cell death.

### 5.3.1 Characterization of PCaNR

Firstly, PCa oligomers were prepared, as shown in Figure 5.3. In the synthesis, RAFT polymerization method was used to construct complex PCa structures. PCa consists of two functional components: an anchoring group for stable binding to NR, and a cationic group as part of the antibacterial function. The first step of synthesis is to prepare RAFT reagent, and

the specific synthesis steps have been completed. Subsequently, NR was prepared by hydrothermal method. These nanorods were then subjected to PCa surface modification using terminal carboxyl groups as anchor points to obtain PCaNR.

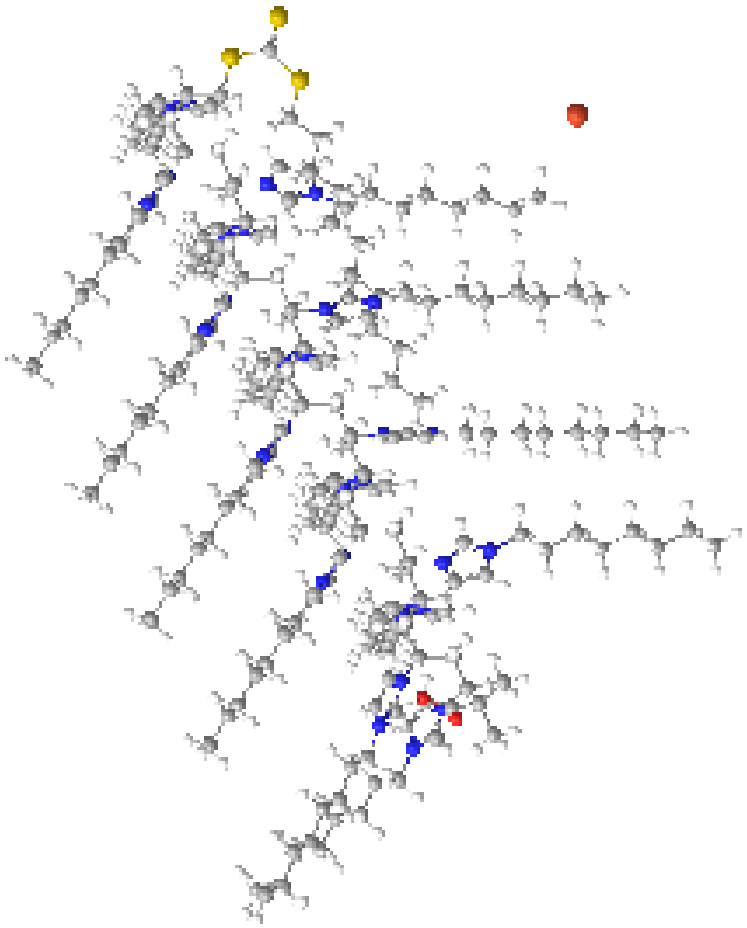

Figure 5.3 The demonstration of PCa molecular structure (ball-and-stick model).

As shown in Figure 5.4, the top view morphology of PCaNR shows that its diameter is about 82.3 nm. The energy dispersive X-ray (EDX) composition mapping was used to compare NR and PCaNR, as shown in Figures 5.5 and 5.6, and the results clearly show the differences in nitrogen and bromine content on the two surfaces.

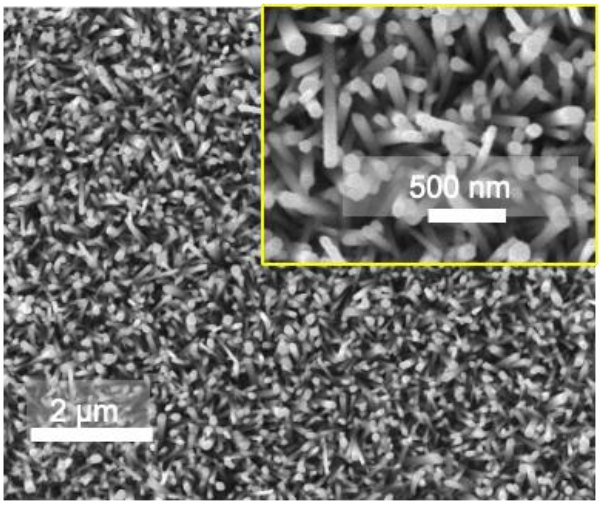


PCaNR

Figure 5.4 SEM images of PCaNR, inset is in higher magnification.

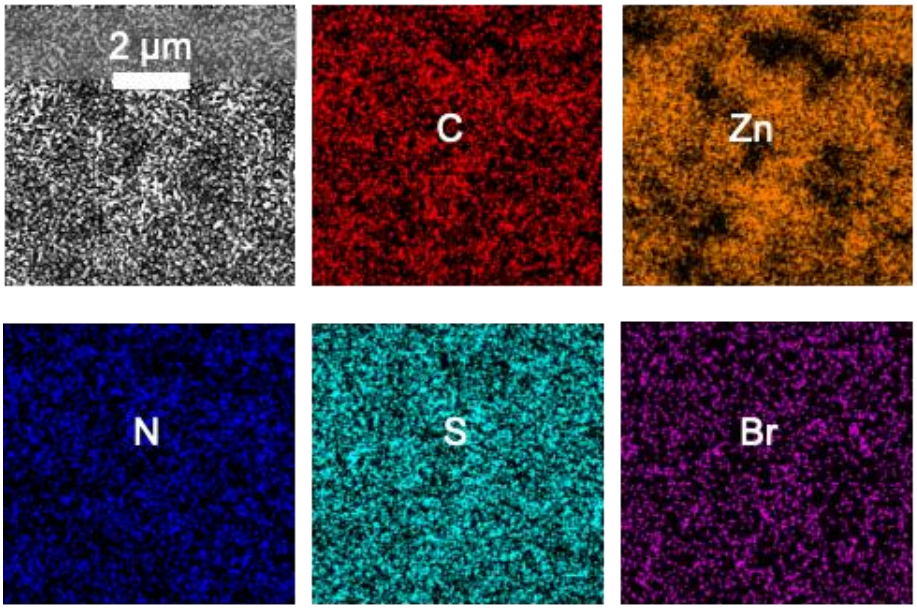


EDX mapping

Figure 5.5 EDX mapping of PCaNR.

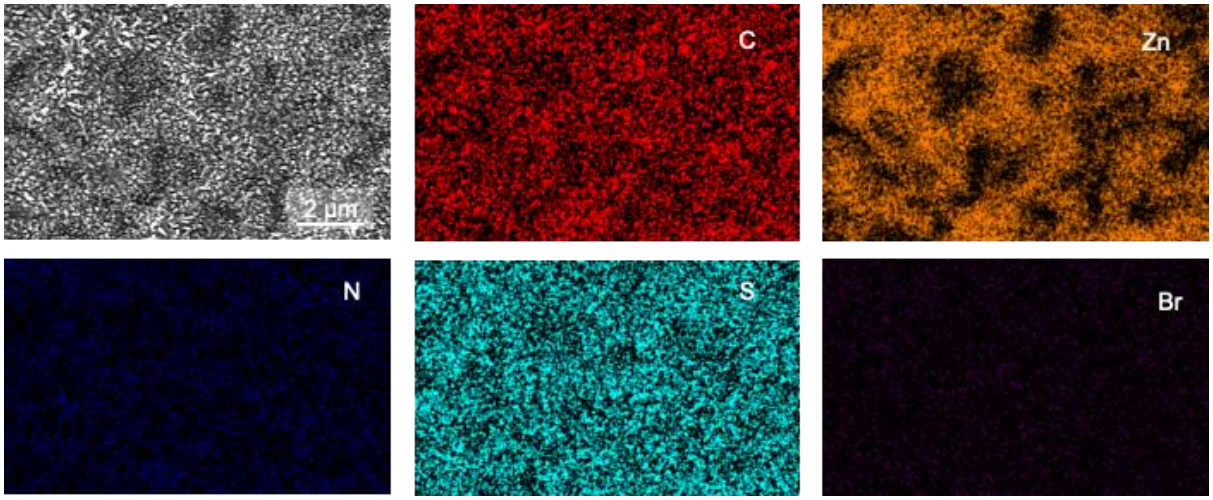


Figure 5.6 EDX mapping of NR.

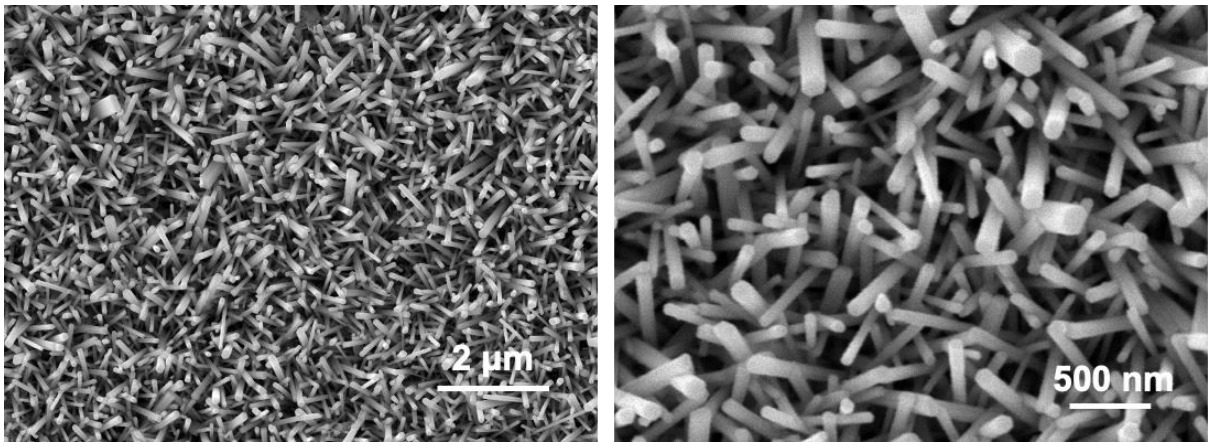


Figure 5.7 SEM images of NR.

In addition, the success of the surface modification was verified by XPS analysis, as shown in Figures 5.8 and 5.9. Compared with NR, the XPS spectra of PCaNR showed characteristic peaks of N 1s and Br 3d at 401 eV and 68 eV, respectively.

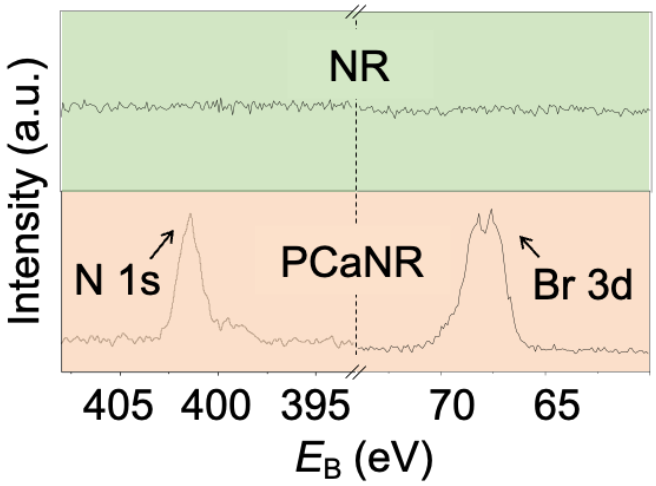


Figure 5.8 High-resolution XPS spectra (N and Br element) of NR (top) and PCaNR (bottom).

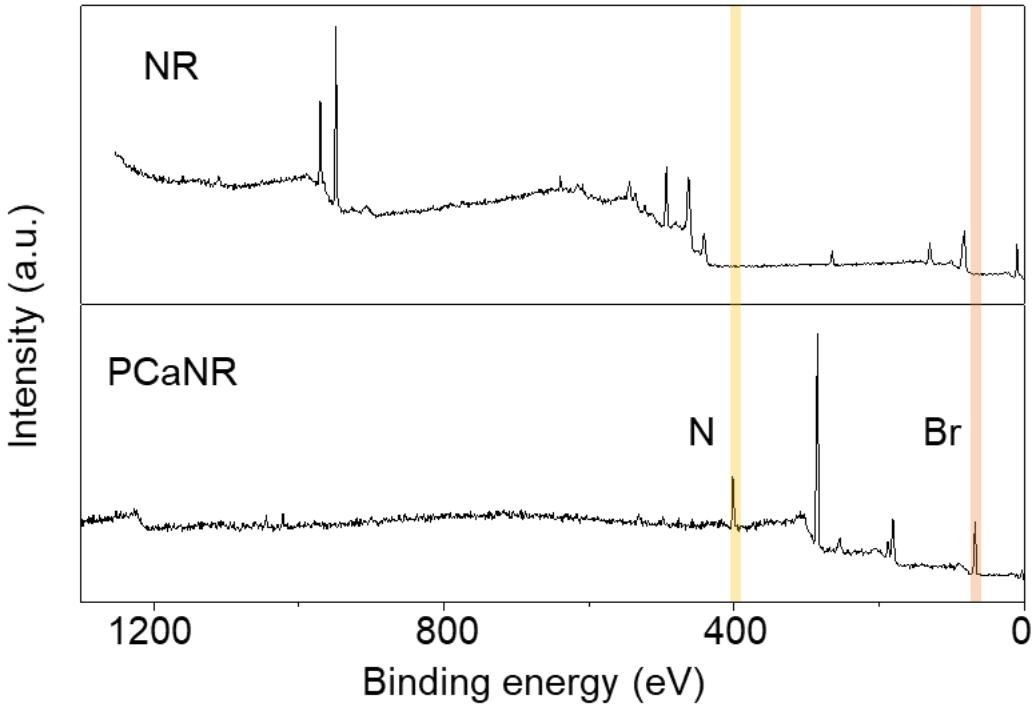


Figure 5.9 XPS spectra of NR and PCaNR confirming successful loading of the N and Br elements.

In Figure 5.10, the water contact Angle (CA) test shows a significant difference in wettability between NR and PCaNR: NR has a contact Angle of about 13.1°, while PCaNR has a contact Angle of about 151.8°. The comparison results proved the effectiveness of the modification process. The successful loading of PCa on the NR surface was further confirmed by FTIR analysis (Figure 5.11). Among them, the absorption peaks at 2920 $cm^{-1}$, 1550 $cm^{-1}$ and 1457 $cm^{-1}$ are attributed to the stretching vibrations of C-H, C-C and C=N bonds, respectively.

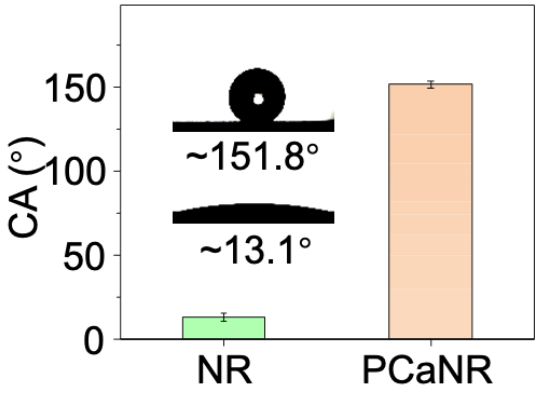


Figure 5.10 Water contact angle of NR and PCaNR, insets show the optical images with different wettability.

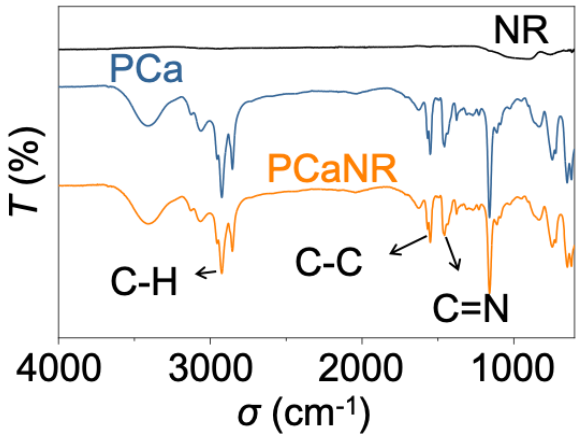


Figure 5.11 FTIR spectra of NR, PCa, and PCaNR.

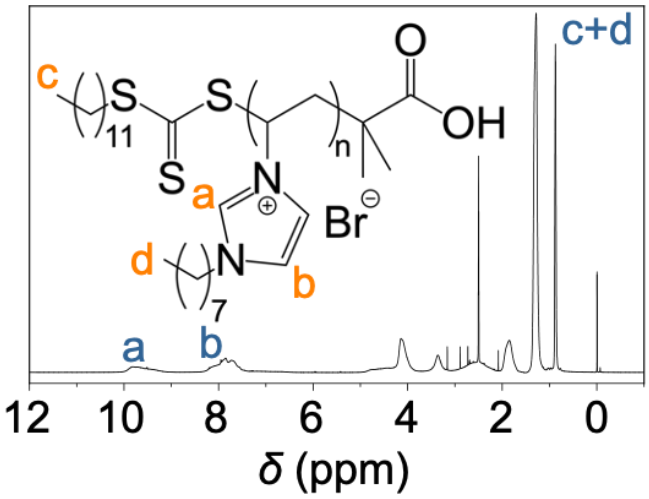


Figure 5.12 NMR spectroscopy of PCa.

The successful synthesis of PCa was also confirmed by $^1$H NMR spectral analysis (Figure 5.12). The signal peaks near 0.87 ppm were attributed to the $CH_3$ ($H_c$) and $CH_3$ ($H_d$) of PCa at the end of RAFT, while the peaks at 7.93 ppm and 9.83 ppm were attributed to CH ($H_a$) and CH ($H_b$) in the imidazole ring, respectively.

To test the hypothesis of nanoclusters formed by head π-π interactions, HRTEM observations and small-angle X-ray scattering (SAXS) analysis were performed. As shown in Figure 5.13, TEM images and corresponding element EDX maps clearly confirm the chemical composition of PCa. In Figure 5.14a, the presence of nanoclusters can be clearly observed, and the representative nanoclusters have been marked with red circles. Its size distribution is shown in Figure 5.14b, with an average diameter of about 3.5nm, which is highly consistent with the result measured by SAXS of about 2.7nm (Figure 5.15), further verifying the hypothesis.

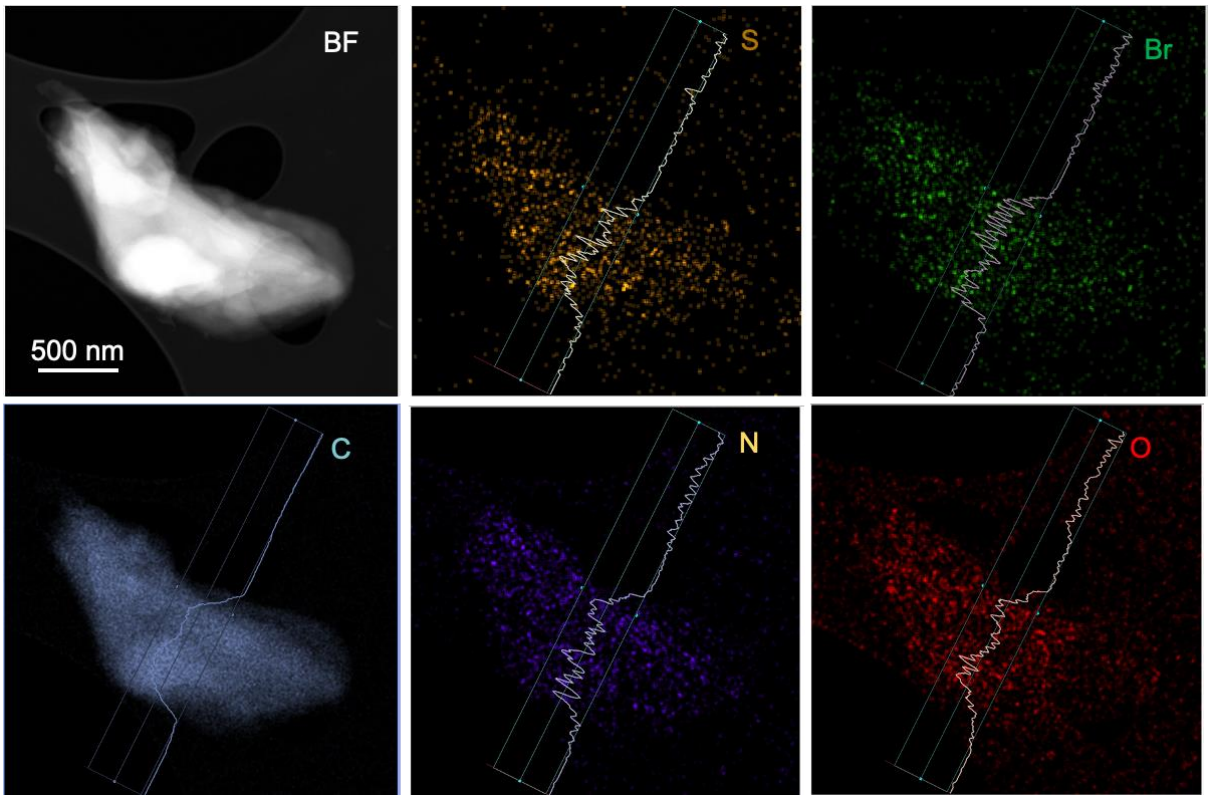


Figure 5.13 TEM image and EDX mapping of S, Br, C, N, O elements.

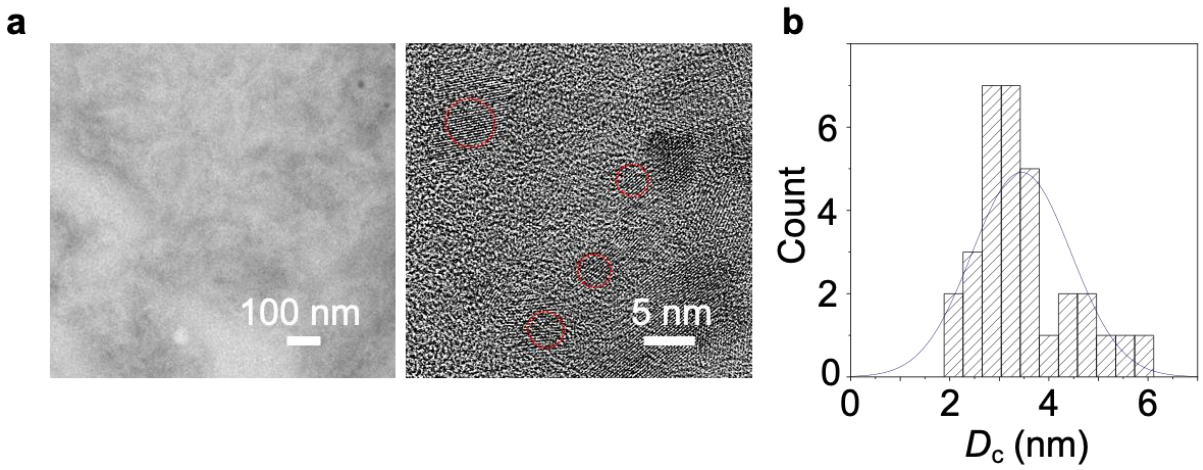


Figure 5.14 a, HRTEM images of PCa. Left is TEM image in a lower magnification. Right is High-resolution TEM image, and the red circles mark the representative well-ordered nanoclusters. b, Histogram of the nanocluster size distribution.

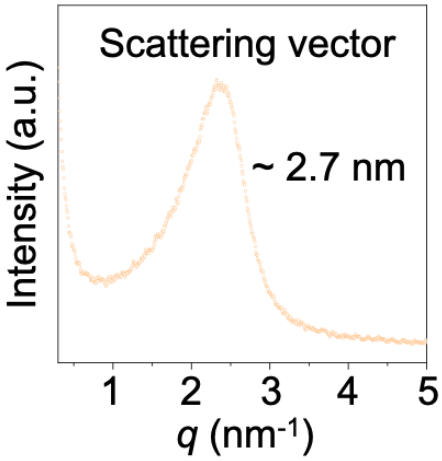


Figure 5.15 SAXS data of PCa.

5.3.2 Bacteria Contact Induced Binding and Killing

The zinc oxide nanorods was chosen as the research object because of their simple preparation method and wide application potential in mechanical sterilization strategies. To evaluate their antimicrobial properties, the bacteria-containing aerosols were sprayed onto three surfaces: bare glass, NR, and PCaNR and allowed the bacteria to come into contact with the surface for a period of time until they were completely killed. As shown in Figure 5.16, it takes only 3 minutes for *E. coli* to be completely killed on PCaNR surfaces, compared to 7 hours and 100 minutes for bare glass and NR surfaces, respectively.

To further understand the bactericidal mechanism, SEM was used to observe the morphological changes of *E. coli* after contact with these three surfaces (Figure 5.17 and 18). The results showed that the bacteria maintained intact cell morphology on the bare glass and NR surfaces, while the cell structure showed significant collapse on the PCaNR surface (Figure 5.19). These preliminary results show that the combination of the designed PCa and biomimetic nanorods can achieve excellent results in contact sterilization, which is characterized by rapid destruction

of bacteria and significant morphological deformation, providing a new idea for the development of advanced antibacterial materials.

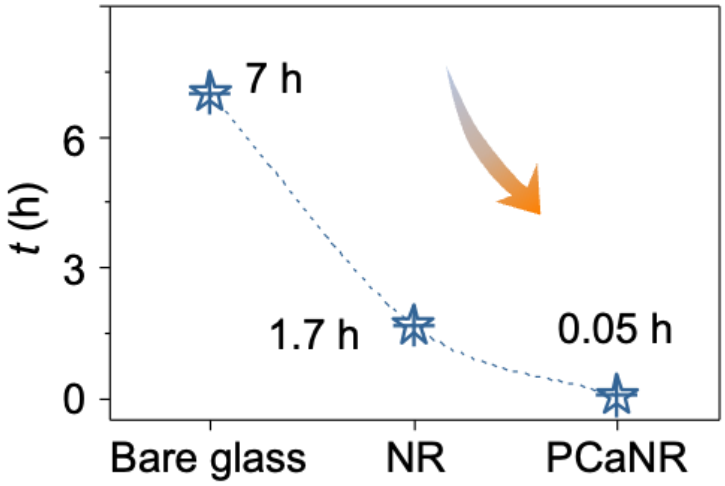


Figure 5.16 Time required for killing all airborne bacteria deposited on the three surfaces (bare glass, NR, PCaNR).

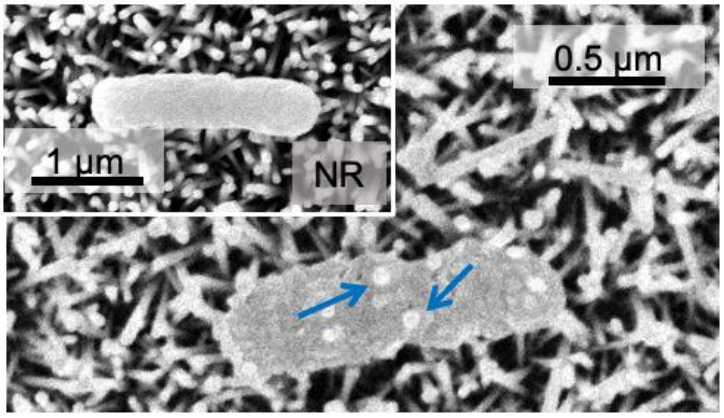


Figure 5.17 SEM observations after airborne *E. coli* deposited on PCaNR, inset is NR, showing disrupted and intact cell morphology.

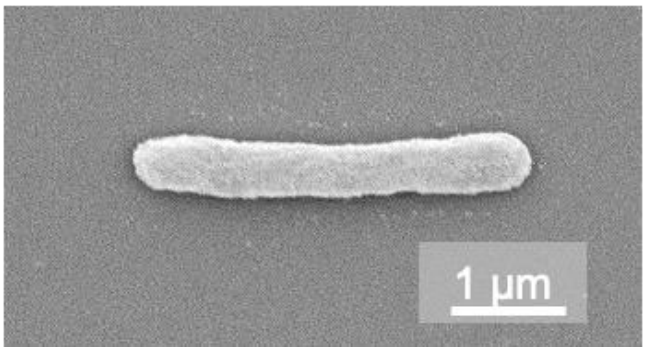


Figure 5.18 SEM observation after airborne *E. coli* deposited on bare glass.

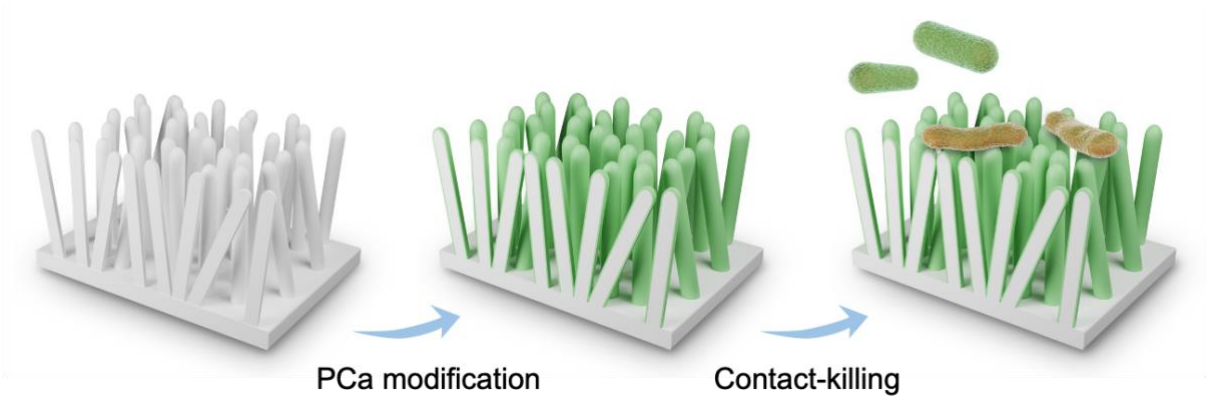


Figure 5.19 Antibacterial properties arising from the synergy of nanostructures and PCa.

*E. coli*, a commonly used bacterial model, was selected to evaluate the antimicrobial performance of PCaNR. To exclude the influence of reactive oxygen species (ROS), the experiment was conducted in the absence of light. To further explore the mechanism and dynamics of bacterial killing, contact killing experiments were conducted using bare glass, NR and PCaNR as contrast surfaces, and antibacterial properties were evaluated by agar plate colony counting. The survival rates of *E. coli* on three surfaces were recorded at different exposure times (see Figure 5.20a). Figure 5.20b clearly shows that the contact sterilization time of PCaNR (3 minutes) is significantly shorter than that of bare glass (about 7 hours) and NR

(about 100 minutes), indicating that the sterilization performance of PCaNR is significantly enhanced.

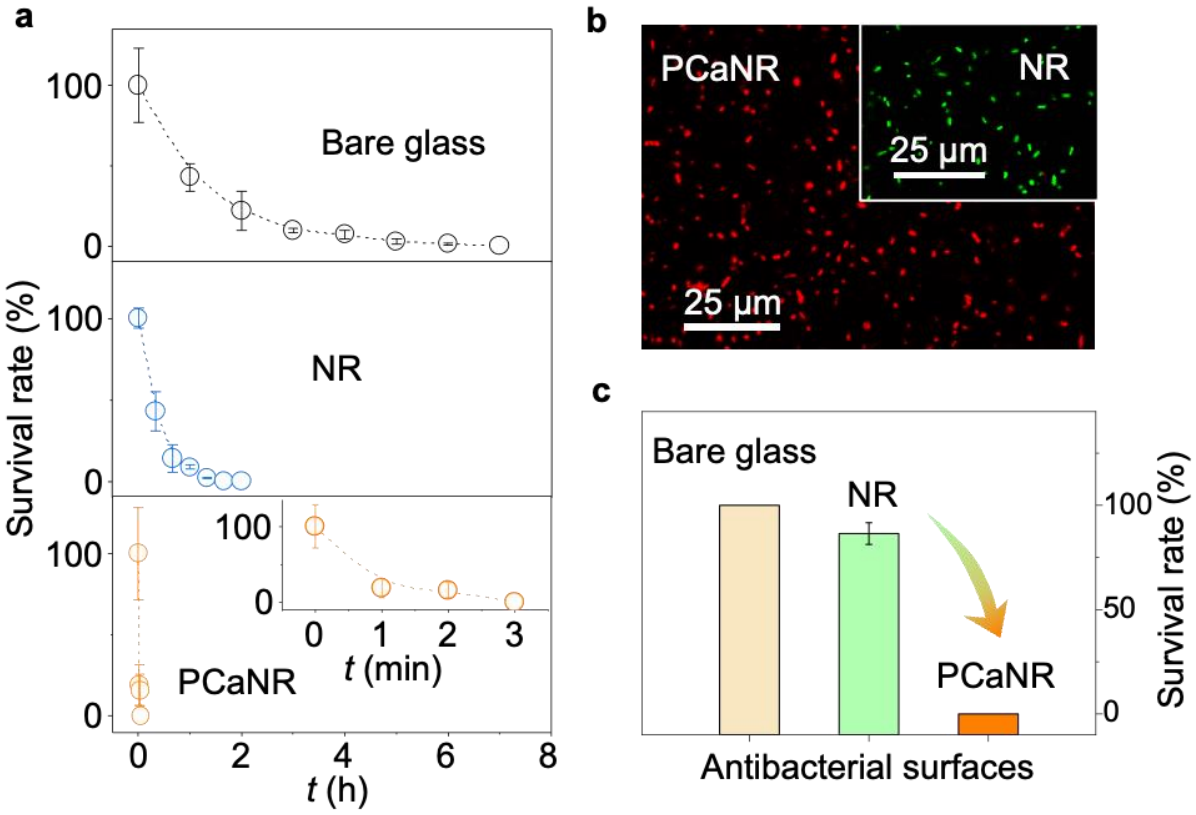


Figure 5.20 Bacteria contact-killing behaviours of PCaNR. a, Time-dependent *E. coli* survival rate on bare glass, NR, PCaNR surfaces. b, Representative fluorescent microscope imaging after airborne *E. coli* deposited on NR, PCaNR surfaces. c, The bacteria survival rate after contact-killing for 3 minutes on three kinds of surfaces. The error bars represent standard deviations and n = 5 for each data point.

*E. coli* suspensions were further sprayed onto three surfaces, maintaining contact for 3 minutes for analysis. Fluorescence microscope imaging results are shown in Figure 5.20b and 5.21, where green fluorescence represents live bacteria and red fluorescence represents dead bacteria. The remarkable contrast between the proportion of live and dead bacteria (see Figure 5.20c)

further highlights the excellent bactericidal efficacy of PCaNR. To verify the excellent bactericidal properties of PCa combined with nanostructures, bare glass and PCa modified glass were prepared (PCa@glass). Figure 5.22a and b show the difference in wettability between the two. The contact Angle of bare glass is about 32°, while the contact Angle of PCa@glass increases to about 93°. XPS spectral analysis (Figure 5.22c) compared the elemental composition of the two surfaces, where the success of the modification was demonstrated by the N 1s and Br 3d peaks at 401 eV and 68 eV at PCa@glass. As shown in Figure 5.22d, the antibacterial experiment results showed that the survival rate of bare glass and PCa@glass was still higher (both greater than 75%) after contact with bacteria. Combining the bactericidal properties of PCa@glass and PCaNR, the combination of nanocluster PCa and NR is the key factor to achieve excellent antibacterial effect.

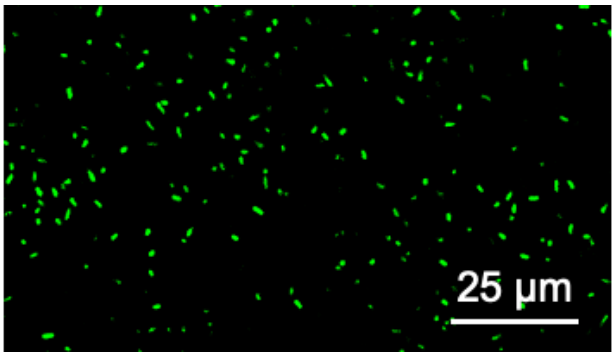


Figure 5.21 Representative fluorescent microscope imaging after airborne *E. coli* deposited on bare glass.

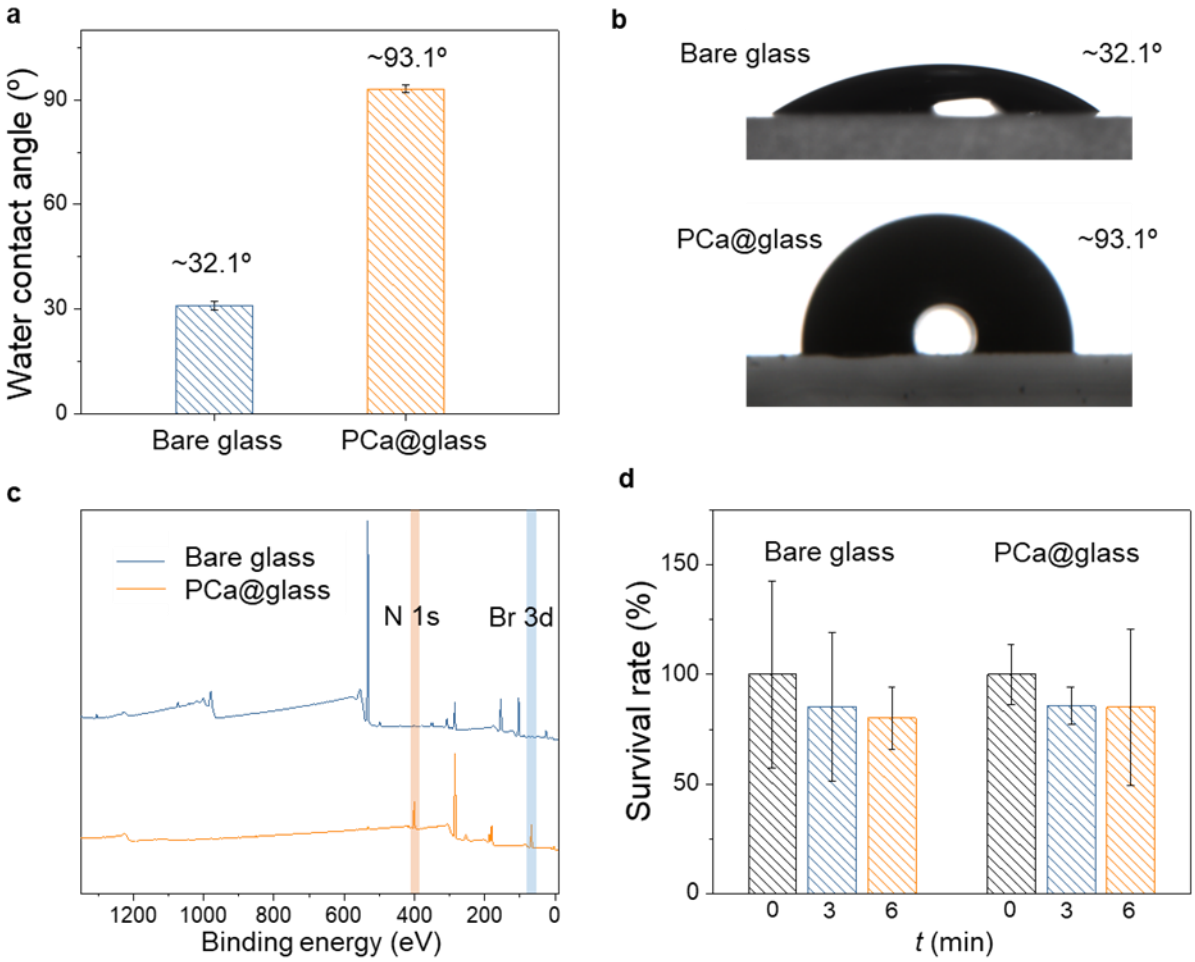


Figure 5.22 Excluding the only role of PCa in the microbicidal performance of PCaNR. a, water contact angle of bare glass and PCa@glass. b, representative optical images of bare glass and PCa@glass. c, XPS spectra of bare glass and PCa@glass. d, *E. coli* survival rate of bare glass and PCa@glass.

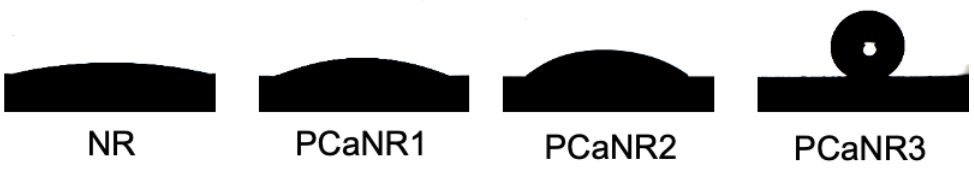


Figure 5.23 Representative optical images of water contact angle on NR and PCaNR1-3.

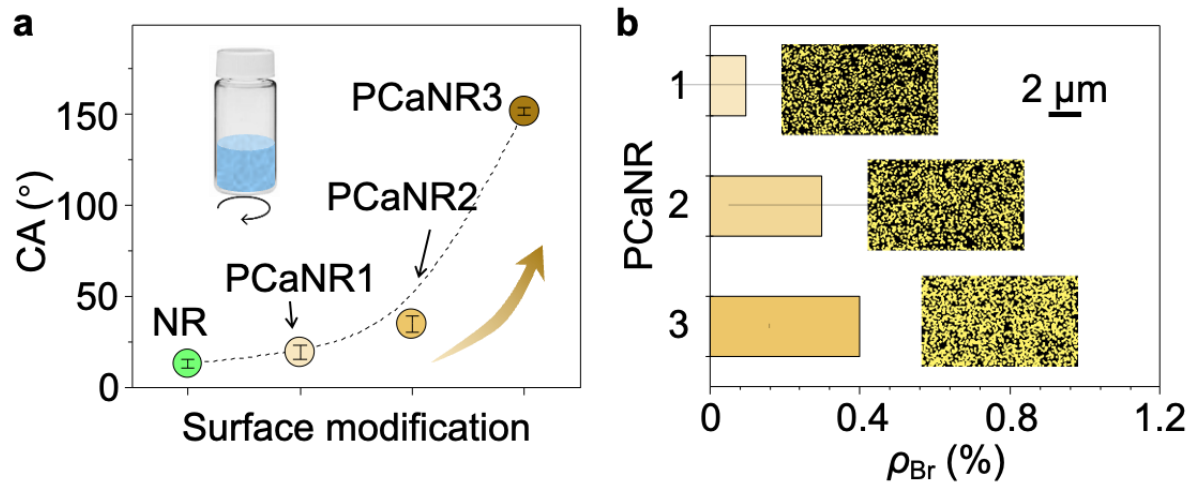


Figure 5.24 a, Water contact angle of NR and PCaNR1-3. b, Br element concentration and EDS mapping of PCaNR1-3.

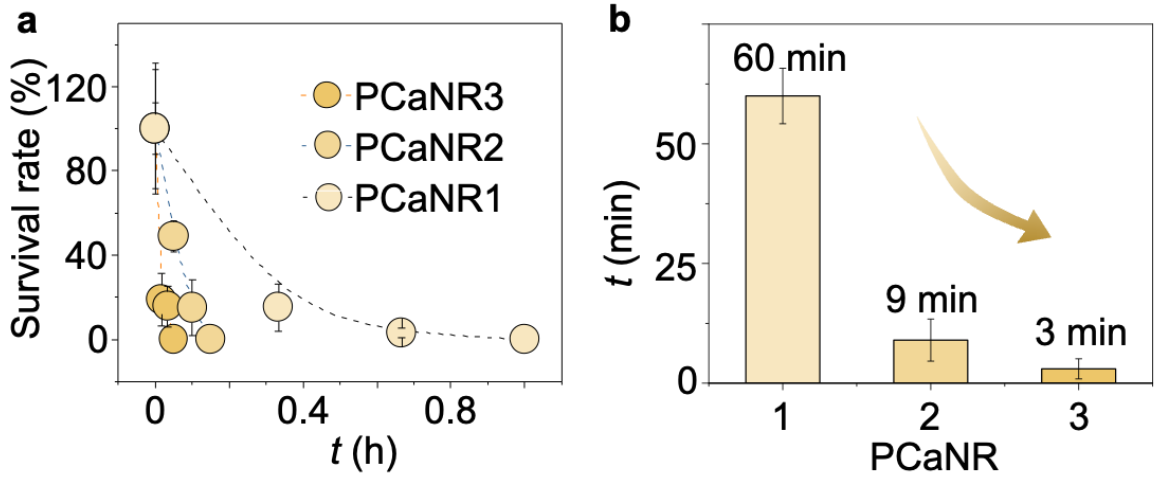


Figure 5.25 a, Time-dependent *E. coli* survival rate on PCaNR1-3 surfaces. b, Time required for killing all airborne bacteria deposited on the three surfaces.

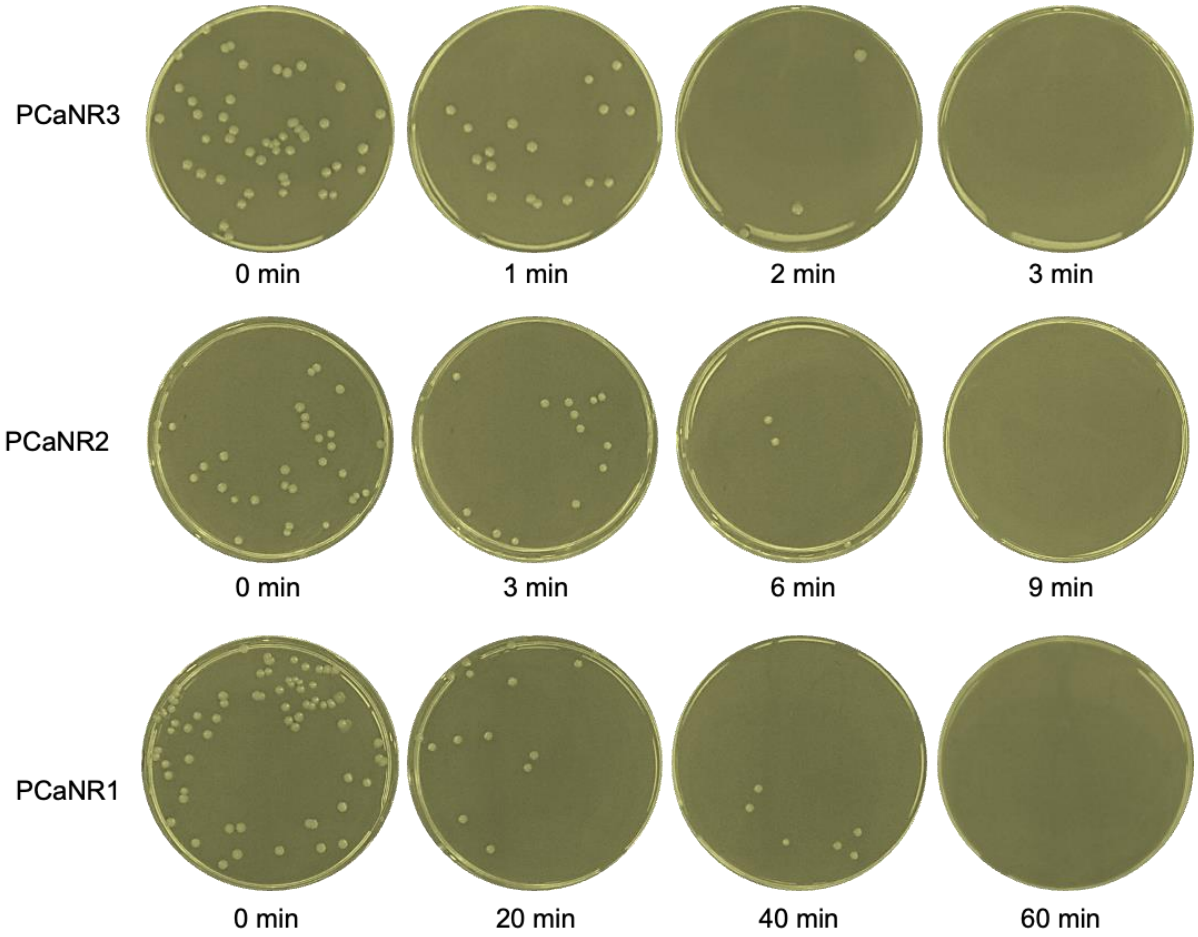


Figure 5.26 Optical images of representative agar plates of sprayed bioaerosol onto PCaNR1-3 for different time periods.

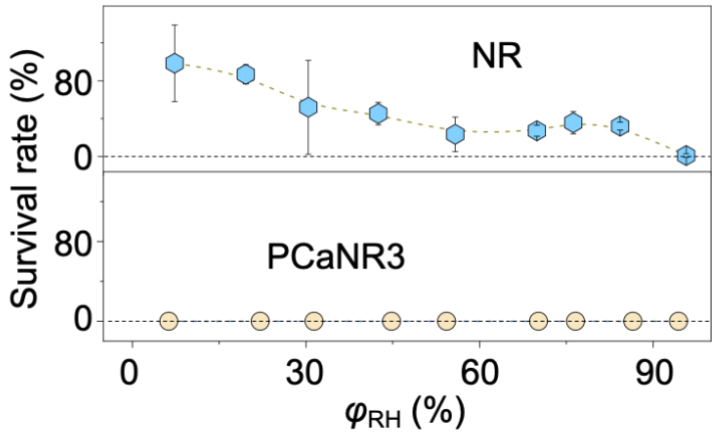


Figure 5.27 *E. coli* survival rate of NR and PCaNR under a series of humidity conditions.

The antimicrobial properties of different types of PCaNR were studied in detail. Three types of PCaNR1-3 were prepared by using PCa methanol solutions with concentrations of 0.001, 0.1 and 10 mol/L, respectively, and their water contact angles were measured (see Figures 5.23 and 5.24a). As the concentration of the solution increases, the surface properties gradually change from hydrophilic to hydrophobic, and eventually form a superhydrophobic surface with a contact angle of up to 150°. In addition, the distribution of bromine elements on different surfaces was analysed through EDX mapping, and the results were shown in Figure 5.24b, which further revealed the differences in composition of the three surfaces.

The results of antibacterial experiments (see Figures 5.25a, b and 5.26) showed that the modified surface significantly shortened the killing contact time of bacteria. Compared with the surface of unmodified NR (1.7 hours of bacterial survival time as shown in Figure 5.20a), PCaNR1-3 achieved a significant reduction in bacterial survival time of 3 minutes, 9 minutes and 1 hour, respectively. These results indicate that PCaNR surfaces have significantly improved antibacterial effects. In addition, PCaNR maintained excellent bactericidal performance under a wide range of ambient humidity conditions (see Figure 5.27), which was significantly better than NR, whose performance decreased significantly with an increase in relative humidity (RH). These findings suggest that nanocluster PCa plays a key role in enhancing mechanical bactericidal.

5.3.3 Bioprotection Application of PCaNR

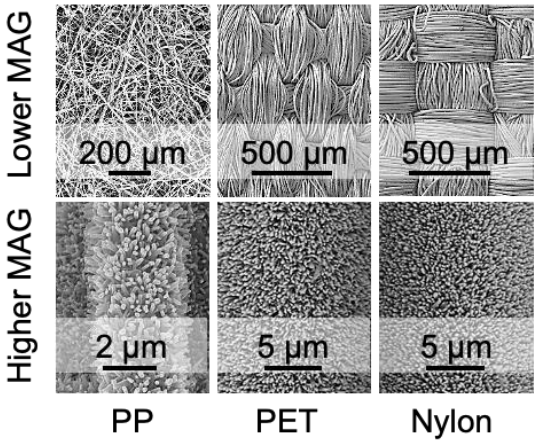


Figure 5.28 SEM images of PP, PET, and Nylon cloth modified with PCaNR.

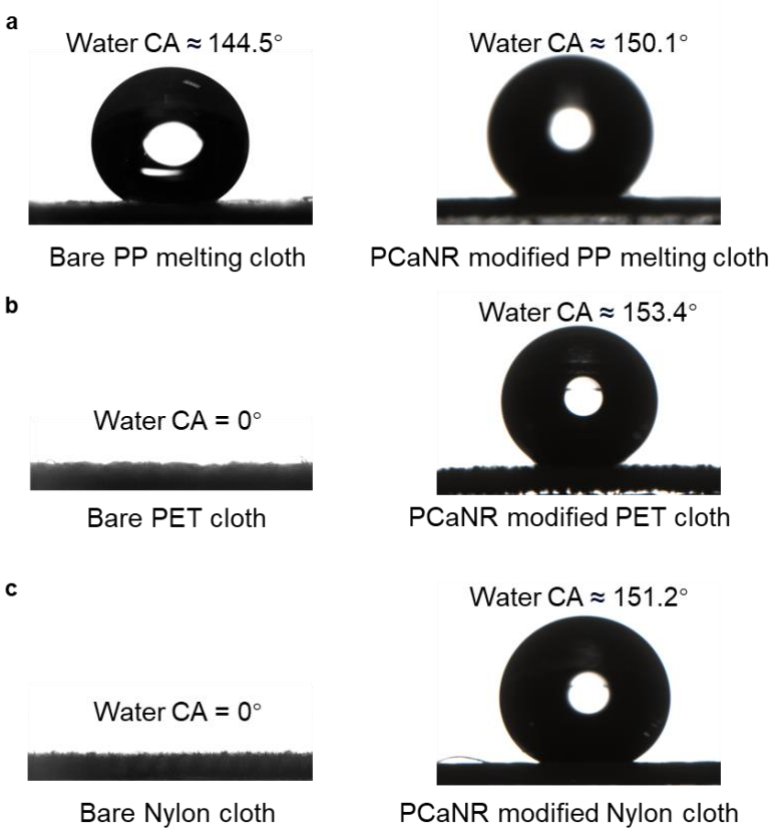


Figure 5.29 Representative optical images of water contact angle on various fabrics.

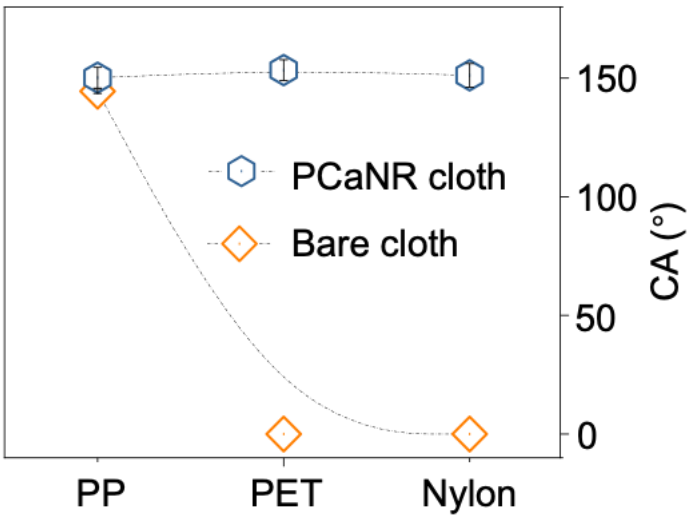


Figure 5.30 Wettability of three kinds of cloth before and after modified.

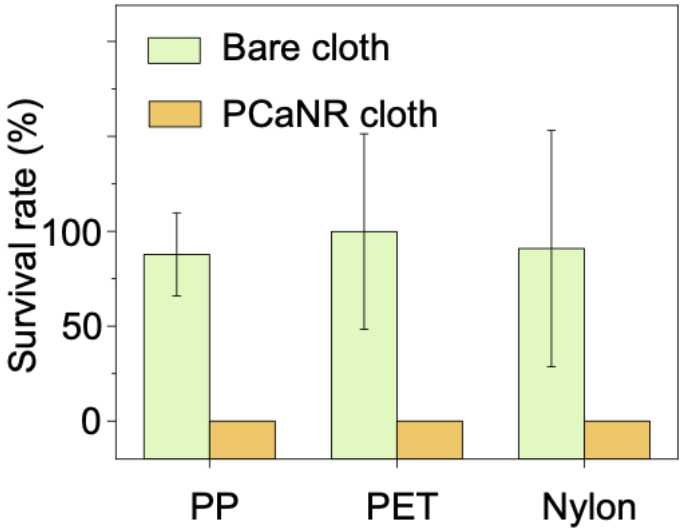


Figure 5.31 Survival rate on bare and PCaNR modified PP, PET, and Nylon cloth.

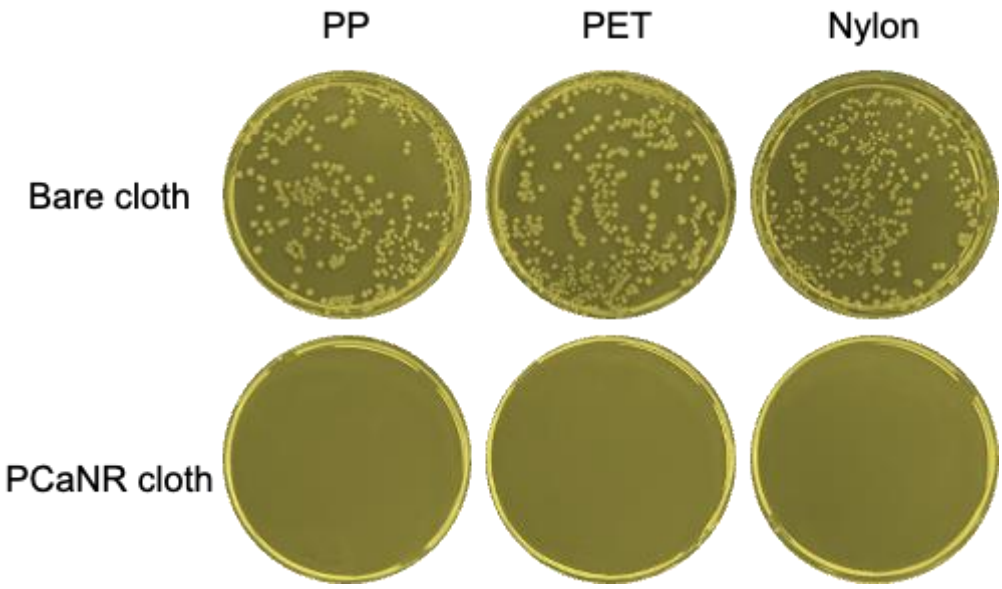


Figure 5.32 Representative optical images of 3-minute antibacterial assay results of bare cloth and PCaNR based cloth.

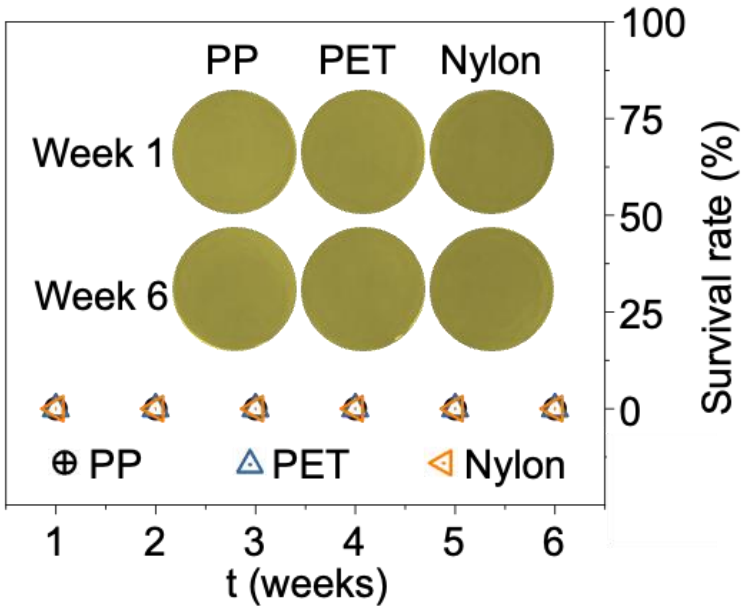


Figure 5.33 Long term antibacterial tests for PCaNR based cloth.

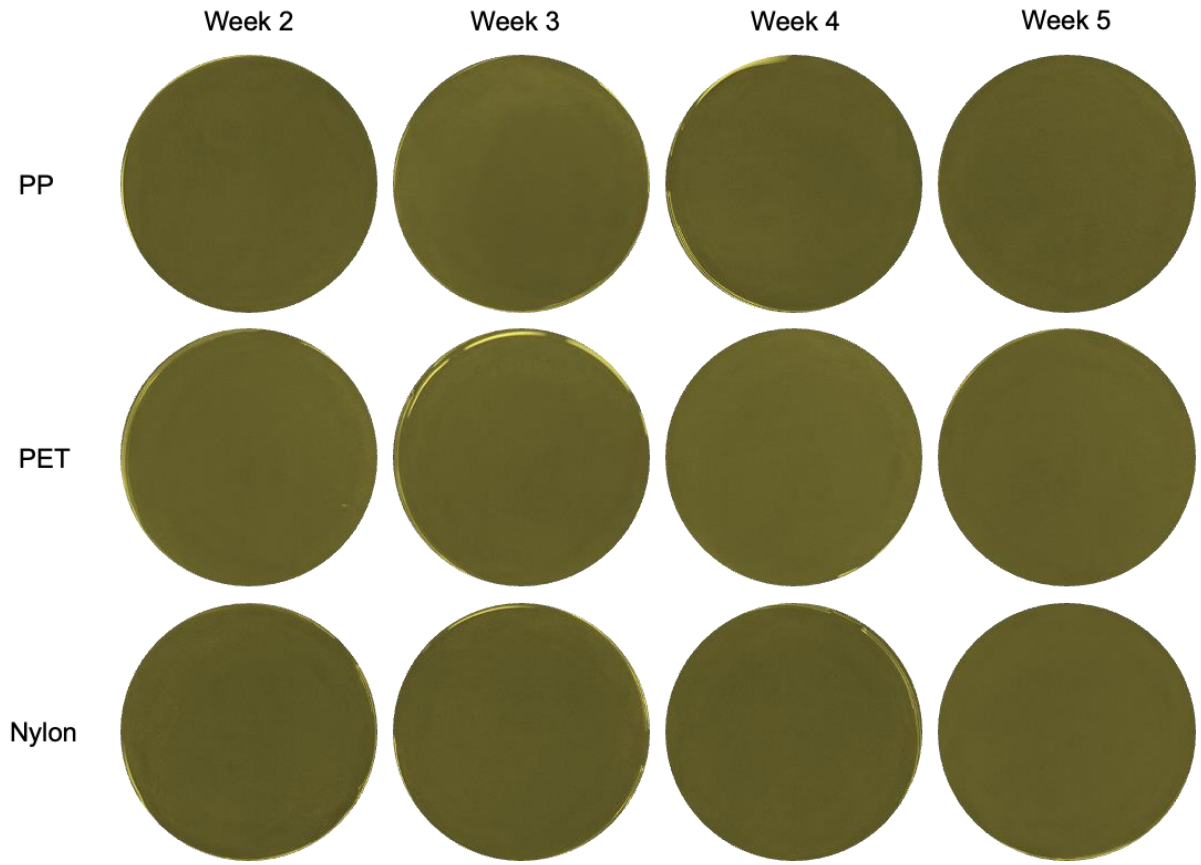


Figure 5.34 Representative optical images of long-term antibacterial assay results for PCaNR based cloth.

The results successfully validate the feasibility of using PCaNR as a bioprotective bactericidal surface layer. For this purpose, three fabric materials were functionalized: melt-blown polypropylene (PP), polyethylene terephthalate (PET) and nylon. The change of the modified fabric fiber morphology is shown in Figure 5.28. Wettability was tested by measuring the water contact Angle of the fabric before and after modification (see Figures 29 and 30). The results showed that PP maintained its original superhydrophobic properties, while PET and nylon significantly improved from hydrophilic to superhydrophobic states, and the water contact Angle exceeded 150°, which further indirectly proved the success of the modification effect.

In the antibacterial efficiency test, the aerosols containing *E. coli* were sprayed onto different fabric surfaces, keeping them in contact for 3 minutes. The results showed that the bacterial survival rates of untreated fabrics were 87% (PP), 90% (PET) and 89% (nylon), respectively. In contrast, the modified fabric surface achieved complete removal of bacteria (see Figures 5.31 and 5.32). To assess the durability of the antimicrobial properties, long-term antimicrobial tests were further performed. The test results (see Figures 5.33 and 5.34) showed that the modified fabric consistently maintained zero bacterial survival during the 6-week experiment, demonstrating excellent antimicrobial stability. Based on the above systematic sterilization test results, the application potential of PCaNR was preliminarily verified in the field of biological protection, becoming a foundation for its popularization in practical protection scenarios.

## 5.4 Conclusions

In this study, a highly effective antibacterial material based on polycationic modified nanostructures (PCaNR) was successfully developed, and its application potential in the field of biological protection was fully verified. Through the charge accumulation effect of polycations and the mechanical bactericidal properties of nanostructures, PCaNR significantly enhances the binding ability of bacterial cell membranes, showing excellent antibacterial properties. The experimental results show that PCaNR can completely kill *E. coli* in bioaerosol in only 3 minutes, and the killing time is much shorter than that of unmodified nanomaterials (about 1.7 hours), which proves the synergistic effect of polycations and nanostructures. In addition, PCaNR can still maintain high antibacterial performance in different humidity environments, showing excellent stability. PCaNR was further applied to the functional modification of textiles to treat melt-blown polypropylene (PP), polyethylene terephthalate (PET) and nylon. The results showed that the modified fabric changed from hydrophilic to superhydrophobic, with a water contact Angle of more than 150°, and significantly improved

antibacterial efficiency. During long-term testing over a period of 6 weeks, the modified fabric consistently maintained zero bacterial survival and demonstrated excellent antimicrobial durability. In summary, PCaNR combines the dual advantages of nanostructures and polycations, providing important support for the efficient removal of bioaerosols and the development of antibacterial textiles, and opening up a new direction for the practical application of biological protective materials.

# 6 Conclusions and Suggestions for Future Research

## 6.1 Conclusions

This study systematically explored the synergistic effect of nanostructure and chemical modification on aerosol bactericidal contact. By introducing three different antimicrobial strategies, a comprehensive killing path was achieved that extends from simple mechanical bactericidal to a combination of mechanical, chemical and electric action.

First, a superhydrophilic fiber layer (based on electrospinning technology) doped with silver nanoparticles is used to efficiently trap and quickly kill bacteria in bioaerosols on the surface of micrometre-scale fibers. The antibacterial effect of silver nanoparticles is coordinated with the high specific surface area and super-hydrophilic properties of the fiber membrane, which realizes the effective elimination of *E. coli* in a relatively short time. However, silver nanoparticles have some cost and potential environmental load problems, so it is necessary to consider economy and environmental safety in practical application.

Secondly, by grafting polyvinyl pyrrolidone (PVP) on the surface of zinc oxide nanorods (NR), this study realized the construction of a superhydrophilic surface and generated liquid bridge tensile force by capillary condensation effect, which could effectively kill pathogens under low humidity conditions. This mechanically stressed bactericidal strategy does not rely on chemical fungicides and helps to reduce the development of drug-resistant strains. However, the superhydrophilic surface may face the problem of reduced efficiency in some specific environments (such as extremely dry conditions), which needs to be further optimized.

Finally, the surface of the nanorods was transformed from hydrophilic to superhydrophobic by polycation (PCa) modification, and strong electrostatic adsorption was achieved in local areas to bind the cell membrane. The strategy can kill aerosol bacteria in a very short time (about 3 minutes), showing that the cationic clusters and nanostructures cooperate to enhance the excellent performance of mechanical and charge interaction. However, the stability and long-term performance of polycationic modification in complex environments (such as air rich in organic pollutants) still need to be further studied.

On the basis of the above research, these antibacterial materials were successfully applied to textile functionalization, and the modification of PP, PET, nylon fabrics were realized. In long-term tests, the modified fabric was able to maintain a zero bacterial survival rate for several weeks, providing important support for the development of practical protective equipment, medical masks and air filtration materials.

## 6.2 Suggestions for Future Research

1. Follow-up studies should systematically evaluate the long-term performance and life of various antibacterial surfaces in complex environments with different humidity, temperature and organic content. At the same time, an improvement scheme should be proposed for the sterilization efficiency under extreme dryness or high humidity conditions.

2. Material durability and safety: It is necessary to further investigate the stability of the material under frequent cleaning, friction, ultraviolet irradiation or chemical disinfection. Ensures high antimicrobial performance after prolonged use and reduces the environmental impact of material wear.

3. In the future, these new antibacterial materials can be integrated with medical protective clothing, masks, high efficiency air filters, air conditioning filters, etc. Through the optimization of the material structure and functional components, the multiple balance of air permeability, comfort, wear resistance and antibacterial property is achieved.

4. Combined with the development trend of sensing technology and smart fabrics, antibacterial textiles are endowed with environmental response and adaptive regulation. In this process, the research on degradable polymers, green synthesis routes and recycling strategies will be strengthened, and the in-depth application of antibacterial materials will be promoted in the field of sustainable fashion and environmental protection.

5. Although the constructed nanostructured surfaces (such as nanofibers and nanorods) exhibit good and lasting antibacterial properties, attention should still be paid to the firmness of their bonding with the fabric substrate in practical applications. Due to insufficient interfacial bonding, the nanostructure may fall off due to external forces such as friction and washing during use and may enter the human body through breathing or skin contact, posing potential health risks. Therefore, improving the interfacial adhesion between the nanostructure and the fiber substrate is crucial to achieve safe and stable practical applications. For example, biomimetic adhesives such as dopamine can be used to enhance interfacial bonding and significantly improve the structural stability and durability of the material under repeated use and external forces [172].

In conclusion, this study provides a multi-dimensional technical reserve for aerosol biosafety protection. Future research should focus on expanding practical application scenarios, optimizing durability and environmental applicability, and combining with the development

direction of intelligence and sustainability, promote antibacterial textiles from the laboratory to a broader field of industry and life.

# References


[1] Singh, N. K.; Sanghvi, G.; Yadav, M.; Padhiyar, H.; Thanki, A. A state-of-the-art review on WWTP associated bioaerosols: Microbial diversity, potential emission stages, dispersion factors, and control strategies. *J. Hazard. Mater.* **2021**, *410*, 124686.

[2] Feng, X.; Hu, P.; Jin, T.; Fang, J.; Tang, F.; Jiang, H.; Lu, C. On-site monitoring of airborne pathogens: recent advances in bioaerosol collection and rapid detection. *Aerobiologia* **2024**, *40* (3), 303-341.

[3] Wang, C. C.; Prather, K. A.; Sznitman, J.; Jimenez, J. L.; Lakdawala, S. S.; Tufekci, Z.; Marr, L. C. Airborne transmission of respiratory viruses. *Science* **2021**, *373* (6558), eabd9149

[4] Zhang, Y.; Cui, J. S.; Chen, K. Y.; Kuo, S. H.; Sharma, J.; Bhatta, R.; Liu, Z.; Ellis-Mohr, A.; An, F. F.; Li, J. H.; et al. A smart coating with integrated physical antimicrobial and strain-mapping functionalities for orthopedic implants. *Sci. Adv.* **2023**, *9* (18), eadg7397.

[5] Linklater, D. P.; Baulin, V. A.; Juodkazis, S.; Crawford, R. J.; Stoodley, P.; Ivanova, E. P. Mechano-bactericidal actions of nanostructured surfaces. *Nat. Rev. Microbiol.* **2021**, *19*, 8-22.

[6] Gao, M. J.; Sun, L.; Wang, Z. Q.; Zhao, Y. B. Controlled synthesis of Ag nanoparticles with different morphologies and their antibacterial properties. *Mater. Sci. Eng., C* **2013**, *33* (1), 397-404.

[7] Macovei, I.; Harabagiu, V.; Burlec, A. F.; Mircea, C.; Horhogea, C. E.; Rimbu, C. M.; Sacarescu, L.; Panainte, A.-D.; Miron, A.; Hancianu, M.; et al. Biosynthesis of silver and gold nanoparticles using Geum urbanum L. rhizome extracts and their biological efficiency. *J. Inorg. Organomet. Polym. Mater.* **2024**, *34*, 5831–5853.

[8] Wang, Y.; Han, Y.; Xu, D.-X. Developmental impacts and toxicological hallmarks of silver nanoparticles across diverse biological models. *Environ. Sci. Ecotechnology* **2024**, *19*, 100325.

[9] Jahan, I.; Bekler, F. M.; Tunc, A.; Guven, K. The effects of silver nanoparticles (AgNPs) on thermophilic bacteria: antibacterial, morphological, physiological and biochemical investigations. *Microorganisms* **2024**, *12* (2), 402.

[10] Hussein, S. Y.; Abbas, T. A.-H. Synthesis and antibacterial activity of ultrasmall silver nanoparticles by pulsed laser ablation in deionized water. *Curr. Nanosci.* **2024**, *20* (3), 409-419.

[11] Hamad, A.; Khashan, K. S.; Hadi, A. Silver nanoparticles and silver ions as potential antibacterial agents. *J. Inorg. Organomet. Polym. Mater.* **2020**, *30* (12), 4811-4828.

[12] Fang, Y.; Hong, C.-Q.; Chen, F.-R.; Gui, F.-Z.; You, Y.-X.; Guan, X.; Pan, X.-h. Green synthesis of nano silver by tea extract with high antimicrobial activity. *Inorg. Chem. Commun.* **2021**, *132*, 108808.

[13] Ahmad, J.; Memon, A. G.; Shaikh, A. A.; Ismail, T.; Giwa, A. S.; Mahmood, A. Insight into single-element nobel metal anisotropic silver nanoparticle shape-dependent selective ROS generation and quantification. *RSC Adv.* **2021**, *11* (14), 8314-8322.

[14] Joubani, M. N.; Zanjanchi, M. A.; Sohrabnezhad, S. A novel Ag/Ag3PO4-IRMOF-1 nanocomposite for antibacterial application in the dark and under visible light irradiation. *Appl. Organomet. Chem.* **2020**, *34* (5), e5575.

[15] Wu, Y. Z.; Liu, P.; Chu, P. K. Mechano-bactericidal activities of orthopedic implants with nanostructured surfaces: Recent advances and prospects. *Adv Mater Interfaces* **2024**, 2400004.

[16] Wu, Y.; Liu, P.; Mehrjou, B.; Chu, P. K. Interdisciplinary-inspired smart antibacterial materials and their biomedical applications. *Adv. Mater.* **2024**, *36* (17), e2305940.

[17] Ivanova, E. P.; Hasan, J.; Webb, H. K.; Truong, V. K.; Watson, G. S.; Watson, J. A.; Baulin, V. A.; Pogodin, S.; Wang, J. Y.; Tobin, M. J.; et al. Natural bactericidal surfaces: Mechanical rupture of Pseudomonas aeruginosa cells by cicada wings. *Small* **2012**, *8* (16), 2489-2494.

[18] Chen, P.; Guo, X. Y.; Li, F. X. Antibiotic resistance genes in bioaerosols: Emerging, non-ignorable and pernicious pollutants. *J. Cleaner Prod.* **2022**, *348*, 131094.

[19] Alipour, M. B.; Davoudi, M.; Farsiani, H.; Sarkhosh, M.; Gharib, S.; Miri, H. H. The effect of medical face masks on inhalation risk of bacterial bioaerosols in hospital waste decontamination station. *Sci. Rep.* **2024**, *14* (1), 26259.

[20] Mbareche, H.; Morawska, L.; Duchaine, C. On the interpretation of bioaerosol exposure measurements and impacts on health. *J. Air Waste Manage. Assoc.* **2019**, *69* (7), 789-804.

[21] van Doremalen, N.; Bushmaker, T.; Morris, D. H.; Holbrook, M. G.; Gamble, A.; Williamson, B. N.; Tamin, A.; Harcourt, J. L.; Thornburg, N. J.; Gerber, S. I.; et al. Aerosol and surface stability of SARS-CoV-2 as compared with SARS-CoV-1. *N. Engl. J. Med.* **2020**, *382* (16), 1564-1567.

[22] Peeri, N. C.; Shrestha, N.; Rahman, M. S.; Zaki, R.; Tan, Z. Q.; Bibi, S.; Baghbanzadeh, M.; Aghamohammadi, N.; Zhang, W. Y.; Haque, U. The SARS, MERS and novel coronavirus (COVID-19) epidemics, the newest and biggest global health threats: what lessons have we learned? *Int. J. Epidemiol.* **2020**, *49* (3), 717-726.

[23] Joseph, J.; Baby, H. M.; Zhao, S.; Li, X. L.; Cheung, K. C.; Swain, K.; Agus, E.; Ranganathan, S.; Gao, J.; Luo, J. N.; et al. Role of bioaerosol in virus transmission and material-based countermeasures. *Exploration (Beijing)* **2022**, *2* (6), 20210038.

[24] Li, M.; Wang, L.; Qi, W.; Liu, Y.; Lin, J. Challenges and perspectives for biosensing of bioaerosol containing pathogenic microorganisms. *Micromachines (Basel)* **2021**, *12* (7).

[25] Li, A. L.; Qiu, X. H.; Jiang, X.; Shi, X. D.; Liu, J. M.; Cheng, Z.; Chai, Q. Q.; Zhu, T. Alteration of the health effects of bioaerosols by chemical modification in the atmosphere: A review. *Fundam. Res.* **2024**, *4* (3), 463-470.

[26] Zhou, L.; Yao, M. S.; Zhang, X.; Hu, B. C.; Li, X. Y.; Chen, H. X.; Zhang, L.; Liu, Y.; Du, M.; Sun, B. C.; et al. Breath-, air- and surface-borne SARS-CoV-2 in hospitals. *J. Aerosol Sci.* **2021**, *152*, 105693.

[27] Stadnytskyi, V.; Bax, C. E.; Bax, A.; Anfinrud, P. The airborne lifetime of small speech droplets and their potential importance in SARS-CoV-2 transmission. *Proc. Natl. Acad. Sci. U. S. A.* **2020**, *117* (22), 11875-11877.

[28] Wang, H. Y.; Peng, L. H.; Li, G. Y.; Zhang, W. P.; Liang, Z. S.; Zhao, H. J.; An, T. C. Photocatalytic ozonation inactivation of bioaerosols by NiFeOOH nanosheets in situ grown on nickel foam. *Appl. Catal., B* **2023**, *324*, 122273.

[29] Xie, W. W.; Li, Y. P.; Bai, W. Y.; Hou, J. L.; Ma, T. F.; Zeng, X. L.; Zhang, L. Y.; An, T. C. The source and transport of bioaerosols in the air: A review. *Front. Environ. Sci. Eng.* **2021**, *15* (3), 44.

[30] Leung, N. H. L. Transmissibility and transmission of respiratory viruses. *Nat. Rev. Microbiol.* **2021**, *19* (8), 528-545.

[31] Bertran, K.; Balzli, C.; Kwon, Y. K.; Tumpey, T. M.; Clark, A.; Swayne, D. E. Airborne transmission of highly pathogenic influenza virus during processing of infected poultry. *Emerging Infect. Dis.* **2017**, *23* (11), 1806-1814.

[32] Chen, W. Z.; Zhang, N.; Wei, J. J.; Yen, H. L.; Li, Y. G. Short-range airborne route dominates exposure of respiratory infection during close contact. *Build. Sci.* **2020**, *176*, 106859.

[33] Cowling, B. J.; Ip, D. K. M.; Fang, V. J.; Suntarattiwong, P.; Olsen, S. J.; Levy, J.; Uyeki, T. M.; Leung, G. M.; Peiris, J. S. M.; Chotpitayasunondh, T.; et al. Aerosol transmission is an important mode of influenza A virus spread. *Nat. Commun.* **2013**, *4*, 1935.

[34] Douwes, J.; Thorne, P.; Pearce, N.; Heederik, D. Bioaerosol health effects and exposure assessment: Progress and prospects. *Ann. Occup. Hyg.* **2003**, *47* (3), 187-200.

[35] Lyu, X.; Luo, Z. W.; Shao, L. Size dependent effectiveness of engineering and administrative control strategies for both short- and long-range airborne transmission control. *Environ. Sci.: Atmos.* **2024**, *4* (1), 43-56.

[36] Dillon, C. F.; Dillon, M. B. Multiscale airborne infectious disease transmission. *Appl. Environ. Microbiol.* **2021**, *87* (4).

[37] Withers, M. R.; Christopher, G. W. Aeromedical evacuation of biological warfare casualties: A treatise on infectious diseases on aircraft. *Mil. Med.* **2000**, *165* (11), 1-21.

[38] Riley, R. L.; Nardell, E. A. Clearing the air: The theory and application of ultraviolet air disinfection. *Am. Rev. Respir. Dis.* **1989**, *139* (5), 1286-1294.

[39] Liu, L. M.; Meng, G.; Laghari, A. A.; Chen, H.; Wang, C.; Xue, Y. M. Reducing the risk of exposure of airborne antibiotic resistant bacteria and antibiotic resistance genes by dynamic continuous flow photocatalytic reactor. *J. Hazard. Mater.* **2022**, *429*.

[40] Eduard, W.; Heederik, D.; Duchaine, C.; Green, B. J. Bioaerosol exposure assessment in the workplace: the past, present and recent advances. *J. Environ. Monit.* **2012**, *14* (2), 334-339.

[41] Heederik, D.; von Mutius, E. Does diversity of environmental microbial exposure matter for the occurrence of allergy and asthma? *J. Allergy Clin. Immunol.* **2012**, *130* (1), 44-50.

[42] Lacey, J.; Dutkiewicz, J. Bioaerosols and occupational lung disease. *J. Aerosol Sci.* **1994**, *25* (8), 1371-1404.

[43] Kraïm-Leleu, M.; Lesage, F. X.; Drame, M.; Lebargy, F.; Deschamps, F. Occupational risk factors for COPD: A case-control study. *Plos One* **2016**, *11* (8).

[44] Tjalvin, G.; Svanes, O.; Bertelsen, R. J.; Hollund, B. E.; Aasen, T. B.; Svanes, C.; Kirkeleit, J. Hypersensitivity pneumonitis in fish processing workers diagnosed by inhalation challenge. *ERJ Open Res.* **2018**, *4* (4).

[45] Liebers, V.; Raulf-Heimsoth, M.; Brüning, T. Health effects due to endotoxin inhalation (review). *Arch. Toxicol.* **2008**, *82* (4), 203-210.

[46] Rowbotham, T. J. Preliminary report on the pathogenicity of Legionella pneumophila for freshwater and soil amoebas. *J. Clin. Pathol.* **1980**, *33* (12), 1179-1183.

[47] Pearson, M. L.; Jereb, J. A.; Frieden, T. R.; Crawford, J. T.; Davis, B. J.; Dooley, S. W.; Jarvis, W. R. Nosocomial transmission of multidrug-resistant Mycobacterium tuberculosis: A risk to patients and healthcare workers. *Ann. Intern. Med.* **1992**, *117* (3), 191-196.

[48] M, B. J.; D, P. Guideline for hand hygiene in health-care settings: recommendations of the healthcare infection control practices advisory committee and the HICPAC/SHEA/APIC/IDSA hand hygiene task force. *Am. J. Infect. Control* **2002**, *30* (8), S1~S46.

[49] Chu, D. K.; Akl, E. A.; Duda, S.; Solo, K.; Yaacoub, S.; Schunemann, H. J.; Review, C.-S. U. Physical distancing, face masks, and eye protection to prevent person-to-person transmission of SARS-CoV-2 and COVID-19: a systematic review and meta-analysis. *Lancet* **2020**, *395* (10242), 1973-1987.

[50] Ghosh, B.; Lal, H.; Srivastava, A. Review of bioaerosols in indoor environment with special reference to sampling, analysis and control mechanisms. *Environ. Int.* **2015**, *85*, 254-272.

[51] Linklater, D. P.; Baulin, V. A.; Juodkazis, S.; Crawford, R. J.; Stoodley, P.; Ivanova, E. P. Mechano-bactericidal actions of nanostructured surfaces. *Nat. Rev. Microbiol.* **2021**, *19* (1), 8-22.

[52] Wang, J. P.; Yang, L. X.; Wang, H. H.; Wang, L. Application of microfluidic chips in the detection of airborne microorganisms. *Micromachines* **2022**, *13* (10).

[53] Cong, J.; Zhang, X. C. How human microbiome talks to health and disease. *Eur. J. Clin. Microbiol. Infect. Dis.* **2018**, *37* (9), 1595-1601.

[54] Mima, K.; Ogino, S.; Nakagawa, S.; Sawayama, H.; Kinoshita, K.; Krashima, R.; Ishimoto, T.; Imai, K.; Iwatsuki, M.; Hashimoto, D.; et al. The role of intestinal bacteria in the development and progression of gastrointestinal tract neoplasms. *Surg. Oncol.* **2017**, *26* (4), 368-376.

[55] Grochowska, M.; Perlejewski, K.; Laskus, T.; Radkowski, M. The role of gut microbiota in gastrointestinal tract cancers. *Arch. Immunol. Ther. Exp.* **2022**, *70* (1).

[56] Tokarz-Deptula, B.; Sliwa-Dominiak, J.; Adamiak, M.; Bak, K.; Deptula, W. Commensal bacteria and immunity of the gastrointestinal, respiratory and genitourinary tracts. *Postepy Hig. Med. Dosw.* **2016**, *70*, 599-609.

[57] Kang, D. H.; Fung, D. Y. C. Development of a medium for differentiation between Escherichia coli and Escherichia coli O157:H7. *J. Food Prot.* **1999**, *62* (4), 313-317.

[58] Pokharel, P.; Dhakal, S.; Dozois, C. M. The diversity of Escherichia coli pathotypes and vaccination strategies against this versatile bacterial pathogen. *Microorganisms* **2023**, *11* (2).

[59] Singha, S.; Thomas, R.; Viswakarma, J. N.; Gupta, V. K. Foodborne illnesses of Escherichia coli O157 origin and its control measures. *J. Food Sci. Technol.* **2023**, *60* (4), 1274-1283.

[60] Xue, X. D.; Zhang, Y. Review of the detection of pathogenic Escherichia coli based-microchip technology. *Anal. Sci.* **2024**.

[61] Sperandio, F. F.; Huang, Y. Y.; Hamblin, M. R. Antimicrobial photodynamic therapy to kill Gram-negative bacteria. *Recent Pat Antiinfect Drug Discov* **2013**, *8* (2), 108-120.

[62] Wu, Y.; Bai, J.; Zhong, K.; Huang, Y.; Gao, H. A dual antibacterial mechanism involved in membrane disruption and DNA binding of 2R,3R-dihydromyricetin from pine needles of Cedrus deodara against Staphylococcus aureus. *Food Chem.* **2017**, *218*, 463-470.

[63] Shallcross, L. J.; Fragaszy, E.; Johnson, A. M.; Hayward, A. C. The role of the Panton-Valentine leucocidin toxin in staphylococcal disease: a systematic review and meta-analysis. *Lancet Infect. Dis.* **2013**, *13* (1), 43-54.

[64] Nadgir, C. A.; Biswas, D. A. Antibiotic resistance and its impact on disease management. *Cureus J. Med. Sci.* **2023**, *15* (4).

[65] Khan, R. T.; Sharma, V.; Khan, S. S.; Rasool, S. Prevention and potential remedies for antibiotic resistance: current research and future prospects. *Front. Microbiol.* **2024**, *15*.

[66] Yuan, X.; Lv, Z. Q.; Zhang, Z. Y.; Han, Y.; Liu, Z. Q.; Zhang, H. J. A review of antibiotics, antibiotic resistant bacteria, and resistance genes in aquaculture: Occurrence, contamination, and transmission. *Toxics* **2023**, *11* (5).

[67] Yapa, P. N.; Munaweera, I.; Weerasekera, M. M.; Weerasinghe, L. Nanoarchitectonics for synergistic activity of multimetallic nanohybrids as a possible approach for antimicrobial resistance (AMR). *J. Biol. Inorg. Chem.* **2024**, *29* (5), 477-498.

[68] Wandiyanto, J. V.; Cheeseman, S.; Truong, V. K.; Al Kobaisi, M.; Bizet, C.; Juodkazis, S.; Thissen, H.; Crawford, R. J.; Ivanova, E. P. Outsmarting superbugs: bactericidal activity of nanostructured titanium surfaces against methicillin- and gentamicin-resistant Staphylococcus aureus ATCC 33592. *J. Mater. Chem. B* **2019**, *7* (28), 4424-4431.

[69] Parmanik, A.; Das, S.; Kar, B.; Bose, A.; Dwivedi, G. R.; Pandey, M. M. Current treatment strategies against multidrug-resistant bacteria: A review. *Curr. Microbiol.* **2022**, *79* (12).

[70] Mitra, S.; Sultana, S. A.; Prova, S. R.; Uddin, T. M.; Islam, F.; Das, R.; Nainu, F.; Sartini, S.; Chidambaram, K.; Alhumaydhi, F. A.; et al. Investigating forthcoming strategies to tackle deadly superbugs: current status and future vision. *Expert Rev. Anti-Infect. Ther.* **2022**, *20* (10), 1309-1332.

[71] Mahizhchi, E.; Sivakumar, D.; Jayaraman, M. Antimicrobial resistance: Techniques to fight AMR in bacteria - A review. *J. Pure Appl. Microbiol.* **2024**, *18* (1), 16-28.

[72] Li, P. P.; Wu, H. X.; Dong, A. Ag/AgX nanostructures serving as antibacterial agents: achievements and challenges. *Rare Met.* **2022**, *41* (2), 519-539.

[73] Levy, S. B.; Marshall, B. Antibacterial resistance worldwide: causes, challenges and responses. *Nat. Med.* **2004**, *10* (12 Suppl), S122-129.

[74] Barbosa, T. M.; Levy, S. B. The impact of antibiotic use on resistance development and persistence. *Drug Resistance Updates* **2000**, *3* (5), 303-311.

[75] Chen, F. N.; Yang, X. D.; Mak, H. K. C.; Chan, D. W. T. Photocatalytic oxidation for antimicrobial control in built environment: A brief literature overview. *Build. Sci.* **2010**, *45* (8), 1747-1754.

[76] Chee, E.; Brown, A. C. Biomimetic antimicrobial material strategies for combating antibiotic resistant bacteria. *Biomater. Sci.* **2020**, *8* (4), 1089-1100.

[77] Zhu, Q.; Guan, J.; Tian, B.; Wang, P. X. Rational design of antibiotic-free antimicrobial contact lenses: Trade-offs between antimicrobial performance and biocompatibility. *Biomater. Adv.* **2024**, *164*.

[78] Ran, B.; Ran, L.; Wang, Z. K.; Liao, J. F.; Li, D. D.; Chen, K. D.; Cai, W. L.; Hou, J. A.; Peng, X. J. Photocatalytic antimicrobials: Principles, design strategies, and applications. *Chem Rev* **2023**, *123* (22), 12371-12430.

[79] Bolashikov, Z. D.; Melikov, A. K. Methods for air cleaning and protection of building occupants from airborne pathogens. *Build. Sci.* **2009**, *44* (7), 1378-1385.

[80] Lu, S. Y.; Meng, G.; Wang, C.; Chen, H. Photocatalytic inactivation of airborne bacteria in a polyurethane foam reactor loaded with a hybrid of MXene and anatase TiO<sub>2</sub> exposing {001} facets. *Chem Eng J* **2021**, *404*.

[81] Memarzadeh, F.; Olmsted, R. N.; Bartley, J. M. Applications of ultraviolet germicidal irradiation disinfection in health care facilities: effective adjunct, but not stand-alone technology. *Am. J. Infect. Control* **2010**, *38* (5), S13-S24.

[82] Montie, T. C.; Kelly-Wintenberg, K.; Roth, J. R. An overview of research using the one atmosphere uniform glow discharge plasma (OAUGDP) for sterilization of surfaces and materials. *IEEE Trans. Plasma Sci.* **2000**, *28* (1), 41-50.

[83] Shimizu, T.; Zimmermann, J. L.; Morfill, G. E. The bactericidal effect of surface micro-discharge plasma under different ambient conditions. *New J. Phys.* **2011**, *13* (2).

[84] Gour, N.; Ngo, K. X.; Vebert-Nardin, C. Anti-infectious surfaces achieved by polymer modification. *Macromol. Mater. Eng.* **2014**, *299* (6), 648-668.

[85] Trifan, A.; Luca, S. V.; Greige-Gerges, H.; Miron, A.; Gille, E.; Aprotosoaie, A. C. Recent advances in tackling microbial multidrug resistance with essential oils: combinatorial and nano-based strategies. *Crit. Rev. Microbiol.* **2020**, *46* (3), 338-357.

[86] Bassegoda, A.; Ivanova, K.; Ramon, E.; Tzanov, T. Strategies to prevent the occurrence of resistance against antibiotics by using advanced materials. *Appl. Microbiol. Biotechnol.* **2018**, *102* (5), 2075-2089.

[87] Liu, W. X.; Qin, Y. K.; Li, P. C. Design of chitosan sterilization agents by a structure combination strategy and their potential application in crop protection. *Molecules* **2021**, *26* (11).

[88] Xu, S. R.; Tan, P.; Tang, Q.; Wang, T.; Ding, Y. K.; Fu, H. Y.; Zhang, Y. C.; Zhou, C. L.; Song, M. D.; Tang, Q. S.; et al. Enhancing the stability of antimicrobial peptides: From design strategies to applications. *Chem Eng J* **2023**, *475*.

[89] Linklater, D. P.; Baulin, V. A.; Le Guevel, X.; Fleury, J. B.; Hanssen, E.; Nguyen, T. H. P.; Juodkazis, S.; Bryant, G.; Crawford, R. J.; Stoodley, P.; et al. Antibacterial action of nanoparticles by lethal stretching of bacterial cell membranes. *Adv. Mater.* **2020**, *32* (52), e2005679.

[90] Jenkins, J.; Mantell, J.; Neal, C.; Gholinia, A.; Verkade, P.; Nobbs, A. H.; Su, B. Antibacterial effects of nanopillar surfaces are mediated by cell impedance, penetration and induction of oxidative stress. *Nat. Commun.* **2020**, *11* (1), 1626.

[91] Perreault, F.; de Faria, A. F.; Nejati, S.; Elimelech, M. Antimicrobial properties of graphene oxide nanosheets: Why size matters. *Acs Nano* **2015**, *9* (7), 7226-7236.

[92] Ivanova, E. P.; Denver P. Linklater; Marco Werner; Vladimir A. Baulin; XiuMei Xu; Nandi Vrancken; Sergey Rubanov; Eric Hanssen; Jason Wandiyanto; Vi Khanh Truong; et al. The multi-faceted mechano-bactericidal mechanism of nanostructured surfaces. *Proc. Natl. Acad. Sci. U. S. A.* **2020**, *117* (23), 12598-12605.

[93] Elbourne, A.; Cheeseman, S.; Atkin, P.; Truong, N. P.; Syed, N.; Zavabeti, A.; Mohiuddin, M.; Esrafilzadeh, D.; Cozzolino, D.; McConville, C. F.; et al. Antibacterial liquid metals: Biofilm treatment via magnetic activation. *Acs Nano* **2020**, *14* (1), 802-817.

[94] Gulzar, N.; Andleeb, S.; Raza, A.; Ali, S.; Liaqat, I.; Raja, S. A.; Ali, N. M.; Khan, R.; Awan, U. A. Acute toxicity, anti-diabetic, and anti-cancerous potential of Trillium govanianum-conjugated silver nanoparticles in Balb/c mice. *Curr. Pharm. Biotechnol.* **2024**, *25* (10), 1304-1320.

[95] Alnsour, A. R.; Daghmash, R. M.; Masadeh, M. M.; Alzoubi, K. H.; Masadeh, M. M.; Bataineh, N. H.; Batayneh, H. H.; Al-Ogaidi, M. S. The pharmaceutical role of silver nanoparticles in treating multidrug-resistant bacteria and biofilms. *Curr. Nanosci.* **2024**, *20* (4), 471-494.

[96] Abbas, R.; Luo, J.; Qi, X.; Naz, A.; Khan, I. A.; Liu, H.; Yu, S.; Wei, J. Silver nanoparticles: Synthesis, structure, properties and applications. *Nanomaterials* **2024**, *14* (17).

[97] Urodkova, E. K.; Uryupina, O. g. Y.; Zhavoronok, E. S.; Grammatikova, N. E.; Kharitonova, T. V.; Senchikhin, I. N. Antibacterial activity of silver nanodispersions in solutions of different molecular weight chitosans. *Chemistryselect* **2023**, *8* (6).

[98] Yan, S. J.; Luan, S. F.; Shi, H. C.; Xu, X. D.; Zhang, J. D.; Yuan, S. S.; Yang, Y. M.; Yin, J. H. Hierarchical polymer brushes with dominant antibacterial mechanisms switching from bactericidal to bacteria repellent. *Biomacromolecules* **2016**, *17* (5), 1696-1704.

[99] Abel, T.; Cohen, J. I.; Engel, R.; Filshtinskaya, M.; Melkonian, A.; Melkonian, K. Preparation and investigation of antibacterial carbohydrate-based surfaces. *Carbohydr. Res.* **2002**, *337* (24), 2495-2499.

[100] Thomas, M.; Montenegro, D.; Castaño, A.; Friedman, L.; Leb, J.; Huang, M. L.; Rothman, L.; Lee, H.; Capodiferro, C.; Ambinder, D.; et al. Polycations. 17. Synthesis and properties of polycationic derivatives of carbohydrates. *Carbohydr. Res.* **2009**, *344* (13), 1620-1627.

[101] Kanazawa, A.; Ikeda, T.; Endo, T. Polymeric phosphonium salts as a novel class of cationic biocides: Effect of side-chain length between main chain and active group on antibacterial activity. *J. Polym. Sci., Part A:Polym. Chem.* **1994**, *32* (10), 1997-2001.

[102] Daaboul, M.; Akgul, B.; Tasdurmazli, S.; Abamor, E. S.; Ozbek, T.; Ozmen, M. M.; Topuzogullari, M. Polycationic nanoparticle-integrated inherently antibacterial cryogels. *Mater. Lett.* **2024**, *368*.

[103] Song, Q.; Chan, S. Y.; Xiao, Z. H.; Zhao, R. X.; Zhang, Y. N.; Chen, X. M.; Liu, T.; Yan, Y. J.; Zhang, B.; Han, F.; et al. Contact-killing antibacterial mechanisms of polycationic coatings: A review. *Prog. Org. Coat.* **2024**, *188*.

[104] Ivanova, E. P.; Hasan, J.; Webb, H. K.; Truong, V. K.; Watson, G. S.; Watson, J. A.; Baulin, V. A.; Pogodin, S.; Wang, J. Y.; Tobin, M. J.; et al. Natural bactericidal surfaces:

Mechanical rupture of Pseudomonas aeruginosa cells by cicada wings. *Small* **2012**, *8* (16), 2489-2494.

[105] Li, J.; Tan, L.; Liu, X. M.; Cui, Z. D.; Yang, X. J.; Yeung, K. W. K.; Chu, P. K.; Wu, S. L. Balancing bacteria-osteoblast competition through selective physical puncture and biofunctionalization of ZnO/polydopamine/arginine-glycine-aspartic acid-cysteine nanorods. *Acs Nano* **2017**, *11* (11), 11250-11263.

[106] Hazell, G.; Fisher, L. E.; Murray, W. A.; Nobbs, A. H.; Su, B. Bioinspired bactericidal surfaces with polymer nanocone arrays. *J. Colloid Interface Sci.* **2018**, *528*, 389-399.

[107] Lin, N.; Berton, P.; Moraes, C.; Rogers, R. D.; Tufenkji, N. Nanodarts, nanoblades, and nanospikes: mechano-bactericidal nanostructures and where to find them. *Adv. Colloid Interface Sci.* **2018**, *252*, 55-68.

[108] Deng, J. J.; Ye, J.; Zhao, Y. L.; Zhu, Y. L.; Wu, T. L.; Zhang, C.; Dong, L. N.; Ouyang, H.; Cheng, X. G.; Wang, X. L. ZnO and hydroxyapatite-modified magnesium implant with a broad spectrum of antibacterial properties and a unique minimally invasive defined degrading capability. *ACS Biomater. Sci. Eng.* **2019**, *5* (9), 4285-4292.

[109] Nakade, K.; Jindai, K.; Sagawa, T.; Kojima, H.; Shimizu, T.; Shingubara, S.; Ito, T. Adhesion and bactericidal properties of a wettability-controlled artificial nanostructure. *ACS Appl. Nano Mater.* **2018**, *1* (10), 5736-5741.

[110] Michalska, M.; Gambacorta, F.; Divan, R.; Aranson, I. S.; Sokolov, A.; Noirot, P.; Laible, P. D. Tuning antimicrobial properties of biomimetic nanopatterned surfaces. *Nanoscale* **2018**, *10* (14), 6639-6650.

[111] Chen, D. W.; Lee, K. Y.; Tsai, M. H.; Lin, T. Y.; Chen, C. H.; Cheng, K. W. Antibacterial application on Staphylococcus aureus using antibiotic agent/zinc oxide nanorod arrays/polyethylethylketone composite samples. *Nanomaterials* **2019**, *9* (5).

[112] Linklater, D. P.; Juodkazis, S.; Ivanova, E. P. Nanofabrication of mechano-bactericidal surfaces. *Nanoscale* **2017**, *9* (43), 16564-16585.

[113] Pang, S. M.; He, Y.; Zhong, R.; Guo, Z. Z.; He, P.; Zhou, C. R.; Xue, B.; Wen, X. J.; Li, H. Multifunctional ZnO/TiO2 nanoarray composite coating with antibacterial activity, cytocompatibility and piezoelectricity. *Ceram. Int.* **2019**, *45* (10), 12663-12671.

[114] Del Valle, A.; Torra, J.; Bondia, P.; Tone, C. M.; Pedraz, P.; Vadillo-Rodriguez, V.; Flors, C. Mechanically induced bacterial death imaged in real time: A simultaneous nanoindentation and fluorescence microscopy study. *ACS Appl. Mater. Interfaces* **2020**, *12* (28), 31235-31241.

[115] Modaresifar, K.; Azizian, S.; Ganjian, M.; Fratila-Apachitei, L. E.; Zadpoor, A. A. Bactericidal effects of nanopatterns: A systematic review. *Acta Biomater.* **2019**, *83*, 29-36.

[116] Valiei, A.; Lin, N.; Bryche, J. F.; McKay, G.; Canva, M.; Charette, P. G.; Nguyen, D.; Moraes, C.; Tufenkji, N. Hydrophilic mechano-bactericidal nanopillars require external forces to rapidly kill bacteria. *Nano Lett.* **2020**, *20* (8), 5720-5727.

[117] Jenkins, J.; Mantell, J.; Neal, C.; Gholinia, A.; Verkade, P.; Nobbs, A. H.; Su, B. Antibacterial effects of nanopillar surfaces are mediated by cell impedance, penetration and induction of oxidative stress. *Nat. Commun.* **2020**, *11* (1).

[118] Dimitrakellis, P.; Ellinas, K.; Kaprou, G. D.; Mastellos, D. C.; Tserepi, A.; Gogolides, E. Bactericidal action of smooth and plasma micro-nanotextured polymeric surfaces with varying wettability, enhanced by incorporation of a biocidal agent. *Macromol. Mater. Eng.* **2021**, *306* (4).

[119] Gao, Q.; Feng, T.; Huang, D. N.; Liu, P.; Lin, P.; Wu, Y.; Ye, Z. M.; Ji, J.; Li, P.; Huang, W. Antibacterial and hydroxyapatite-forming coating for biomedical implants based on polypeptide-functionalized titania nanospikes. *Biomater. Sci.* **2020**, *8* (1), 278-289.

[120] Ivanova, E. P.; Linklater, D. P.; Werner, M.; Baulin, V. A.; Xu, X.; Vrancken, N.; Rubanov, S.; Hanssen, E.; Wandiyanto, J.; Truong, V. K.; et al. The multi-faceted mechano-bactericidal mechanism of nanostructured surfaces. *Proc. Natl. Acad. Sci. U. S. A.* **2020**, *117* (23), 12598-12605.

[121] Tan, R.; Marzolini, N.; Jiang, P.; Jang, Y. Bio-inspired polymer thin films with non-close-packed nanopillars for enhanced bactericidal and antireflective properties. *ACS Appl. Polym. Mater.* **2020**, *2* (12), 5808-5816.

[122] Ye, J.; Deng, J. J.; Chen, Y. T.; Yang, T.; Zhu, Y. L.; Wu, C. X.; Wu, T. L.; Jia, J. Y.; Cheng, X. G.; Wang, X. L. Cicada and catkin inspired dual biomimetic antibacterial structure for the surface modification of implant material. *Biomater. Sci.* **2019**, *7* (7), 2826-2832.

[123] Le Clainche, T.; Linklater, D.; Wong, S.; Le, P.; Juodkazis, S.; Le Guevel, X.; Coll, J. L.; Ivanova, E. P.; Martel-Frachet, V. Mechano-bactericidal titanium surfaces for bone tissue engineering. *ACS Appl. Mater. Interfaces* **2020**, *12* (43), 48272-48283.

[124] Shimada, T.; Yasui, T.; Yonese, A.; Yanagida, T.; Kaji, N.; Kanai, M.; Nagashima, K.; Kawai, T.; Baba, Y. Mechanical rupture-based antibacterial and cell-compatible $ZnO/SiO_2$ nanowire structures formed by bottom-up approaches. *Micromachines (Basel)* **2020**, *11* (6).

[125] Li, X.; Tsui, K. H.; Tsoi, J. K. H.; Green, D. W.; Jin, X. Z.; Deng, Y. Q.; Zhu, Y. M.; Li, X. G.; Fan, Z. Y.; Cheung, G. S. P. A nanostructured anti-biofilm surface widens the efficacy against spindle-shaped and chain-forming rod-like bacteria. *Nanoscale* **2020**, *12* (36), 18864-18874.

[126] Linklater, D.; Ivanova, E. P. Challenges to the design and testing of antimicrobial nanostructured surfaces. *Microbiology Australia* **2023**.

[127] Zhao, X. Y.; Xu, Z. H.; Wei, Z. X.; Sun, Y.; Zhou, Q. Nature-inspired mechano-bactericidal nanostructured surfaces with photothermally enhanced antibacterial performances. *Prog. Org. Coat.* **2023**, *182*.

[128] Feng, H. Q.; Wang, G. M.; Jin, W. H.; Zhang, X. M.; Huang, Y. F.; Gao, A.; Wu, H.; Wu, G. S.; Chu, P. K. Systematic study of inherent antibacterial properties of magnesium-based biomaterials. *ACS Appl. Mater. Interfaces* **2016**, *8* (15), 9662-9673.

[129] Kaur, R.; Liu, S. Antibacterial surface design - Contact kill. *Prog. Surf. Sci.* **2016**, *91* (3), 136-153.

[130] Wandiyanto, J. V.; Tamanna, T.; Linklater, D. P.; Truong, V. K.; Al Kobaisi, M.; Baulin, V. A.; Joudkazis, S.; Thissen, H.; Crawford, R. J.; Ivanova, E. P. Tunable morphological changes of asymmetric titanium nanosheets with bactericidal properties. *J. Colloid Interface Sci.* **2020**, *560*, 572-580.

[131] Wang, G. M.; Jiang, W. J.; Mo, S.; Xie, L. X.; Liao, Q.; Hu, L. S.; Ruan, Q. D.; Tang, K. W.; Mehrjou, B.; Liu, M. T.; et al. NNonleaching antibacterial concept demonstrated by in situ construction of 2D nanoflakes on magnesium. *Adv Sci* **2020**, *7* (1).

[132] Wang, G. M.; Tang, K. W.; Jiang, W. J.; Liao, Q.; Li, Y.; Liu, P.; Wu, Y. Z.; Liu, M. T.; Wang, H. Y.; Li, B.; et al. Quantifiable relationship between antibacterial efficacy and electro-mechanical intervention on nanowire arrays. *Adv. Mater.* **2023**, *35* (19).

[133] Wu, Y. Z.; Xiao, D. Z.; Liu, P.; Liao, Q.; Ruan, Q. D.; Huang, C.; Liu, L. L.; Li, D.; Zhang, X. L.; Li, W.; et al. Nanostructured conductive polypyrrole for antibacterial components in flexible wearable devices. *Research* **2023**, *2023*.

[134] Anitha, V. C.; Banerjee, A. N.; Joo, S. W.; Min, B. K. Morphology-dependent low macroscopic field emission properties of titania/titanate nanorods synthesized by alkali-controlled hydrothermal treatment of a metallic Ti surface. *Nanotechnology* **2015**, *26* (35).

[135] Oungoulian, S. R.; Durney, K. M.; Jones, B. K.; Ahmad, C. S.; Hung, C. T.; Ateshian, G. A. Wear and damage of articular cartilage with friction against orthopedic implant materials. *J. Biomech.* **2015**, *48* (10), 1957-1964.

[136] Pham, V. T. H.; Truong, V. K.; Quinn, M. D. J.; Notley, S. M.; Guo, Y. C.; Baulin, V. A.; Al Kobaisi, M.; Crawford, R. J.; Ivanova, E. P. Graphene induces formation of pores that kill spherical and rod-shaped bacteria. *Acs Nano* **2015**, *9* (8), 8458-8467.

[137] Peng, M. K.; Hu, F. Y.; Du, M. T.; Mai, B. J.; Zheng, S. R.; Liu, P.; Wang, C. H.; Chen, Y. S. Hydrothermal growth of hydroxyapatite and ZnO bilayered nanoarrays on magnesium alloy surface with antibacterial activities. *Front. Mater. Sci.* **2020**, *14* (1), 14-23.

[138] Morel, J.; McNeilly, O.; Grundy, S.; Brown, T.; Gunawan, C.; Amal, R.; Scott, J. A. Nanoscale titanium surface engineering via low-temperature hydrothermal etching for enhanced antimicrobial properties. *ACS Appl. Mater. Interfaces* **2023**, *15* (39), 46247-46260.

[139] Bright, R.; Hayles, A.; Wood, J.; Palms, D.; Brown, T.; Barker, D.; Vasilev, K. Surfaces containing sharp nanostructures enhance antibiotic efficacy. *Nano Lett.* **2022**, *22* (16), 6724-6731.

[140] Liu, Z. T.; Yi, Y. Z.; Song, L. J.; Chen, Y. X.; Tian, L. M.; Zhao, J.; Ren, L. Q. Biocompatible mechano-bactericidal nanopatterned surfaces with salt-responsive bacterial release. *Acta Biomater.* **2022**, *141*, 198-208.

[141] Li, K.; Chen, J.; Xue, Y.; Ding, T. X.; Zhu, S. B.; Mao, M. T.; Zhang, L.; Han, Y. Polymer brush grafted antimicrobial peptide on hydroxyapatite nanorods for highly effective antibacterial performance. *Chem Eng J* **2021**, *423*.

[142] Zhang, L.; Xue, Y.; Gopalakrishnan, S.; Li, K.; Han, Y.; Rotello, V. M. Antimicrobial peptide-loaded pectolite nanorods for enhancing wound-healing and biocidal activity of titanium. *ACS Appl. Mater. Interfaces* **2021**, *13* (24), 28764-28773.

[143] Zhang, X. Y.; Zhang, G. N.; Chai, M. Z.; Yao, X. H.; Chen, W. Y.; Chu, P. K. Synergistic antibacterial activity of physical-chemical multi-mechanism by TiO2 nanorod arrays for safe biofilm eradication on implant. *Bioact. Mater.* **2021**, *6* (1), 12-25.

[144] Zhao, L. D.; Liu, T. Q.; Li, X. Q.; Cui, Q. Q.; Wu, Q. Q.; Wang, X.; Song, K. D.; Ge, D. Low-temperature hydrothermal synthesis of novel 3D hybrid nanostructures on titanium surface with mechano-bactericidal performance. *ACS Biomater. Sci. Eng.* **2021**, *7* (6), 2268-2278.

[145] Bright, R.; Fernandes, D.; Wood, J.; Palms, D.; Burzava, A.; Ninan, N.; Brown, T.; Barker, D.; Vasilev, K. Long-term antibacterial properties of a nanostructured titanium alloy surface: An in vitro study. *Mater. Today Bio* **2022**, *13*.

[146] Li, P.; Li, J.; Feng, X.; Li, J.; Hao, Y.; Zhang, J.; Wang, H.; Yin, A.; Zhou, J.; Ma, X.; et al. Metal-organic frameworks with photocatalytic bactericidal activity for integrated air cleaning. *Nat. Commun.* **2019**, *10* (1), 2177.

[147] Andra, S.; Balu, S. k.; Jeevanandam, J.; Muthalagu, M. Emerging nanomaterials for antibacterial textile fabrication. *Naunyn-Schmiedeberg's Arch. Pharmacol.* **2021**, *394* (7), 1355-1382.

[148] Knibbs, L. D.; Johnson, G. R.; Kidd, T. J.; Cheney, J.; Grimwood, K.; Kattenbelt, J. A.; O'Rourke, P. K.; Ramsay, K. A.; Sly, P. D.; Wainwright, C. E.; et al. Viability of Pseudomonas aeruginosa in cough aerosols generated by persons with cystic fibrosis. *Thorax* **2014**, *69* (8), 740-745.

[149] Khan, A. U.; Zahoor, M.; Rehman, M. U.; Ikram, M.; Zhu, D. C.; Umar, M. N.; Ullah, R.; Ali, E. A. Bioremediation of azo dye brown 703 by Pseudomonas aeruginosa: an effective treatment technique for dye-polluted wastewater. *Microbiol. Res.* **2023**, *14* (3), 1049-1066.

[150] Vihodceva, S.; Ramata-Stunda, A.; Pumpure, A. Evaluation of dermal toxicity of antibacterial cotton textile coated by sol-gel technology. *J. Text. Inst.* **2018**, *109* (7), 961-966.

[151] Gao, Y.; Bach Truong, Y.; Zhu, Y.; Louis Kyratzis, I. Electrospun antibacterial nanofibers: Production, activity, andin vivoapplications. *J. Appl. Polym. Sci.* **2014**, *131* (18).

[152] Si, Y.; Zhang, Z.; Wu, W.; Fu, Q.; Huang, K.; Nitin, N.; Ding, B.; Sun, G. Daylight-driven rechargeable antibacterial and antiviral nanofibrous membranes for bioprotective applications. *Sci. Adv.* **2018**, *4*, eaar5931.

[153] Cheung, Y. H.; Ma, K.; van Leeuwen, H. C.; Wasson, M. C.; Wang, X.; Idrees, K. B.; Gong, W.; Cao, R.; Mahle, J. J.; Islamoglu, T.; et al. Immobilized regenerable active chlorine within a zirconium-based MOF textile composite to eliminate biological and chemical threats. *J. Am. Chem. Soc.* **2021**, *143* (40), 16777-16785.

[154] Alhaji, N. M. I.; Sujatha, S. Synthesis of plant-mediated metal silver nanoparticles for fabric coating. In *ICETMT*, Bangalore, INDIA, 2022

Feb 10-11, 2022; 2022; Vol. 62, pp 5684-5689. DOI: 10.1016/j.matpr.2022.05.115.

[155] Stabryla, L. M. M.; Moncure, P. J. J.; Millstone, J. E. E.; Gilbertson, L. M. M. Particle-driven effects at the bacteria interface: A nanosilver investigation of particle shape and dose metric. *ACS Appl. Mater. Interfaces* **2023**, *15*, 39027−39038.

[156] Yuan, G.; Cranston, R. Recent advances in antimicrobial treatments of textiles. *Text. Res. J.* **2008**, *78* (1), 60-72.

[157] Naebe, M.; Haque, A. N. M. A.; Haji, A. Plasma-assisted antimicrobial finishing of textiles: A review. *Engineering* **2022**, *12*, 145-163.

[158] Gao, W. R.; Wang, X. M.; Xu, W. Q.; Xu, S. P. Luminescent composite polymer fibers: In situ synthesis of silver nanoclusters in electrospun polymer fibers and application. *Mater. Sci. Eng., C* **2014**, *42*, 333-340.

[159] Abu Bakar, N.; Yusoff, N. N.; Azmi, F. S. N.; Shapter, J. G. A review of metal nanoparticle-based surface-enhanced raman scattering substrates for severe acute respiratory syndrome coronavirus 2 (SARS-CoV-2) detection special collection: Distinguished Australian researchers. *Aggregate* **2023**, *4* (5), e339.

[160] Tripathi, N.; Goshisht, M. K. Recent advances and mechanistic insights into antibacterial activity, antibiofilm activity, and cytotoxicity of silver nanoparticles. *ACS Appl. Bio Mater.* **2022**, *5* (4), 1391-1463.

[161] Zare, E. N.; Zheng, X.; Makvandi, P.; Gheybi, H.; Sartorius, R.; Yiu, C. K. Y.; Adeli, M.; Wu, A.; Zarrabi, A.; Varma, R. S.; et al. Nonspherical metal-based nanoarchitectures: Synthesis and impact of size, shape, and composition on their biological activity. *Small* **2021**, *17* (17), 2007073.

[162] Vankayala, R.; Kuo, C. L.; Sagadevan, A.; Chen, P. H.; Chiang, C. S.; Hwang, K. C. Morphology dependent photosensitization and formation of singlet oxygen (1Δg) by gold and silver nanoparticles and its application in cancer treatment. *J. Mater. Chem. B* **2013**, *1* (35), 4379-4387.

[163] Lu, Z. S.; Xiao, J.; Wang, Y.; Meng, M. In situ synthesis of silver nanoparticles uniformly distributed on polydopamine-coated silk fibers for antibacterial application. *J. Colloid Interface Sci.* **2015**, *452*, 8-14.

[164] Afandy, H. H.; Sabir, D. K.; Aziz, S. B. Antibacterial activity of the green synthesized plasmonic silver nanoparticles with crystalline structure against gram-positive and gram-negative bacteria. *Nanomaterials* **2023**, *13* (8), 1327.

[165] Morsy, R.; Hosny, M.; Reicha, F.; Elnimr, T. Developing a potential antibacterial long-term degradable electrospun gelatin -based composites mats for wound dressing applications. *React. Funct. Polym.* **2017**, *114*, 8-12.

[166] Singh, C.; Mehata, A. K.; Priya, V.; Malik, A. K.; Setia, A.; Suseela, M. N. L.; Vikas; Gokul, P.; Samridhi; Singh, S. K.; et al. Bimetallic Au-Ag nanoparticles: advanced nanotechnology for tackling antimicrobial resistance. *Molecules* **2022**, *27* (20), 7059.

[167] Zheng, S.; Du, M.; Miao, W.; Wang, D.; Zhu, Z.; Tian, Y.; Jiang, L. 2D prior spreading inspired from Chinese Xuan papers. *Adv Funct Mater* **2018**, *28* (49), 1800832.

[168] Majumder, S.; Matin, M. A.; Sharif, A.; Arafat, M. T. Understanding solubility, spinnability and electrospinning behaviour of cellulose acetate using different solvent systems. *Bull. Mater. Sci.* **2019**, *42* (4).

[169] Yang, G.; Li, X. L.; He, Y.; Ma, J. K.; Ni, G. L.; Zhou, S. B. From nano to micro to macro: Electrospun hierarchically structured polymeric fibers for biomedical applications. *Prog. Polym. Sci.* **2018**, *81*, 80-113.

[170] Pham, Q. P.; Sharma, U.; Mikos, A. G. Electrospinning of polymeric nanofibers for tissue engineering applications: A review. *Tissue Eng.* **2006**, *12* (5), 1197-1211.

[171] Kamarudin, D.; Hashim, N. A.; Ong, B. H.; Faried, M.; Suga, K.; Umakoshi, H.; Wan Mahari, W. A. Alternative fouling analysis of PVDF UF membrane for surface water treatment: The credibility of silver nanoparticles. *J. Membr. Sci.* **2022**, *661*.

[172] Kamarudin, D.; Awanis Hashim, N.; Ong, B. H.; Kakihana, Y.; Higa, M.; Matsuyama, H. Multiple effect of thermal treatment approach on PVDF membranes: Permeability enhancement and silver nanoparticles immobilization. *J. Environ. Chem. Eng.* **2021**, *9* (4).

[173] Mathew, A.; Hasan, J.; Singamneni, S.; Yarlagadda, P. K. D. Nanospikes on customized 3D-printed titanium implant surface inhibits bacterial colonization. *Adv. Eng. Mater.* **2023**, *25* (8).

[174] Ye, J.; Li, B.; Li, M.; Zheng, Y. F.; Wu, S. L.; Han, Y. Formation of a ZnO nanorods-patterned coating with strong bactericidal capability and quantitative evaluation of the contribution of nanorods-derived puncture and ROS-derived killing. *Bioact. Mater.* **2022**, *11*, 181-191.

[175] Ye, J.; Li, B.; Zheng, Y. F.; Wu, S. L.; Chen, D. F.; Han, Y. Eco-friendly bacteria-killing by nanorods through mechano-puncture with top selectivity. *Bioact. Mater.* **2022**, *15*, 173-184.

[176] Huo, J. J.; Jia, Q. Y.; Wang, K.; Chen, J. J.; Zhang, J. H.; Li, P.; Huang, W. Metal-phenolic networks assembled on $TiO_2$ nanospikes for antimicrobial peptide deposition and osteoconductivity enhancement in orthopedic applications. *Langmuir* **2023**, *39* (3), 1238-1249.

[177] Cui, Q.; Liu, T.; Li, X.; Song, K.; Ge, D. Nanopillared polycarbonate surfaces having variable feature parameters as bactericidal coatings. *ACS Appl. Nano Mater.* **2020**, *3* (5), 4599-4609.

[178] Clainche, T. L.; Linklater, D.; Wong, S.; Le, P.; Juodkazis, S.; Guevel, X. L.; Coll, J. L.; Ivanova, E. P.; Martel-Frachet, V. Mechano-bactericidal titanium surfaces for bone tissue engineering. *ACS Appl. Mater. Interfaces* **2020**, *12* (43), 48272-48283.

[179] Arias, S. L.; Devorkin, J.; Spear, J. C.; Civantos, A.; Allain, J. P. Bacterial envelope damage inflicted by bioinspired nanostructures grown in a hydrogel. *ACS Appl. Bio Mater.* **2020**, *3* (11), 7974-7988.

[180] Yang, L.; Hu, J.; Qin, J. The van der Waals force between arbitrary-shaped particle and a plane surface connected by a liquid bridge in humidity environment. *Granular Matter* **2014**, *16* (6), 903-909.

[181] Yang, Q.; Sun, P. Z.; Fumagalli, L.; Stebunov, Y. V.; Haigh, S. J.; Zhou, Z. W.; Grigorieva, I. V.; Wang, F. C.; Geim, A. K. Capillary condensation under atomic-scale confinement. *Nature* **2020**, *588* (7837), 250-253.

[182] Fisher, L. R.; Gamble, R. A.; Middlehurst, J. The Kelvin equation and the capillary condensation of water. *Nature* **1981**, *290*, 575-576.

[183] Hirst, W. Dimensional changes accompanying capillary condensation. *Nature* **1947**, *159*, 267-268.

[184] Wu, Y. Z.; Ruan, Q. D.; Huang, C.; Liao, Q.; Liu, L. L.; Liu, P.; Mo, S.; Wang, G. M.; Wang, H. Y.; Chu, P. K. Balancing the biocompatibility and bacterial resistance of polypyrrole by optimized silver incorporation. *Biomater. Adv.* **2022**, *134*, 112701.

[185] Liu, X. L.; Xu, Y. J.; Wu, Z. Q.; Chen, H. Poly(N-vinylpyrrolidone)-modified surfaces for biomedical applications. *Macromol. Biosci.* **2013**, *13* (2), 147-154.

[186] Luan, S. F.; Zhao, J.; Yang, H. W.; Shi, H. C.; Jin, J.; Li, X. M.; Liu, J. C.; Wang, J. W.; Yin, J. H.; Stagnaro, P. Surface modification of poly(styrene-

-(ethylene-

-butylene)-

-styrene) elastomer via UV-induced graft polymerization of

-vinyl pyrrolidone. *Colloid Surface B* **2012**, *93*, 127-134.

[187] Zhao, Y.; A, H.; Cheung, Y. H.; Lam, Y.; Tang, J.; Li, H.; Yang, Z.; Xin, J. H. Capillary condensation mediated fluidic straining for enhanced bacterial inactivation. *Adv Funct Mater* **2024**, *34* (32).

[188] Wang, X. Y.; Xia, Z. P.; Wang, H. L.; Wang, D.; Sun, T. W.; Hossain, E.; Pang, X.; Liu, Y. F. Cell-membrane-coated nanoparticles for the fight against pathogenic bacteria, toxins, and inflammatory cytokines associated with sepsis. *Theranostics* **2023**, *13* (10), 3224-3244.

[189] Conner, S. D.; Schmid, S. L. Regulated portals of entry into the cell. *Nature* **2003**, *422* (6927), 37-44.

[190] Groves, J. T.; Kuriyan, J. Molecular mechanisms in signal transduction at the membrane. *Nat Struct Mol Biol* **2010**, *17* (6), 659-665.

[191] Silhavy, T. J.; Kahne, D.; Walker, S. The bacterial cell envelope. *Csh Perspect Biol* **2010**, *2* (5).

[192] Sarkar, D.; Dhar, M.; Das, A.; Mandal, S.; Phukan, A.; Manna, U. Covalent crosslinking chemistry for controlled modulation of nanometric roughness and surface free energy. *Chem Sci* **2024**, *15* (13), 4938-4951.

[193] Huang, Y.; Chandran Suja, V.; Yang, M.; Malkovskiy, A. V.; Tandon, A.; Colom, A.; Qin, J.; Fuller, G. G. Interfacial stresses on droplet interface bilayers using two photon fluorescence lifetime imaging microscopy. *J. Colloid Interface Sci.* **2024**, *653*, 1196-1204.

[194] Huang, W. Y. C.; Boxer, S. G.; Ferrell, J. J. r. Membrane localization accelerates association under conditions relevant to cellular signaling. *Proc. Natl. Acad. Sci. U. S. A.* **2024**, *121* (10), e2319491121.

[195] Cao, Z. Q.; Mi, L.; Mendiola, J.; Ella-Menye, J. R.; Zhang, L.; Xue, H.; Jiang, S. Y. Reversibly switching the function of a surface between attacking and defending against bacteria. *Angew Chem Int Edit* **2012**, *51* (11), 2602-2605.

[196] Zhao, S.; Li, Z. Y.; Yin, S. Y.; Chen, Q. D.; Sun, H. B.; Wen, L. P.; Jiang, L.; Sun, K. Mimicking the competitive interactions to reduce resistance induction in antibacterial actions. *Chem. Eng. J.* **2023**, *454*, 140215.

[197] Caudill, E. R.; Hernandez, R. T.; Johnson, K. P.; O'Rourke, J. T.; Zhu, L. C.; Haynes, C. L.; Feng, Z. V.; Pedersen, J. A. Wall teichoic acids govern cationic gold nanoparticle interaction with Gram-positive bacterial cell walls. *Chem Sci* **2020**, *11* (16), 4106-4118.

[198] Gleue, L.; Schupp, J.; Zimmer, N.; Becker, E.; Frey, H.; Tuettenberg, A.; Helm, M. Stability of alkyl chain-mediated lipid anchoring in liposomal membranes. *Cells* **2020**, *9* (10), 2213.

[199] Zeng, Z. L.; Pu, K. Y. Improving cancer immunotherapy by cell membrane-camouflaged nanoparticles. *Adv Funct Mater* **2020**, *30* (43).

[200] de Sousa, K. M.; Linklater, D. P.; Baulin, V. A.; Dekiwadia, C.; Mayes, E.; Murdoch, B. J.; Le, P. H.; Fluke, C. J.; Boshkovikj, V.; Wen, C. E.; et al. Understanding the influence of serum proteins adsorption on the mechano-bactericidal efficacy and immunomodulation of nanostructured titanium. *Adv Mater Interfaces* **2024**, *11*, 2301021.

[201] Chopra, D.; Guo, T. Q.; Jayasree, A.; Gulati, K.; Ivanovski, S. Bioinspired, bioactive, and bactericidal: Anodized nanotextured dental implants. *Adv Funct Mater* **2024**, *34*, 2314031.

[202] Xing, Z. Y.; Guo, J. S.; Wu, Z. H.; He, C.; Wang, L. Y.; Bai, M. R.; Liu, X. K.; Zhu, B. H.; Guan, Q. Y.; Cheng, C. Nanomaterials-enabled physicochemical antibacterial therapeutics: toward the antibiotic-free disinfections. *Small* **2023**, *19* (50), 2303594.

[203] Song, N. N.; Yu, Y.; Zhang, Y. N.; Wang, Z. D.; Guo, Z. J.; Zhang, J. L.; Zhang, C. B.; Liang, M. M. Bioinspired hierarchical self-assembled nanozyme for efficient antibacterial treatment. *Adv. Mater.* **2023**, *36* (10), 2210455.

[204] Peng, L.; Zhu, H. J.; Wang, H. B.; Guo, Z. B.; Wu, Q. Y.; Yang, C.; Hu, H. Y. Hydrodynamic tearing of bacteria on nanotips for sustainable water disinfection. *Nat. Commun.* **2023**, *14* (1), 5734.

[205] Locock, K. E. S.; Michl, T. D.; Stevens, N.; Hayball, J. D.; Vasilev, K.; Postma, A.; Griesser, H. J.; Meagher, L.; Haeussler, M. Antimicrobial polymethacrylates synthesized as mimics of tryptophan-rich cationic peptides. *Acs Macro Lett* **2014**, *3* (4), 319-323.

[206] Zhao, Y.; Luo, Y.; Chai, Y.; Lam, Y.; Gong, Y.; Chen, K.; Lu, G.; Xia, G.; Chang, Y.; Yang, M.; et al. Precise oligomer organization enhanced electrostatic interactions for efficient cell membrane binding. *Nano Lett.* **2025**, *25* (21), 8488-8494.

[207] Wang, H.; Shi, X. F.; Yu, D. F.; Zhang, J.; Yang, G.; Cui, Y. X.; Sun, K. J.; Wang, J. B.; Yan, H. K. Antibacterial activity of geminized amphiphilic cationic homopolymers. *Langmuir* **2015**, *31* (50), 13469-13477.

[208] Nikfarjam, N.; Ghomi, M.; Agarwal, T.; Hassanpour, M.; Sharifi, E.; Khorsandi, D.; Ali Khan, M.; Rossi, F.; Rossetti, A.; Nazarzadeh Zare, E.; et al. Antimicrobial ionic liquid-based materials for biomedical applications. *Adv Funct Mater* **2021**, *31* (42), 2104148.

[209] Fu, T. R.; Smith, S.; Camarasa-Gómez, M.; Yu, X. F.; Xue, J. Y.; Nuckolls, C.; Evers, F.; Venkataraman, L.; Wei, S. J. Enhanced coupling through π-stacking in imidazole-based molecular junctions. *Chem Sci* **2019**, *10* (43), 9998-10002.

[210] Lai, J. T.; Filla, D.; Shea, R. Functional polymers from novel carboxyl-terminated trithiocarbonates as highly efficient RAFT agents. *Macromolecules* **2002**, *35* (18), 6754-6756.

[211] Huang, X.; Hu, J.; Li, Y.; Xin, F.; Qiao, R.; Davis, T. P. Engineering organic/inorganic nanohybrids through raft polymerization for biomedical applications. *Biomacromolecules* **2019**, *20* (12), 4243-4257.